AD_____

Award Number: W81XWH-11-1-0756

TITLE: Pediatric Glioblastoma Therapies Based on Patient-Derived Stem Cell Resources

PRINCIPAL INVESTIGATOR: Patrick Paddison

CONTRACTING ORGANIZATION: Fred Hutchinson Cancer Research Center
Seattle, WA 98109

REPORT DATE: November 2014

TYPE OF REPORT: FINAL

PREPARED FOR: U.S. Army Medical Research and Materiel Command
Fort Detrick, Maryland 21702-5012

DISTRIBUTION STATEMENT: Approved for Public Release;
Distribution Unlimited

The views, opinions and/or findings contained in this report are those of the author(s) and should not be construed as an official Department of the Army position, policy or decision unless so designated by other documentation.

REPORT DOCUMENTATION PAGE

Form Approved
OMB No. 0704-0188

1. REPORT DATE	2. REPORT TYPE	3. DATES COVERED
November 2014	Final	1Sep2011 - 31Aug2014

4. TITLE AND SUBTITLE

Pediatric Glioblastoma Therapies Based on Patient-Derived Stem Cell Resources

5a. CONTRACT NUMBER
W81XWH-11-1-0756

5b. GRANT NUMBER

5c. PROGRAM ELEMENT NUMBER

6. AUTHOR(S)

Patrick Paddison

E-Mail: paddison@fredhutch.org

5d. PROJECT NUMBER

5e. TASK NUMBER

5f. WORK UNIT NUMBER

7. PERFORMING ORGANIZATION NAME(S) AND ADDRESS(ES)

Fred Hutchinson Cancer Research Center

1100 Fairview Ave N, J6-300

Seattle, WA 98109-4433

8. PERFORMING ORGANIZATION REPORT

9. SPONSORING / MONITORING AGENCY NAME(S) AND ADDRESS(ES)

U.S. Army Medical Research and Materiel Command
Fort Detrick, Maryland 21702-5012

10. SPONSOR/MONITOR'S ACRONYM(S)

11. SPONSOR/MONITOR'S REPORT NUMBER(S)

12. DISTRIBUTION / AVAILABILITY STATEMENT

Approved for Public Release; Distribution Unlimited

13. SUPPLEMENTARY NOTES

14. ABSTRACT

Gliomas comprise ~60% of cases among pediatric brain tumors. To date, there are few resources available to study and manipulate pediatric brain tumor cells, to evaluate whether pediatric tumor will have fundamental different responses to the new therapeutic regimes. Since glioma stem cell lines have been successfully isolated from adults, in this proposal we aim to isolate and characterize GSC populations from pediatric patients. In the past two years we have successfully derived and cultured eight patient-derived pediatric glioma stem cell lines. In the past year we have continued molecular and phenotypic characterization of these lines. This characterization included analysis of gene expression and patient-specific gene mutations, and also proof-of-concept shRNA screens. In addition we have begun to identify candidate therapeutic targets using the pediatric GBM isolates. So far, this effort has led to two promising candidate molecules for precision pediatric brain tumor therapeutics.

15. SUBJECT TERMS

Glioblastoma multiforme, glioma stem cell, brain tumor-initiating cell, pediatric brain tumor, RNAi, functional genetics

16. SECURITY CLASSIFICATION OF:			17. LIMITATION OF ABSTRACT	18. NUMBER OF PAGES	19a. NAME OF RESPONSIBLE PERSON
a. REPORT	b. ABSTRACT	c. THIS PAGE			USAMRMC
U	U	U	UU	76	19b. TELEPHONE NUMBER *(include area code)*

Table of Contents

Pediatric Glioblastoma therapies based on patient-derived stem cell resources – Final Report
Award Number: W81XWH-11-1-0756
PI: Patrick Paddison, PhD

INTRODUCTION

Glioblastoma multiforme (GBM) is the most aggressive and common form of brain cancer in adults, and is among the deadliest cancers with a median survival period of 12-14 months. GBM tumors appear to be hierarchically organized suggestive of a cancer stem cell origin. Consistent with this notion, tumor-initiating, glioma stem cells (GCS) have recently been isolated that retain the development potential and specific genetic alterations found in the patient's tumor. When used to generate tumors in the cortex of mice, these cells give rise to patient-specific molecular signatures and histological features.

Gliomas comprise ~60% of cases among pediatric brain tumors. To date, there are few resources available to study and manipulate pediatric brain tumor cells, to evaluate whether pediatric tumors will have fundamental different responses to the new therapeutic regimes. Since glioma stem cell lines have been successfully isolated from adults, in this proposal we aimed to isolate GSC population from pediatric patients. Collaborating with Dr. Xiao-Nan Li at Texas Children's Hospital, Dr. Paddison's group had access to ten orthotopic mouse lines harboring tumors derived from ten different pediatric glioma cases. In these orthotopic xenograft models, patient tumor samples were injected directly into the cortex of recipient NOD-SCID mice, where upon the patient tumor regrew with similar molecular and pathological characteristics observed in the tumor of origin. In this grant, we derived and characterized pediatric GSC lines and assessed whether they diverge from adult GSCs with respect to genes and networks required for proliferation and survival.

BODY

In this proposal, Dr. Paddison takes a step towards defining new therapeutic strategies for pediatric glioma by applying adult GSC isolation and culture techniques to derive pediatric glioma stem cells and then assessing whether pediatric isolates diverge from adult GBM patients with respect to genes and networks required for proliferation and survival.

Study Design: Pediatric GSC lines will be isolated from ten pediatric patient tumors. All ten lines will be characterized for stem cell properties, including expression of progenitor makers, capacity for multi-lineage differentiation, and tumor formation. Finally, lines will be examined for requirement of 6 genes essential to adult GSCs and, more broadly, for pathways required for proliferation and/or survival using a shRNA shot-gun screening approach.

Specific Aim 1: To isolate pediatric glioma stem cell populations in defined monolayer growth culture conditions.

Task 1: Isolation of pediatric GSC lines. Animal subjects (FHCRC): 30 NOD/SCID mice.

1a. Shipment of 10 mice from Texas children's hospital, FHCRC quarantine, and regulatory review (months 1-4).

1b. Passage of tumors to new recipient NOD/SCID mice and plating of tumor-derived cells material (months 1-6).

1d. Passaging of tumor isolates in GSC culture conditions (months 3-9).

1e. Freeze down of early passage and further expansion of GSC lines (months 4-12).

In aim 1, we proposed to isolate pediatric glioma stem cell lines from existing orthotopic mouse lines harboring tumors derived from different pediatric glioma cases. Adult GSC lines retain patient-specific molecular signatures and karyotype when isolated and cultured in monolayers on laminin coated plastic in the serum-free culture media supplemented with EGF and FGF-2 (6, 7). While multiple adult GSC lines have been successfully isolated (6, 7), there are currently no pediatric GSC lines available for comparison studies. The isolation of pediatric lines will allow identification of pediatric-specific glioma networks and vulnerabilities, which may be absent or altered in adult tumors.

We report that each of the PDX-pediatric brain tumor models listed in Table 1 successfully used for isolate tumor sphere cultures in GSC expansion media (N2B27 neural basal media (Stemcell Technologies) supplemented with EGF and FGF-2 (20ng/mL each)(7)). Since ability to generate tumor spheres during in vitro culture correlates with tumor initiating cell activity (8, 9), this suggests that we have successfully isolated and cultured tumor initiating cells from each tumor. Importantly, we have been successful at passaging, expanding and freezing tumor sphere cultures, achieving a key goal and milestone for aim 1. However, we found that only two lines GSC-1406 and GSC-1502 were suitable for experimentation as monolayer cultures (Table 1) due to slow growth after monolayer conversion or failure of neurosphere-to-monolayer conversion. As a result, in Aims 2 and 3 we focused studies on GSC-1406 and GSC-1502 cells. However, we will continue to use the other isolates for follow up biological studies in the future. GSC-1502 cells have appeared in multiple manuscripts focused on identifying novel drug targets since their isolation for this grant – one of which has been published (10) and three others are in submission.

Table 1 shows the summary of progress of Task 1 from **Tasks 1a-d**, revealing which pediatric tumor models could be isolated as monolayer culture and which were further characterized in Aims 2 and 3. Importantly, **Task 1e** was also completed for all isolates, albeit we had to freeze down some isolates after expansion in "sphere" culture rather than monolayer culture, since we were unsuccessful in converting them. However, the end goal of creating a pediatric brain tumor resource was achieved for this Aim.

Specific Aim 2: To perform molecular and phenotypic characterization of pediatric glioma stem cell isolates.

Task 2: Characterization of pediatric GSC lines.

2a. Growth rate/doubling time (months 10-15).

2b. Tumor sphere formation assays (months 10-15).

2c. Detection of expression of neural progenitor and lineage markers (months 13-15).

2d. Gene expression profiles (months 14-18).

2e. CNV analysis (months 14-18).

2f. Tumor formation assays (months 19-24).

In aim 2, we proposed to perform molecular and phenotypic characterization of pediatric isolates from Aim 1 to determine whether they: (1) harbor glioma stem cell characteristics; (2) fall into one or more adult GBM subclasses; and (3) are capable of initiating tumors (outlined in the Tasks above).

We have made significant progress for this aim. We were successful at completing all tasks listed above for GSC-1406 and GSC-1502 cells and partly successful for other isolates listed in Table 1. Both of these isolates grow robustly in monolayer culture with doubling times <60hrs (**Task 2a**) and as tumor spheres (**Task 2b**). We further were able to create a method for developmentally subtyping these isolates (**Tasks 2c and 2d**).

We classified pediatric GSC isolates according to the scheme proposed for adult GBMs (11, 12) based on an 840 gene list predictive of Proneural, Neural, Classical and Mesenchymal subtypes (Figure 2). In order to classify GSC isolates by signatures produced by The Cancer Genome Atlas (i.e., classical, mesenchymal, neural, and proneural) (11, 13), we developed the following procedure. We first performed RNA-seq on GSC cultures (n=3) using an Illumina HiSeq 2000 according to the manufacturer's instructions (FHCRC Genomics Shared Resource). RNA-Seq reads are then aligned to the GRCh37/hg19 assembly using Tophat (14) and counted for gene associations against the UCSC genes database with HTSeq, a python package for analysis of high-throughput sequencing data (15). The R language of statistical computing is then used for further analysis (16). All data is combined and normalized using a trimmed mean of M-values (TMM) method from the R package, edgeR (17-19). Normalized counts are then log transformed, and the means across all the cell lines were used to calculate relative gene expression levels. The GSC line data is then clustered using a Manhattan distance complete-linkage method to establish leaflets. Previously 173 glioma cell lines were subtyped using the expression of 840 signature genes (11). Our samples are clustered using 790 of these genes. The associations of our cell lines to those in publication are determined by minimum Manhattan distance to expression centroids produced by ClaNC. If a gene is expressed consistently in a particular subtype by absolute distance, then that is counted as a 1 and the number of associated genes in each category is summed. As a validation, the four subtypes are clearly distinguished when the method is applied to the 173 glioma lines described previously (11). The results demonstrate that GSC-1406 is consistent with a "proneural" GBM and GSC-1502 "mesenchymal" GBM (Figure 1). Importantly, these subtypes account for over half of all GBM, suggesting that these isolates should prove to be important glioma models.
We further completed **Task 2e**, which was to examine genomic regions with gains and losses in GSC isolates for GSC-1406 and GSC-1502 isolates (Figure 2). The detection of copy number variations (CNVs) was carried out via Control-FREEC v7.2 (20, 21). The software package was downloaded from http://bioinfo-out.curie.fr/projects/freec/. The paired-end alignment files of the tumor sample and its control, either CB660 or VM, were used as the input. R scripts provide by the software were used to add the significance to the predicted CNVs and the visualization of the results.

In addition, we also performed exome-sequencing on GSC-1502, which revealed that this isolate has mutations characteristic of mesenchymal glioma, including *NF1* and *TP53*, among others. Importantly, we were able to confirm that all original isolates of pediatric brain tumors (Table 1), robustly form tumors when serially engrafted into immunodeficient recipient mice (**Task 2f**).

In addition, we assessed pediatric isolates in terms of their ability to form tube-like endothelial structures in vitro, which may be important for tumor-microenvironment interactions and represent a novel tumor-specific lineage (22, 23). The 1406 but not the 1502 isolate shows ability to differentiate and form tube-

like structures in endothelial tube formation assays. We've also started access degree of expression of endothelial cell markers such as CD105, which may correlate with tumor aggressiveness in adult GBMs. In year 2, we extended this analysis to include differentiation conditions that promote GBM-derived pericytes (2) that interact with endothelial cells and may be a key feature of GBM differentiation programs. Through a collaboration with Dr. Shideng Bao (Cleveland Clinic) we have begun to assess the ability of the pediatric glioma cell lines to convert into pericytes using Dr. Bao's fluorescent reporter systems (2) and have confirmed expression of pericyte-specific genes in pediatric glioma stem cell lines. These results suggest that similar to adult brain tumors pediatric ones have the ability to form pericytes (Figure 3).

Specific Aim 3: To determine whether adult and pediatric GSCs share common proliferation and survival networks.

Task 3: Characterization of pediatric GSC lines.

3a. Examining lentiviral transduction and shRNA knockdown in GSC lines (months 22-24).

3b. Short and long-term outgrowth assays for gene knockdowns essential to adult GSCs (months 25-29).

3c. RNAi barcode screens for two pediatric GSC lines (months 30-33).

3d. Data analysis and manuscript submission (months 35-36).

In aim 3, we proposed to examine RNAi hits that have been validated as essential for adult GSC proliferation or survival in pediatric GSC isolates. In addition, we further proposed to perform preliminary shRNA “shot gun” screens to be performed on two pediatric GSC lines to obtain functional genetic “finger prints” to compare to adult GSCs screen results. We were able to make significant progress on each task associated with this Aim.

Our studies primarily focused on the GSC-1502 pediatric isolate for proof of concept experiments. This included examination of RNAi and CRISPR-Cas9 mediated gene inhibition for a variety of gene targets, including BUB1B, ZNF131, and PKMYT1 (Figures 4-6) (**Task 3a**). As a result, these results have been integrated into one published manuscript (10) and two that are currently in submission. Importantly, this analysis included both short and long-term assays for gene knockdowns essential to adult GSCs (**Task 3b**). Figure 4 shows that GSC-1502 cells are insensitive to BUB1B knockdown, a target which came out of an RNAi screen for adult GBM targets. We found that 1502 cells were resistant to BUB1B knockdown similar to untransformed cells. For GBM and genetically transformed cells sensitive to BUB1B knockdown, mechanistic studies revealed that these cells have altered sister KT dynamics during metaphase, which likely favor KT-MT instability. We investigated this possibility that 1052 cells lack this KT conformational change during mitosis. This was indeed the case. As shown in Figure 1, the interkinetochore distances (IKDs), or the maximum distance achieved between sister KTs when stable end-on MT attachment has occurred (24), in 1502 cells fell into the range of cells insensitive to BUB1B inhibition. This result emphasizes the notion that pediatric brain tumors may differ substantially from those observed in adults. We are currently analyzing other pediatric isolates for short and long IKDs and sensitivity to BUB1B knockdown. If successful, these studies may identify IKDs as a biomarker for pediatric GBM that predicts sensitivity to perturbation of KT-MT interactions.

At the same time, we performed a proof-of-concept shRNA screen in 1502 cells. This screen assayed ~20 genes that scored as being differentially required for adult GBM cell expansion, as compared to human NSCs. For this assay, a human mini-pooled lentiviral shRNA library of ~100 shRNAs was used to infect 1502 cells and one NSC cell (CB660) at a representation of ~1000 fold and a multiplicity of infection (MOI) of ~1 in parallel. Cells were then selected by puromycin to remove uninfected population and divided into 3 replicates. Cells were kept for three weeks, encompassing approximately 10 cell doublings. Afterwards, DNA was harvested and viral inserts containing unique target sequence were PCR amplified. The PCR product went through a column purification procedure to remove primers and genomic DNA and then subjected to Illumina high-throughput sequencing. In this analysis, shRNAs lost in the GSC population represent candidate gene targets that may be required by tumor outgrowth. The shRNA screen and Bar-code array analysis will be performed as previously described (3-5). This analysis revealed that multiple candidate genes differentially required in 1502 cells (Figure 5). In particular, we find PHF5A as a common target between adult GBM isolates and 1502. This is an exciting result, since we have shown that PHF5A knockdown in adult GSCs inhibits RNA splicing of an unusual class of exons with distinctive 3' splice sites, leading to defects in constitutive and alternative splicing in thousands of essential genes, including many required for cell cycle progression. This suggests that at least this pediatric GBM isolate has the same novel requirement for PHF5A to maintain proper exon recognition. This could suggest that classes of compounds affecting 3' splice recognition may be effective against pediatric brain tumors.

In addition, from the results published in (1) we have found a novel vulnerability in ZNF131 for pediatric isolate 1502 (Figure 6). According to motif analysis ZNF131 encodes a BTB/POZ zinc finger protein, and thus might act as a transcriptional regulator. We are currently pursuing the hypothesis that ZNF131 transcriptionally regulates HAUS5, a component of Augmin protein complex, and that this regulation is crucial for maintenance of 1502 and other tumor isolate viability. We present additional data regarding this hypothesis in Figures 6-8. These figures show that ZNF131 regulates steady-state levels of HAUS5, through maintenance of RNA Polymerase activity at the HAUS5 promoter. Importantly, the Augmin complex is known to facilitate centrosome-independent microtubule nucleation along the mitotic spindle by recruiting the gamma tubulin ring complex to microtubules. Our discovery suggests that the Augmin complex represents another key therapeutic target for at least a subset of pediatric gliomas. Future studies will aim to validate this result in other pediatric brain tumor isolates and to begin to develop small molecule inhibition strategies for HAUS5 and the Augmin complex.

For completion of **Task 3c**, we preformed two types of screens. First, we performed RNAi screens targeting 319 epigenetic factors in adult and pediatric glioma isolates and also in neural stem cells, a non-transformed candidate cell of origin control for gliomas (1, 10). Our results from this screen are presented in **Table 2**. The goal of this screen is to identify key epigenetic factors that are required for maintenance of expression of survival and self-renewal circuits in adult and pediatric glioma stem cells. However, this functional set has the added advantage of targeting genes with drugable enzymatic activities. As a result we are already collaborating with Cheryl Arrowsmith of the Structural Genomics Consortium at University of Toronto, who has helped develop cell permeable inhibitors of the Set1-like multiprotein histone methyltransferase complex, two members of which scored in our screen. We have also acquired an improved RNAi library, which will help facilitate this process (~10 shRNA per gene rather than only 3 for our current one).

The second type of screens we performed were genome-wide CRISPR-Cas9 gene knockout screens. Before attempting CRISPR-Cas9 screens, we first examined the efficacy of delivering a CRISPR-Cas9 targeting system by lentiviral (LV) transduction in human GSC and NSC isolates. Consistent with previous reports, an all-in-one LV-sgRNA:Cas9 platform system was highly effective at targeting reporter and endogenous genes in both GSCs and NSC isolates, including: randomly integrated copies of *EGFP* (>85%) (Figure 9), a non-essential endogenous gene, *TP53*, assayed by western blot, and an essential gene, *MCM2* (25), assayed by viability of *in vitro* expanded cells. In each case, we were able to observe profound reduction in target gene activity in GSCs and NSCs. Importantly, peak suppression occurred 10-14 days post-infection and non-targeting sgRNA controls had no effect on cell viability.

Given these successful demonstrations of gene editing, we next performed genome-wide screens using two adult GSC isolates, 0131, 0827, and 1502, and two control NSC lines, CB660 and U5 (Figure 10). The screens were performed using a "shot gun" approach where GSCs and NSCs were transduced with a LV pool containing a human CRISPR-Cas9 library composed of 64,751 unique sgRNAs targeting 18,080 genes (26) and out grown in self-renewal conditions for ~3 weeks. For the primary screen readout, we deep sequenced library sgRNAs from transduced cell populations before and after outgrowth, and then used edgeR (empirical analysis of digital gene expression in R) (17) to assess changes in individual sgRNA representation, which identified 99.8% of all sgRNAs in the pool. Based on normalized read counts, each screen replicate tightly clustered at Day 0 and displayed cell type-specific differences after expansion. EdgeR analysis revealed thousands of significantly scoring sgRNAs for each screen, representing both candidate essential and growth limiting genes

To validate screen results, we performed parallel screens with the a retest sgRNA pool both *in vitro* in GSCs and NSCs and *in vivo* in brain tumors derived from GSCs. These approaches again used sgRNA-seq of a day 0 population versus populations after 3 weeks of outgrowth *in vitro* or post-tumor formation *in vivo* as the readout. These approaches yielded 17 genes (7 essential and 10 GSC-sensitive) that retested prominently both *in vitro* and *in vivo*. Both *in vitro* and *in vivo* retests yielded *PKMYT1* as the top GSC-lethal gene (Figure 11).

PKMYT1 (aka *Myt1*) encodes a dual specificity protein kinase homologous to *WEE1* that localizes to the endoplasmic reticulum-Golgi complex and, at least *in vitro,* can inhibit cyclin B-CDK1 activity, by phosphorylating CDK1's ATP binding domain at Thr14 and to a lesser extent Tyr15 (27, 28). In follow up studies we show that PKMYT1 acts redundantly with Wee1 to inhibit Cyclin B-CDK1 activity via CDK1-Tyr15 phosphorylation and prevent premature entry into mitosis in NSCs. However, in GSCs this redundancy is lost, likely as a result of oncogenic signaling, causing GBM-specific lethality. Our results suggest that PKMYT1 is a candidate drug target for both adult and pediatric gliomas.

KEY RESEARCH ACCOMPLISHMENTS

- Isolation and propagation of tumor initiating cells from eight pediatric brain tumor patients.
- Development of methodology for classification of GBM tumors from RNA-seq data
- Preliminary mutation scan for two GBM tumor isolates
- Preliminary examination of GBM-lethal candidates from adult GBM isolate screens in a pediatric GBM isolate
- Isolation and propagation of tumor initiating cells in monolayer culture from 8 pediatric glioma patients
- Development and use of methodology for classification of GBM tumors from RNA-seq data
- In depth mutation scan and RNA-seq comparisons for 1502 glioma isolate and development of genomics analysis pipeline

- Confirmation of GBM-lethal candidates from adult GBM isolate screens in a pediatric GBM isolate
- RNAi and CRISPR-Cas9 screens in 1502 GSC line for key epigenetic factors and gene in general required for pediatric glioma stem cell self-renewal

REPORTABLE OUTCOMES

Manuscripts:

- Ding Y Ding Y, Hubert CG, Herman J, Corrin P, Toledo CM, Skutt-Kakaria K, Vazquez J, Basom R, Zhang B, Risler JK, Pollard SM, Nam DH, Delrow JJ, Zhu J, Lee J, DeLuca J, Olson JM, **Paddison PJ**. Cancer-specific requirement for BUB1B/BUBR1 in human brain tumor isolates and genetically transformed cells**. Cancer Discov**. 3(2):198-211, 2013. PMID: 23154965; PMCID: PMC3632446.

- Hubert CG, Bradley RK, Ding Y, Toledo CM, Herman J, Skutt-Kakaria K, Girard EJ, Davison J, Berndt J, Corrin P, Hardcastle J, Basom R, Delrow JJ, Webb T, Pollard SM, Lee J, Olson JM, **Paddison PJ**. Genome-wide RNAi screens in human brain tumor isolates reveal a novel viability requirement for PHF5A. **Genes and Dev.** 27(9):1032-45, 2013. PMID: 23651857. PMCID: PMC3656321.

- Toledo CM, Herman J, Olsen JB, Ding Y, Corrin P, Girad E, Olson JM, Emili A, DeLuca J, and **Paddison PJ.** BuGZ is required for Bub3 stability, Bub1 kinetochore function, and chromosome alignment. **Dev. Cell** 28(3):282-94, 2014. PMID: 24462187; PMCID: PMC3995079.

- Herman J, Toledo CM, Olson JM, DeLuca J, and **Paddison PJ.** Molecular Pathways: Regulation and Targeting of Kinetochore-Microtubule Attachment in Cancer. **Clin Cancer Res.** 2014 Aug 7. pii: clincanres.0645.2014. PMID: 25104085

Abstracts: None

Presentations:

- PEW Scholar Meeting, Vieques, Puerto Rico, 2013
- RNAi Research & Therapeutics Conference, San Francisco, CA, 2013
- Institute for Stem Cell and Regenerative Medicine, University of Washington, Seattle, WA, 2013
- Institute for Systems Biology, Seattle WA, 2014
- Society of NeuroOncology's CNS Anticancer Drug Discovery and Development Meeting, Miami 2014**.**

Licenses applied for and/or issued:

- Compositions and methods for treating cancer. Hubert C, Paddison P, Olson J, Bradley R. Application No. 61/712,725

Degrees obtained that are supported by this award:

- Chris Hubert, PhD

Development of cell lines, tissue or serum repositories:

- Isolation and propagation of tumor initiating cells from eight pediatric brain tumor patients

Infomatics such as databases and animal models, etc.:

- Development of methodology for classification of GBM tumors from RNA-seq data and exome sequencing and shRNA screening.

Funding applied for based on work supported by this award:

- Pardee Foundation and 3 NIH R01s.
- Principal Investigator, “Uncovering cancer-specific molecular requirements for Glioblastoma multiforme,” Listwin Family Foundation
- Principal Investigator, “Evolution of cancer specific molecular requirements for Glioblastoma multiforme,” NCI / NIH R21 CA170722-01 2012 - 2014
- Investigator, "Identification of Small Molecule Inhibitors of PHF5A for Glioblastoma," R01 CA193841-01

Employment or research opportunities applied for and/or received based on experience/training supported by this award: none during this reporting period:

- Yu Ding, Investigator II, Novartis Institutes for Biomedical Research, China, (January 2015)
- Chris Hubert, Postdoctoral Fellow, Rich Lab, Lerner Research Institute, Cleveland Clinic, (September 2013)

CONCLUSION: This proposal has succeeded in accomplishing the following: the isolation of glioma stem cells from high and low grade pediatric gliomas; the development of glioma stem cell-driven cancer models; and the identification of novel candidate therapeutic targets for pediatric glioma. Thus, these studies have led to tangible progress for pediatric glioma by creating in vitro resources, where few exist, and have begun to specifically address the question of whether aggressive pediatric brain tumors have similar vulnerabilities to adults. The integration of functional genetic data from our functional genetic screens in defined populations of glioma-initiating cells will act as a valuable comparison data set for genomic data sets arising for pediatric glioma (e.g., TCGA-style profiling). Finally, in collaboration with Dr. Jim Olson's group (FHCRC) we have already begun creating a team of researchers solely focused on translating these results to both adult and pediatric brain tumors.

Personnel funded by this award:

Patrick J Paddison, PhD, PI
James M. Olson, MD, PhD, Mentor
Yu Ding, PhD, Postdoctoral Fellow
Phillip Corrin, Research Technician

REFERENCES

1. Hubert CG, Bradley RK, Ding Y, Toledo CM, Herman J, Skutt-Kakaria K, Girard EJ, Davison J, Berndt J, Corrin P, Hardcastle J, Basom R, Delrow JJ, Webb T, Pollard SM, Lee J, Olson JM, Paddison PJ. Genome-wide RNAi screens in human brain tumor isolates reveal a novel viability requirement for PHF5A. Genes Dev. 2013;27(9):1032-45. Epub 2013/05/09. doi: 10.1101/gad.212548.112. PubMed PMID: 23651857; PMCID: 3656321.
2. Cheng L, Huang Z, Zhou W, Wu Q, Donnola S, Liu JK, Fang X, Sloan AE, Mao Y, Lathia JD, Min W, McLendon RE, Rich JN, Bao S. Glioblastoma stem cells generate vascular pericytes to support vessel function and tumor growth. Cell. 2013;153(1):139-52. doi: 10.1016/j.cell.2013.02.021. PubMed PMID: 23540695; PMCID: 3638263.
3. Paddison PJ, Silva JM, Conklin DS, Schlabach M, Li M, Aruleba S, Balija V, O'Shaughnessy A, Gnoj L, Scobie K, Chang K, Westbrook T, Cleary M, Sachidanandam R, McCombie WR, Elledge SJ, Hannon GJ. A resource for large-scale RNA-interference-based screens in mammals. Nature. 2004;428(6981):427-31. doi: 10.1038/nature02370. PubMed PMID: 15042091.
4. Silva JM, Li MZ, Chang K, Ge W, Golding MC, Rickles RJ, Siolas D, Hu G, Paddison PJ, Schlabach MR, Sheth N, Bradshaw J, Burchard J, Kulkarni A, Cavet G, Sachidanandam R, McCombie WR, Cleary MA, Elledge SJ, Hannon GJ. Second-generation shRNA libraries covering the mouse and human genomes. Nat Genet. 2005;37(11):1281-8. doi: 10.1038/ng1650. PubMed PMID: 16200065.
5. Luo J, Emanuele MJ, Li D, Creighton CJ, Schlabach MR, Westbrook TF, Wong KK, Elledge SJ. A genome-wide RNAi screen identifies multiple synthetic lethal interactions with the Ras oncogene. Cell. 2009;137(5):835-48. Epub 2009/06/06. doi: S0092-8674(09)00529-7 [pii] 10.1016/j.cell.2009.05.006. PubMed PMID: 19490893; PMCID: 2768667.
6. Lee J, Kotliarova S, Kotliarov Y, Li A, Su Q, Donin NM, Pastorino S, Purow BW, Christopher N, Zhang W, Park JK, Fine HA. Tumor stem cells derived from glioblastomas cultured in bFGF and EGF more closely mirror the phenotype and genotype of primary tumors than do serum-cultured cell lines. Cancer Cell. 2006;9(5):391-403. Epub 2006/05/16. doi: 10.1016/j.ccr.2006.03.030. PubMed PMID: 16697959.
7. Pollard SM, Yoshikawa K, Clarke ID, Danovi D, Stricker S, Russell R, Bayani J, Head R, Lee M, Bernstein M, Squire JA, Smith A, Dirks P. Glioma stem cell lines expanded in adherent culture have tumor-specific phenotypes and are suitable for chemical and genetic screens. Cell Stem Cell. 2009;4(6):568-80. Epub 2009/06/06. doi: 10.1016/j.stem.2009.03.014. PubMed PMID: 19497285.
8. Singh SK, Hawkins C, Clarke ID, Squire JA, Bayani J, Hide T, Henkelman RM, Cusimano MD, Dirks PB. Identification of human brain tumour initiating cells. Nature. 2004;432(7015):396-401. Epub 2004/11/19. doi: nature03128 [pii]10.1038/nature03128. PubMed PMID: 15549107.
9. Galli R, Binda E, Orfanelli U, Cipelletti B, Gritti A, De Vitis S, Fiocco R, Foroni C, Dimeco F, Vescovi A. Isolation and characterization of tumorigenic, stem-like neural precursors from human glioblastoma. Cancer Res. 2004;64(19):7011-21. Epub 2004/10/07. doi: 64/19/7011 [pii]10.1158/0008-5472.CAN-04-1364. PubMed PMID: 15466194.
10. Ding Y, Hubert CG, Herman J, Corrin P, Toledo CM, Skutt-Kakaria K, Vazquez J, Basom R, Zhang B, Risler JK, Pollard SM, Nam DH, Delrow JJ, Zhu J, Lee J, DeLuca J, Olson JM, Paddison PJ. Cancer-Specific requirement for BUB1B/BUBR1 in human brain tumor isolates and genetically transformed cells. Cancer discovery. 2013;3(2):198-211. Epub 2012/11/17. doi: 10.1158/2159-8290.CD-12-0353. PubMed PMID: 23154965; PMCID: 3632446.
11. Verhaak RG, Hoadley KA, Purdom E, Wang V, Qi Y, Wilkerson MD, Miller CR, Ding L, Golub T, Mesirov JP, Alexe G, Lawrence M, O'Kelly M, Tamayo P, Weir BA, Gabriel S, Winckler W, Gupta S, Jakkula L, Feiler HS, Hodgson JG, James CD, Sarkaria JN, Brennan C, Kahn A, Spellman PT, Wilson RK, Speed TP, Gray JW, Meyerson M, Getz G, Perou CM, Hayes DN. Integrated genomic analysis identifies clinically relevant subtypes of glioblastoma characterized

by abnormalities in PDGFRA, IDH1, EGFR, and NF1. Cancer Cell. 2010;17(1):98-110. Epub 2010/02/05. doi: S1535-6108(09)00432-2 [pii] 10.1016/j.ccr.2009.12.020. PubMed PMID: 20129251; PMCID: 2818769.

12. Lottaz C, Beier D, Meyer K, Kumar P, Hermann A, Schwarz J, Junker M, Oefner PJ, Bogdahn U, Wischhusen J, Spang R, Storch A, Beier CP. Transcriptional profiles of CD133+ and CD133- glioblastoma-derived cancer stem cell lines suggest different cells of origin. Cancer Res. 2010;70(5):2030-40. Epub 2010/02/11. doi: 0008-5472.CAN-09-1707 [pii] 10.1158/0008-5472.CAN-09-1707. PubMed PMID: 20145155.
13. Phillips HS, Kharbanda S, Chen R, Forrest WF, Soriano RH, Wu TD, Misra A, Nigro JM, Colman H, Soroceanu L, Williams PM, Modrusan Z, Feuerstein BG, Aldape K. Molecular subclasses of high-grade glioma predict prognosis, delineate a pattern of disease progression, and resemble stages in neurogenesis. Cancer Cell. 2006;9(3):157-73. Epub 2006/03/15. doi: S1535-6108(06)00056-0 [pii] 10.1016/j.ccr.2006.02.019. PubMed PMID: 16530701.
14. Trapnell C, Roberts A, Goff L, Pertea G, Kim D, Kelley DR, Pimentel H, Salzberg SL, Rinn JL, Pachter L. Differential gene and transcript expression analysis of RNA-seq experiments with TopHat and Cufflinks. Nat Protoc. 2012;7(3):562-78. Epub 2012/03/03. doi: 10.1038/nprot.2012.016 nprot.2012.016 [pii]. PubMed PMID: 22383036.
15. Anders S. HTSeq: Analysing high-throughput sequencing data with Python 2010. Available from: http://www-huber.embl.de/users/anders/HTSeq/.
16. R Development Core Team. R: A language and environment for statistical computing. Vienna: R Foundation for Statistical Computing; 2011.
17. Robinson MD, McCarthy DJ, Smyth GK. edgeR: a Bioconductor package for differential expression analysis of digital gene expression data. Bioinformatics. 2010;26(1):139-40. Epub 2009/11/17. doi: btp616 [pii] 10.1093/bioinformatics/btp616. PubMed PMID: 19910308; PMCID: 2796818.
18. Robinson MD, Smyth GK. Moderated statistical tests for assessing differences in tag abundance. Bioinformatics. 2007;23(21):2881-7. Epub 2007/09/21. doi: btm453 [pii] 10.1093/bioinformatics/btm453. PubMed PMID: 17881408.
19. Robinson MD, Smyth GK. Small-sample estimation of negative binomial dispersion, with applications to SAGE data. Biostatistics. 2008;9(2):321-32. Epub 2007/08/31. doi: kxm030 [pii] 10.1093/biostatistics/kxm030. PubMed PMID: 17728317.
20. Boeva V, Zinovyev A, Bleakley K, Vert JP, Janoueix-Lerosey I, Delattre O, Barillot E. Control-free calling of copy number alterations in deep-sequencing data using GC-content normalization. Bioinformatics. 2011;27(2):268-9. Epub 2010/11/18. doi: 10.1093/bioinformatics/btq635. PubMed PMID: 21081509; PMCID: 3018818.
21. Boeva V, Popova T, Bleakley K, Chiche P, Cappo J, Schleiermacher G, Janoueix-Lerosey I, Delattre O, Barillot E. Control-FREEC: a tool for assessing copy number and allelic content using next-generation sequencing data. Bioinformatics. 2012;28(3):423-5. Epub 2011/12/14. doi: 10.1093/bioinformatics/btr670. PubMed PMID: 22155870; PMCID: 3268243.
22. Wang R, Chadalavada K, Wilshire J, Kowalik U, Hovinga KE, Geber A, Fligelman B, Leversha M, Brennan C, Tabar V. Glioblastoma stem-like cells give rise to tumour endothelium. Nature. 2010;468(7325):829-33. Epub 2010/11/26. doi: nature09624 [pii]10.1038/nature09624. PubMed PMID: 21102433.
23. Ricci-Vitiani L, Pallini R, Biffoni M, Todaro M, Invernici G, Cenci T, Maira G, Parati EA, Stassi G, Larocca LM, De Maria R. Tumour vascularization via endothelial differentiation of glioblastoma stem-like cells. Nature. 2010;468(7325):824-8. Epub 2010/11/26. doi: nature09557 [pii] 10.1038/nature09557. PubMed PMID: 21102434.
24. DeLuca JG, Gall WE, Ciferri C, Cimini D, Musacchio A, Salmon ED. Kinetochore microtubule dynamics and attachment stability are regulated by Hec1. Cell. 2006;127(5):969-82. Epub 2006/11/30. doi: S0092-8674(06)01408-5 [pii]10.1016/j.cell.2006.09.047. PubMed PMID: 17129782.

25. O'Donnell M, Langston L, Stillman B. Principles and concepts of DNA replication in bacteria, archaea, and eukarya. Cold Spring Harbor perspectives in biology. 2013;5(7). Epub 2013/07/03. doi: 10.1101/cshperspect.a010108. PubMed PMID: 23818497; PMCID: 3685895.
26. Shalem O, Sanjana NE, Hartenian E, Shi X, Scott DA, Mikkelsen TS, Heckl D, Ebert BL, Root DE, Doench JG, Zhang F. Genome-scale CRISPR-Cas9 knockout screening in human cells. Science. 2014;343(6166):84-7. doi: 10.1126/science.1247005. PubMed PMID: 24336571.
27. Booher RN, Holman PS, Fattaey A. Human Myt1 is a cell cycle-regulated kinase that inhibits Cdc2 but not Cdk2 activity. J Biol Chem. 1997;272(35):22300-6. Epub 1997/08/29. PubMed PMID: 9268380.
28. Liu F, Stanton JJ, Wu Z, Piwnica-Worms H. The human Myt1 kinase preferentially phosphorylates Cdc2 on threonine 14 and localizes to the endoplasmic reticulum and Golgi complex. Mol Cell Biol. 1997;17(2):571-83. Epub 1997/02/01. PubMed PMID: 9001210; PMCID: 231782.

SUPPORTING DATA

Table 1: Pediatric Brain Tumor Models Used for Aims 1-3

Pediatric Model	Patient	Sex	Neurosphere	Monolayer	RNA-seq	Mutation	CNV	shRNA screen[1]	CRISPR-Cas9 screen[2]
IC-1128GBM-VI	8 y 7 mo	Male	Y	N					
IC-1406GBM-V	5 y	Female	Y	Y	Y	Y	Y		
IC-1502GBM-I	4 y 8 mo	Female	Y	Y	Y	Y	Y	Y	Y
IC-1621GBM-IV	6 y	Male	Y	nd					
IC-2305GBM	9 y	Male	Y	Y*					
IC-3704GBM-III	12 y	Male	Y	Y					
IC-3752GBM-rIV	5 y	Female	Y	nd					
IC-A46GBM-r V	16 y 11 mo	Female	Y	nd					

Y=Yes; N=No; nd=not determined

*doubling time >60hrs

[1]shRNA screen for epigenetic factors restricting stem cell self-renewal.

[2]Genome-wide CRISPR-Cas9 screen for genes lethal to pediatric stem-like cells

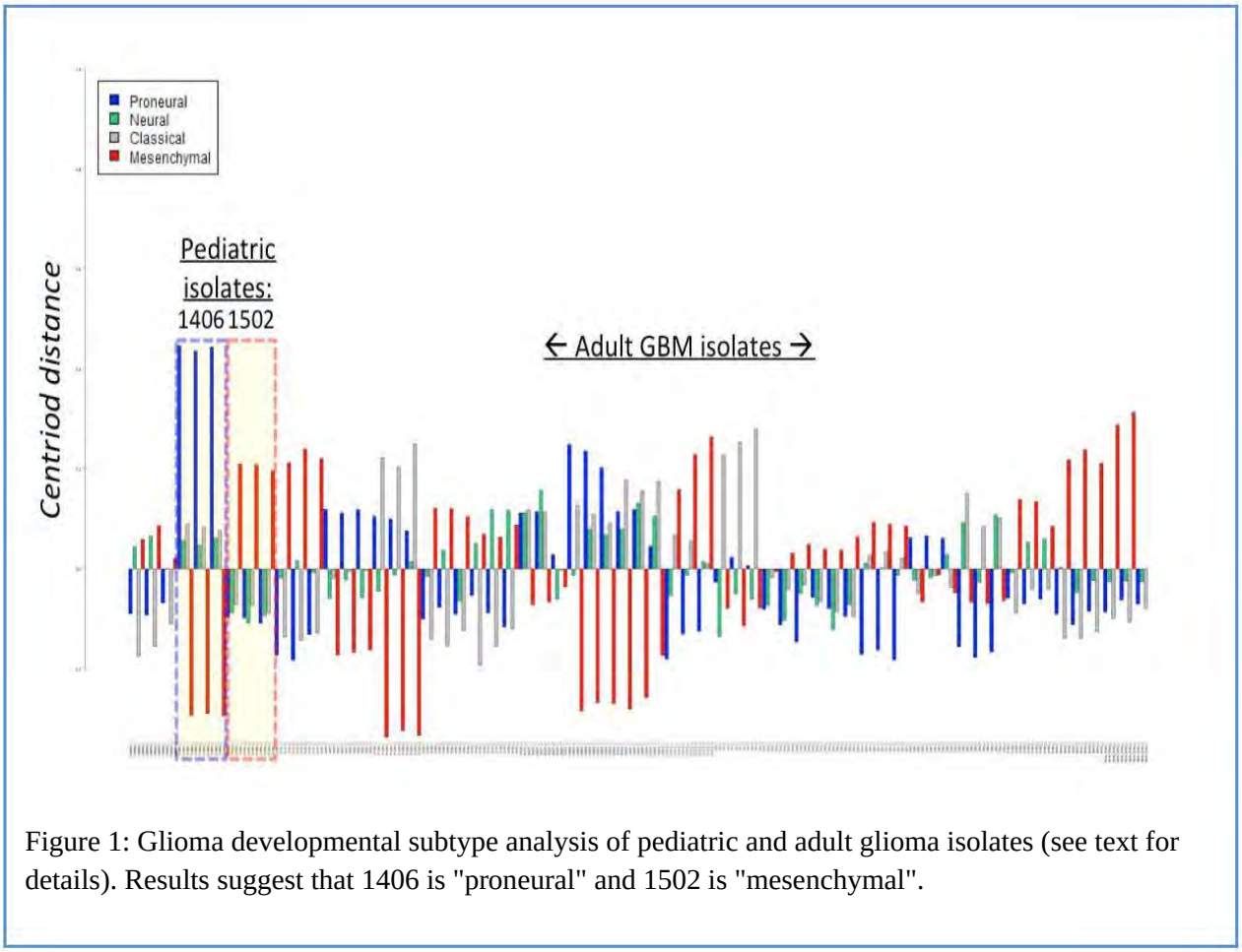

Figure 1: Glioma developmental subtype analysis of pediatric and adult glioma isolates (see text for details). Results suggest that 1406 is "proneural" and 1502 is "mesenchymal".

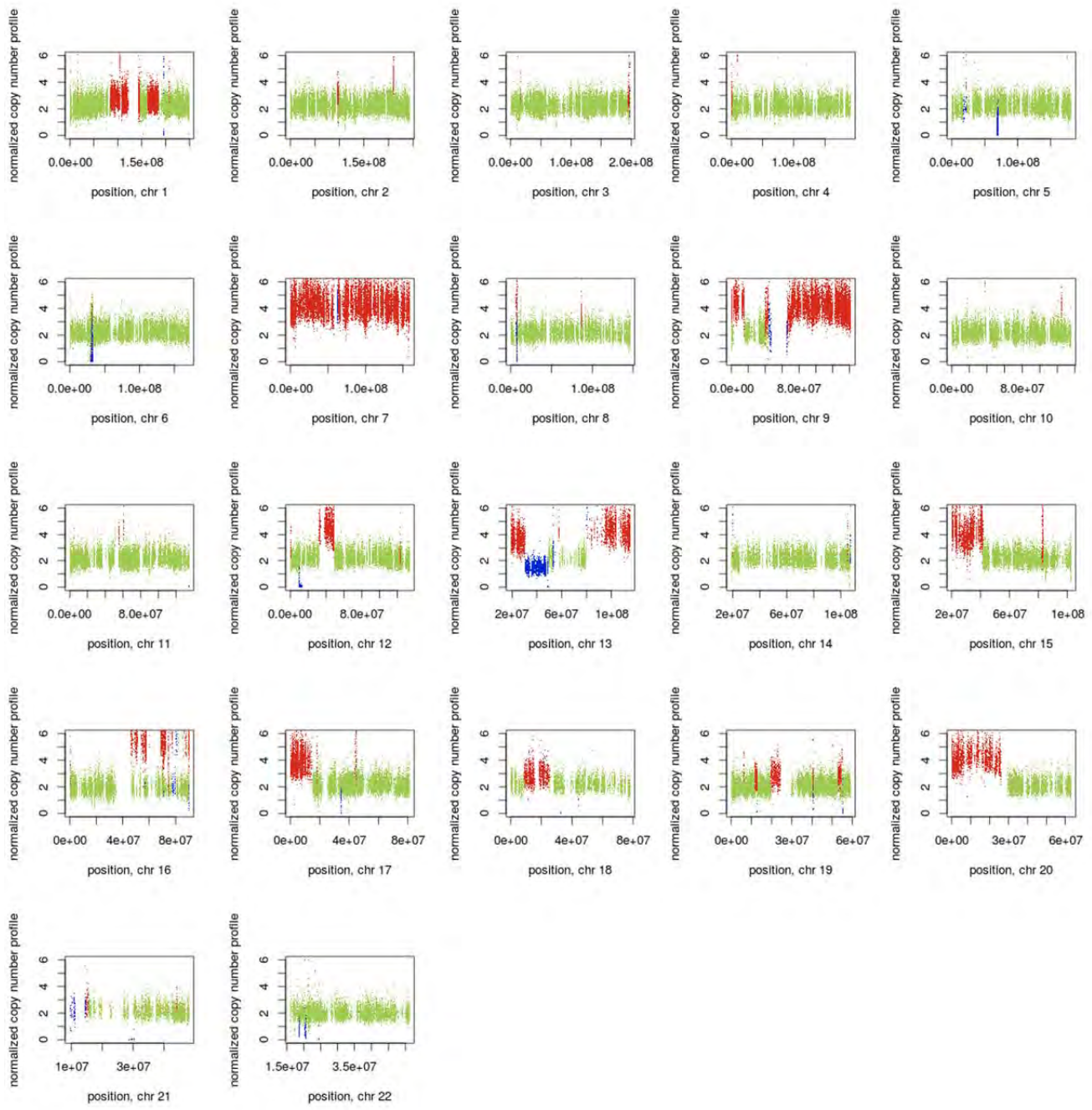

Figure 2: Copy number variation analysis for pediatric GSC isolate 1502. Each graph represents a single chromosome; red and blue dots indicate gains and losses respectively.

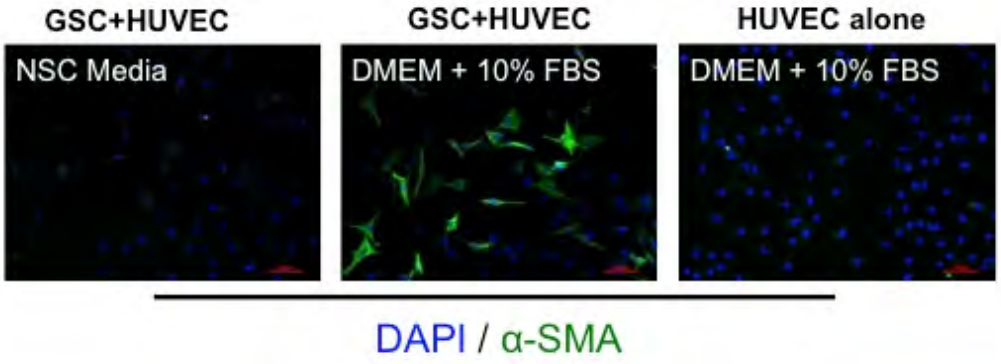

Figure 3. Pericyte differentiation of GSCs co-cultured with human endothelial cells (HUVECs). A recent study demonstrated that GSCs have the capacity to form functioning pericytes, a cell type important for blood vessel generation, structure, and function, as well as for maintenance of the blood-brain barrier maintenance (2) . A 1:1 admixture of GSCs and HUVECs (or HUVECs alone, right panel) was seeded onto laminin coated dishes followed by treatment normal NSC expansion media (left panel) or DMEM + 10% FBS for seven days. Afterwards, cells were fixed and stained for DNA content (DAPI) and alpha smooth muscle actin (α-SMA), a key marker of pericytes which is not expressed in self-renewing GSCs or normally dividing HUVECs. The middle panel shows dramatic induction of α-SMA in GSCs co-cultured with HUVECs. This will be used as a phenotype assay in Aim 2 for our panel of pediatric GSCs isolated from Aim 1.

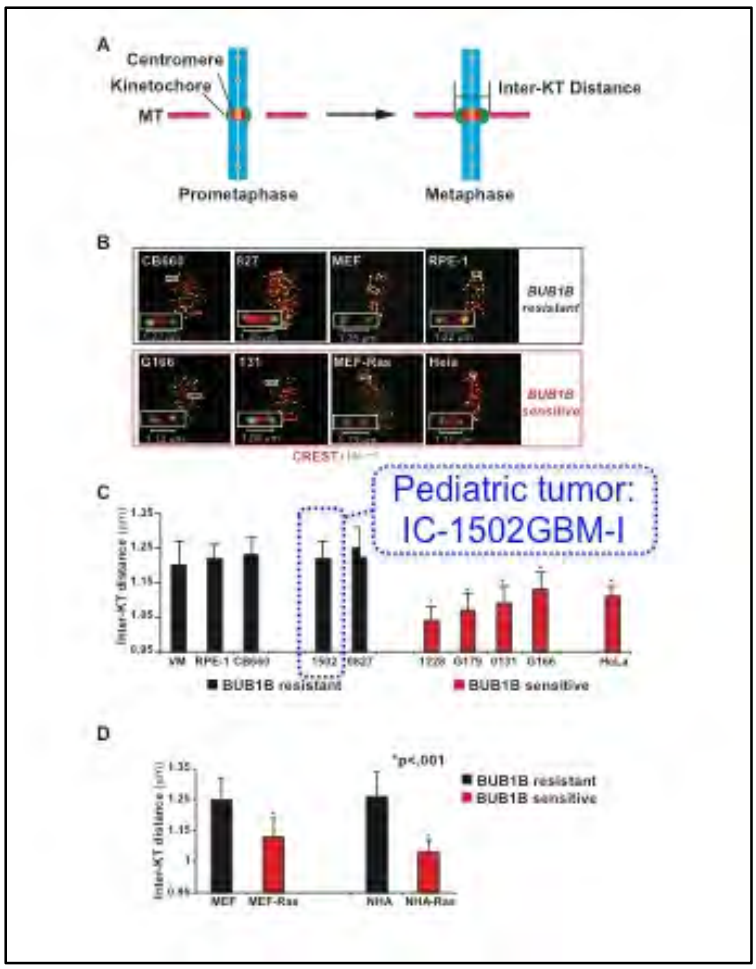

Figure 4. Measurement of inter-kinetochore distance (IKD) in BUB1B resistant and sensitive cells. To identify new candidate therapeutic targets for Glioblastoma multiforme (GBM), we combined functional genetics and GBM network modeling to identify kinases required for the growth of patient-derived GBM stem cells, but which are dispensable to proliferating human neural stem cells (NSCs). This approach yielded BUB1B/BUBR1, a critical mitotic spindle checkpoint player, as the top scoring GBM-lethal kinase. Mechanistic studies revealed that BUB1B's GLEBs domain activity is required to suppress lethal kinetochore-microtubule (KT-MT) attachment defects in GBM isolates and genetically transformed cells with altered sister KT dynamics, which likely favor KT-MT instability. We found that 1502 pediatric GSC cells were resistant to BUB1B knockdown. To determine whether KT dynamics were altered in resistant and sensitive cells, we measured inter-kinetochore distance (IKD): the maximum distance achieved between sister KTs when stable end-on MT attachment has occurred (24). Unlike most adult GBM cells, and also Ras-transformed cells, 1502 cells did not show the characteristic conformation change in KTs, i.e., short IKDs, which correlates with BUB1B sensitivity. This suggests that for pediatric brain tumor targeting BUB1B activity and/or KT-MT function would not be a good therapeutic strategy. More generally, it suggests that pediatric brain tumors may differ from adults in their genetic vulnerabilities. *Figure panels:* (A) Cartoon showing IKD measurement. (B) Measurement of IKDs in BTICs, NSCs, MEF, MEF-Ras, RPE and Hela cells using immunofluorescent staining of kinetochores. Constitutive associated centromere network (CCAN/CREST) proteins (red) and outer kinetochore protein, Hec1, (green) were visualized to identify kinetochore pairs. IKDs were measured between Hec1 centroids using Applied Precision Softworx software package. (C-D) Quantification of IKDs from (B). *denotes p<.001 by student's t-test.

Figure 5. Preliminary validation screen of adult GBM-lethal genes in Pediatric GBM isolates. Pediatric GSC 1502 cells and human neural stem cells were infected with lentiviral shRNA pool targeting ~20 adult GBM lethal gene candidates at a representation of ~1000 fold and a multiplicity of infection (MOI) of ~1 in parallel. Cells were then selected by puromycin to remove uninfected population and divided into 3 replicates. Cells were grown for three weeks. Afterwards, DNA was harvested and viral inserts containing unique target sequence were PCR amplified. The PCR product went through a column purification procedure to remove primers and genomic DNA and then subjected to Illumina high-throughput sequencing. In this analysis, shRNAs lost in the GSC population represent candidate gene targets that may be required by tumor outgrowth. The shRNA screen was performed as previously described (3-5).

The graph, below, shows the relative representation of various shRNAs at the end of the expansion period relative to human NSCs. These shRNAs also scored as specifically lethal to three adult GSC lines. Thus, these may represent common therapeutic targets between pediatric and adult brain cancers. If true, downstream efforts, e.g., drug development, would prioritize such targets, which would provide the best therapeutic windows and target both adult and pediatric cancers.

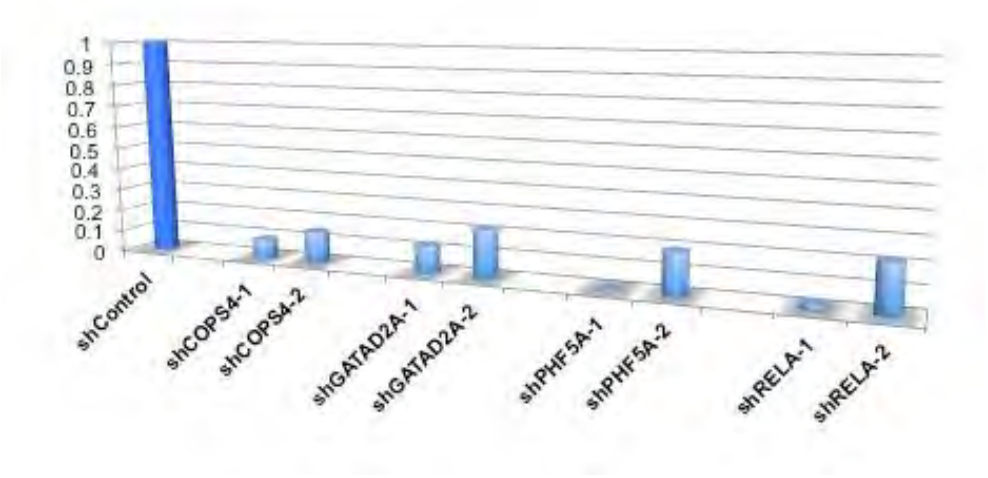

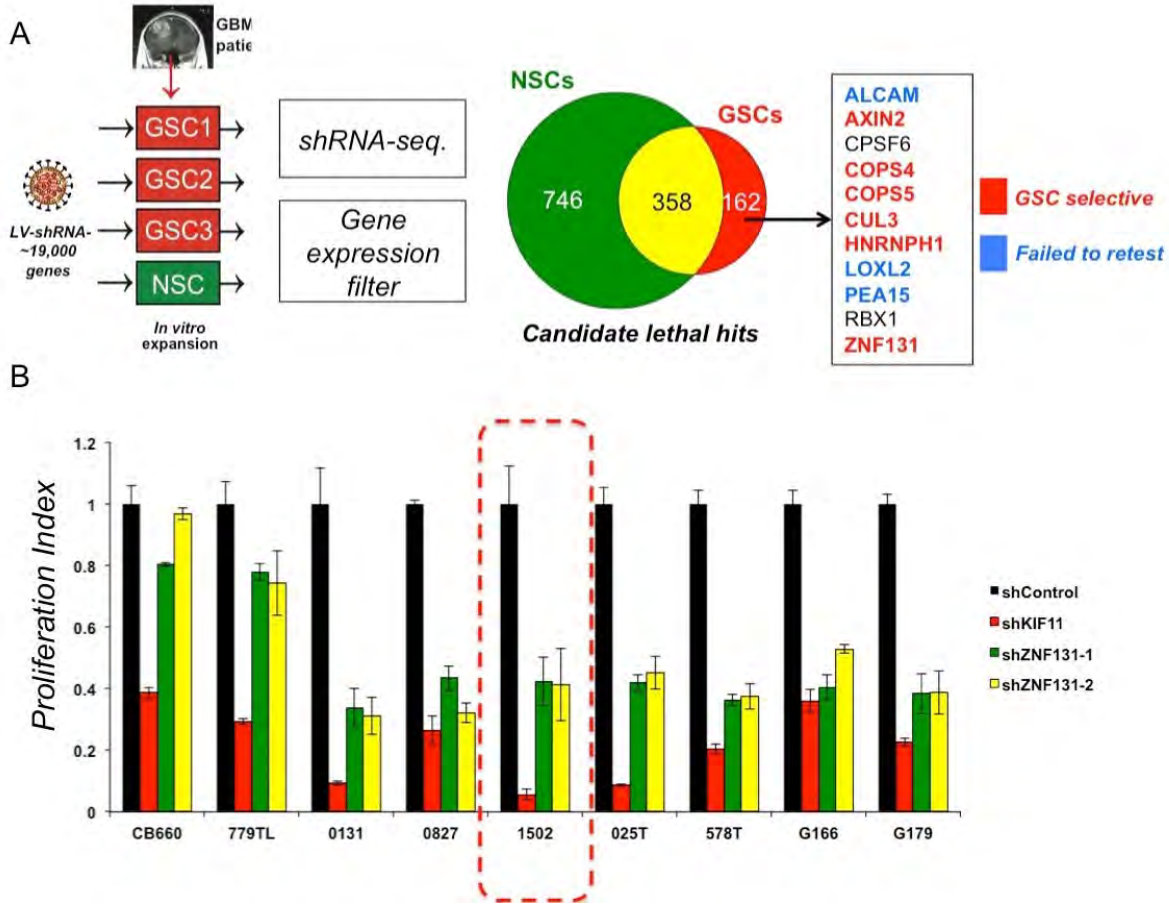

Figure 6. Genome-wide screens from (1) in patient-derived GBM stem-like cells and control neural stem cells revealed an novel candidate ZNF131 (**A**). ZNF131 was further validated in outgrowth assays for viability using both adult and pediatric GSCs (**B**). ZNF131 showed specific lethality in tumor isolates. Pediatric isolate 1502 is highlighted in red-hashes. Note that KIF11 knockdown acts as an essential gene control and the CB660 and 779TL are both human fetal neural stem cell isolates used as candidate cell-of-origin controls for GSCs.

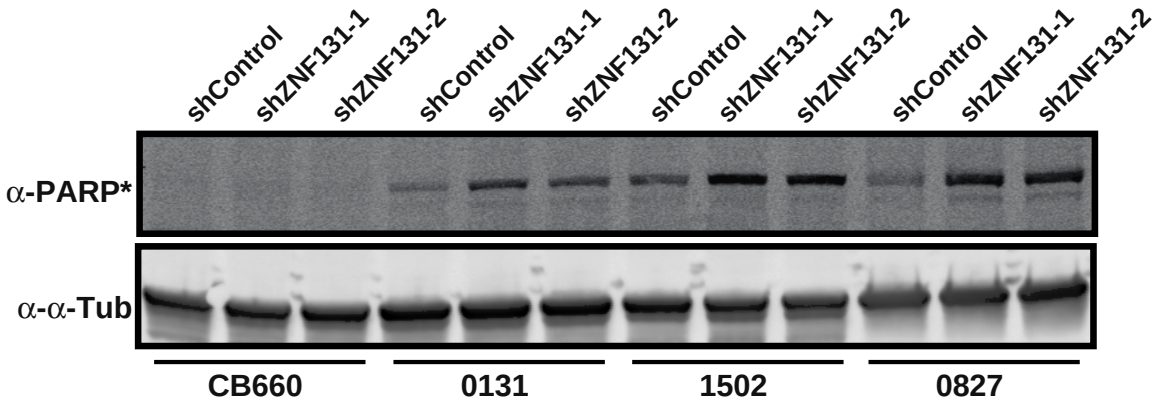

Figure 7. Knockdown of ZNF131 in patient-derived GBM stem-like cells but not control neural stem cells triggers apoptosis in multiple GSC isolates including pediatric glioma isolate 1502. Note that KIF11 knockdown acts as an essential gene control and the CB660 is human fetal neural stem cell isolates used as candidate cell-of-origin controls for GSCs.

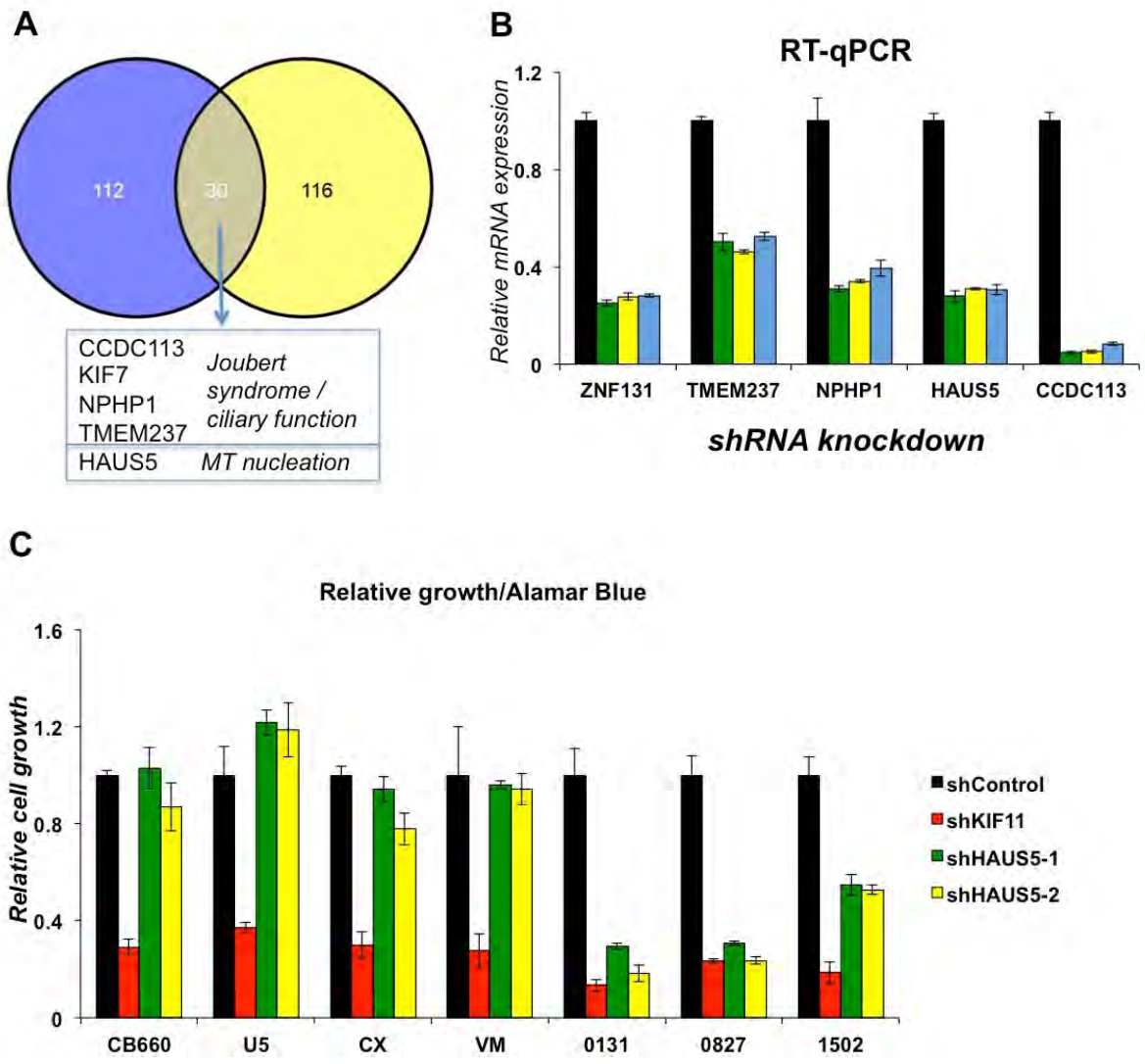

Figure 8. ZNF131 function relevant for GSC viability is regulation of steady state levels of HAUS5 mRNA. **A**) Gene expression analysis (using RNA-seq) after ZNF131 knockdown in two different GSC lines converged on only a few genes which showed lower mRNA levels after knockdown. This included genes involved in cilium function and HAUS5, an Augmin complex gene. **B**) Validation of genes called out in A by RT-qPCR after knockdown with shRNA control (black), shZNF131-1 (green), shZN131-2 (yellow), and shZNF131-3 (blue). **C**) Knockdown retests of genes shown in B) revealed that only HAUS5 is differentially required by GSCs (not shown). Shown are is examination of shHAUS5 in NSCs (CB660, U5, CX, VM) and GSCs (0131, 0827, 1502). Only GSCs shown loss of viability upon that only patient-derived GBM stem-like cells but not control neural stem cells triggers apoptosis in multiple GSC isolates including pediatric glioma isolate 1502. Note that KIF11 knockdown acts as an essential gene control and the CB660 is human fetal neural stem cell isolates used as candidate cell-of-origin controls for GSCs.

Table 2: Results from a shRNA screen comparing adult and pediatric GSCs to NSCs, attempting to identify new therapeutic targets from among 319 epigenetic regulatory factors**.**

Gene	Predicted Function	shRNAs scoring	Specificity?
ASH2L	Set1-like multiprotein histone methyltransferase complex	3	Adult/Pediatric
DPY30	Set1-like multiprotein histone methyltransferase complex	4	Pediatric
KAT5	Histone acetyltransferase	3	Pediatric
KAT8	Histone acetyltransferase H4K16ac	4	Pediatric
PARP2	Poly ADP-ribosyl transferase-like 2 protein	3	Pediatric
PBRM1	Protein polybromo-1	4	Pediatric
PRDM11	PR Domain-Containing Protein 11	4	Pediatric
SIN3B	Transcriptional repressor	4	Pediatric
SIRT7	NAD^+-dependent deacetylase	4	Adult/Pediatric
USP22	Deubiquitinating enzyme	4	Pediatric

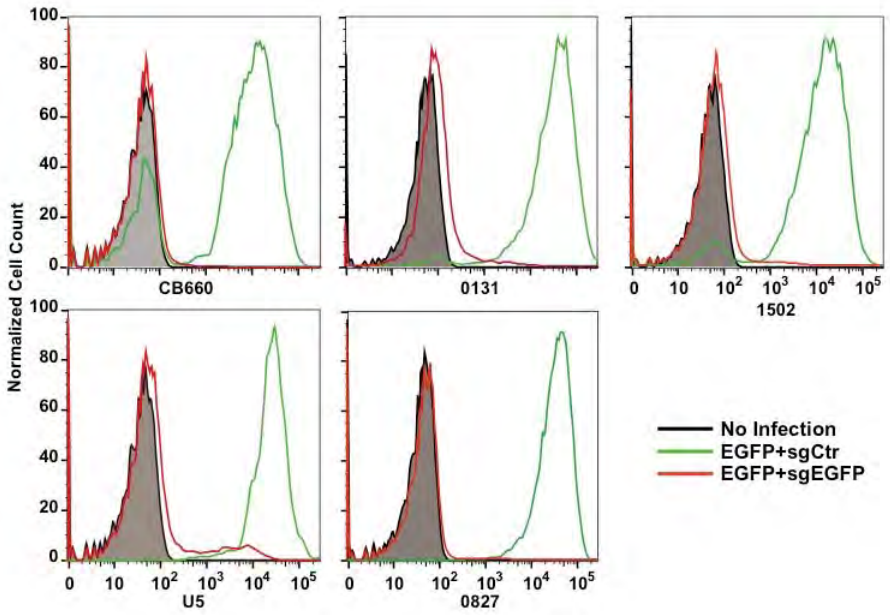

Figure 9. Validation of CRISPR-Cas9 gene editing strategies in adult and pediatric GSCs along with NSCs. sgEGFP:Cas9 was used to target stably expressed H2B-EGFP in GSCs and NSCs. Cells were first infectedwith LV-EGFP-H2B at MOI>2 and passaged for 1 week, and then infected with sgControl or sgEGFP at MOI<1, selected, outgrown for 14 days, and flow analyzed.

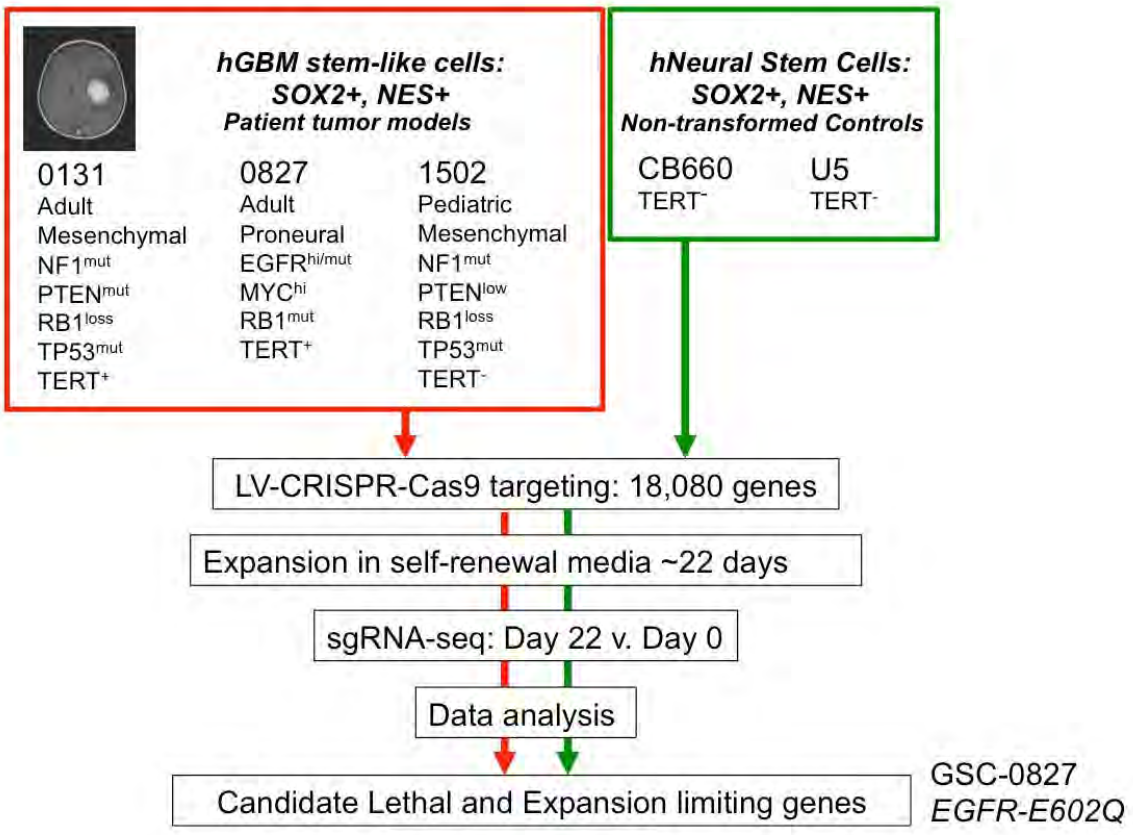

Figure 10. Overview of Genome-wide CRISPR-Cas9 KO screens in GSCs and NSCs**.**

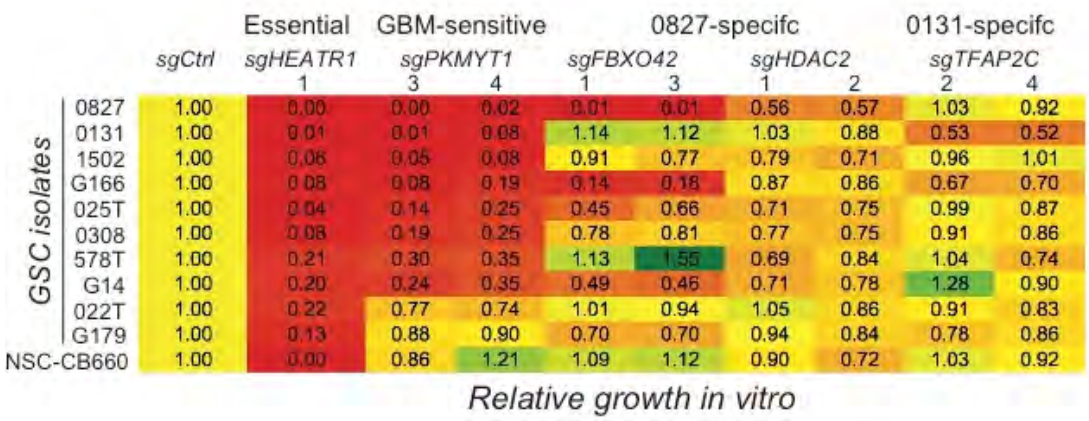

Figure 11. PKMYT1 is generally required for viability of adult and pediatric GSC isolates. To further evaluate retesting sgRNA screen hits, we next examined targeting of *PKMYT1, FBXO42, HDAC2, TFAP2C* and *HEATR1* in 10 different GSC isolates along with NSCs using *in vitro* viability assays and two control sgRNAs. The results revealed that *PKMYT1* was required for viability in 8 of these isolates, while *HDAC2* and *TFAP2C* requirement appeared more specific to GSC-0827 and GSC-0131 cells,respectively. Shown are the normalized *In vitro* viability assays retest results for individual sgRNAs in multiple GSC isolates for genes indicated. Samples were outgrown for 12 days following selection or cultured for 18 days following selection and counted with each split every 5-7 days to determine total cell number, and normalized to sgControl.

Published OnlineFirst November 15, 2012; DOI: 10.1158/2159-8290.CD-12-0353

RESEARCH ARTICLE

Cancer-Specific Requirement for BUB1B/BUBR1 in Human Brain Tumor Isolates and Genetically Transformed Cells

Yu Ding[1], Christopher G. Hubert[2], Jacob Herman[7], Philip Corrin[1], Chad M. Toledo[1], Kyobi Skutt-Kakaria[1,6], Julio Vazquez[3], Ryan Basom[4], Bin Zhang[5], Jennifer K. Risler[4], Steven M. Pollard[8], Do-Hyun Nam[9], Jeffery J. Delrow[4], Jun Zhu[3], Jeongwu Lee[10], Jennifer DeLuca[7], James M. Olson[2], and Patrick J. Paddison[1]

ABSTRACT

To identify new candidate therapeutic targets for glioblastoma multiforme, we combined functional genetics and glioblastoma network modeling to identify kinases required for the growth of patient-derived brain tumor–initiating cells (BTIC) but that are dispensable to proliferating human neural stem cells (NSC). This approach yielded BUB1B/BUBR1, a critical mitotic spindle checkpoint player, as the top-scoring glioblastoma lethal kinase. Knockdown of BUB1B inhibited expansion of BTIC isolates, both *in vitro* and *in vivo*, without affecting proliferation of NSCs or astrocytes. Mechanistic studies revealed that BUB1B's GLE2p-binding sequence (GLEBS) domain activity is required to suppress lethal kinetochore–microtubule (KT–MT) attachment defects in glioblastoma isolates and genetically transformed cells with altered sister KT dynamics, which likely favor KT–MT instability. These results indicate that glioblastoma tumors have an added requirement for BUB1B to suppress lethal consequences of altered KT function and further suggest that sister KT measurements may predict cancer-specific sensitivity to BUB1B inhibition and perhaps other mitotic targets that affect KT–MT stability.

SIGNIFICANCE: Currently, no effective therapies are available for glioblastoma, the most frequent and aggressive brain tumor. Our results suggest that targeting the GLEBS domain activity of BUB1B may provide a therapeutic window for glioblastoma, as the GLEBS domain is nonessential in untransformed cells. Moreover, the results further suggest that sister KT distances at metaphase may predict sensitivity to anticancer therapeutics targeting KT function. *Cancer Discov; 3(2); 198–211. ©2012 AACR.*

See related commentary by Venere et al., p. 141.

Authors' Affiliations: [1]Human Biology Division, [2]Clinical Research Division, [3]Scientific Imaging Shared Resource, and [4]Genomics Shared Resource, Fred Hutchinson Cancer Research Center; [5]Sage Bionetworks, Seattle; [6]The Evergreen State College, Olympia, Washington; [7]Department of Biochemistry and Molecular Biology, Colorado State University, Fort Collins, Colorado; [8]Cancer Institute, University College London, London, United Kingdom; [9]Institute for Refractory Cancer Research, Samsung Medical Center, Seoul, Korea; and [10]Stem Cell Biology and Regenerative Medicine, Lerner Research Institute, Cleveland Clinic, Cleveland, Ohio

Note: Supplementary data for this article are available at Cancer Discovery Online (http://cancerdiscovery.aacrjournals.org/).

Corresponding Author: Patrick J. Paddison, Fred Hutchinson Cancer Research Center, 1100 Fairview Avenue North, C3-168, Seattle, WA 98109. Phone: 206-667-4312; Fax: 206-667-4023; E-mail: paddison@fhcrc.org

doi: 10.1158/2159-8290.CD-12-0353

Published OnlineFirst November 15, 2012; DOI: 10.1158/2159-8290.CD-12-0353

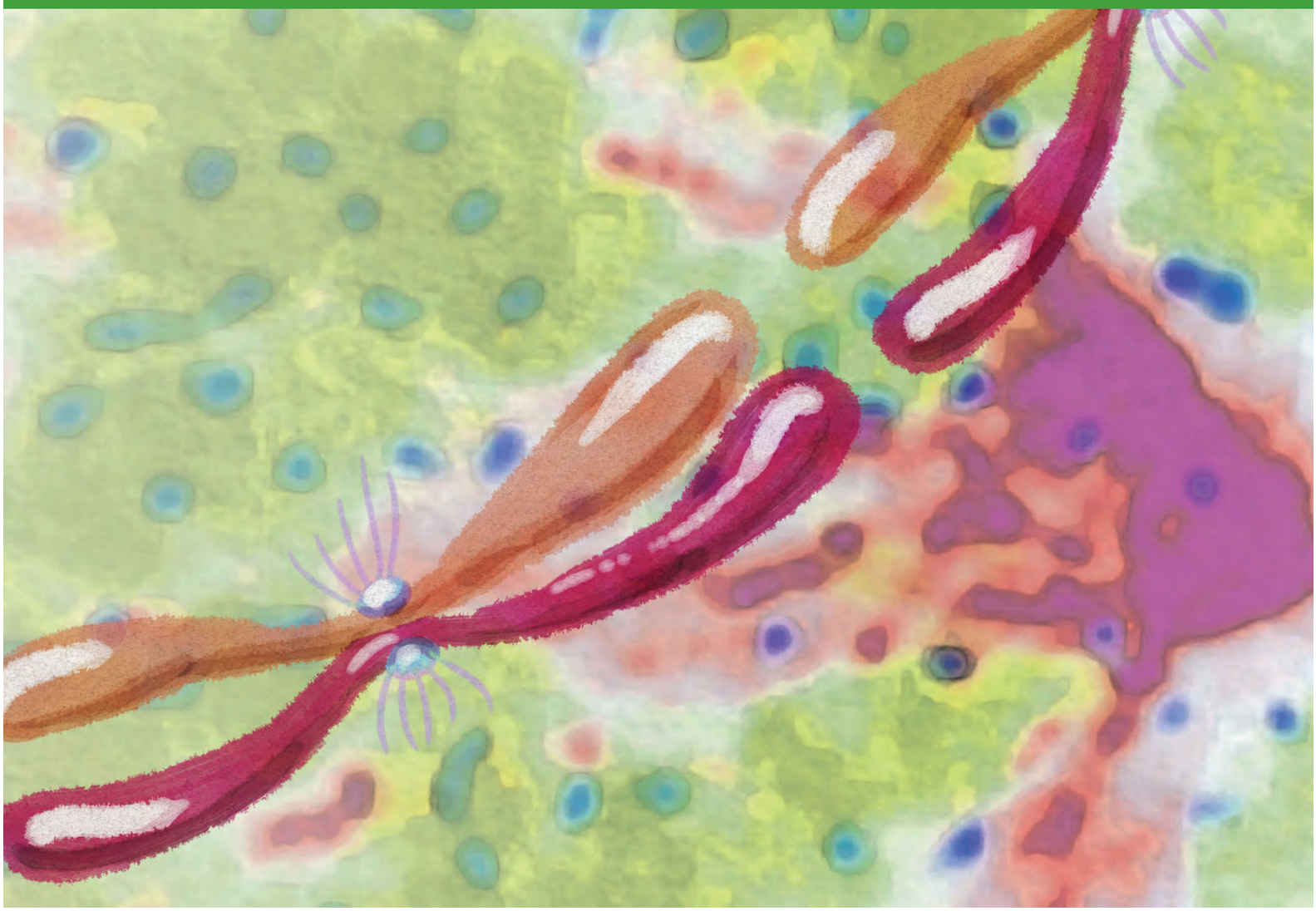

INTRODUCTION

Glioblastoma multiforme is the most aggressive and common form of brain cancer in adults (1). Currently, no effective therapies are available for glioblastoma. Even with standard of care treatments, such as surgery, radiation, and chemotherapy, approximately 90% of adult patients die within 2 years of diagnosis (2). Both adult and pediatric brain tumors seem to be hierarchically organized, suggestive of a cancer stem cell origin (3–6). Consistent with this notion, brain tumor-initiating cells (BTIC) have recently been isolated that retain the development potential and specific genetic alterations found in the patient's tumor (3, 4, 7, 8). When implanted into the cortex of rodents, BTICs give rise to glioblastoma-like tumors with patient-specific molecular signatures and histologic features (5–8). Expression of neural progenitor molecular networks may contribute to the aggressive behavior of glioblastoma tumors through enhancing self-renewal or developmental programs (9), DNA repair pathways (10), angiogenesis (11), and/or invasiveness (12). Given the likelihood of BTIC-driven maintenance and spread of glioblastoma, effective cell-based therapies will likely have to target the stem cell.

Recently, a new method for deriving and maintaining BTICs was developed in which adult BTICs can be isolated and grown in serum-free, defined monolayer culture (7, 8). By this method, BTICs can retain tumor-initiating potential and tumor-specific genetic and epigenetic signatures over extended outgrowth periods (13). Here, we sought to take advantage of this BTIC culture system to find evidence for the cancer-lethal hypothesis: that transformed cells, compared with "normal" cells, harbor novel molecular vulnerabilities as a direct consequence of cancer-causing genetic alterations (14). Although multiple studies have addressed the question of cancer lethality in serum-derived cell lines (15, 16), there remain lingering questions of applicability to human cancers, as serum-derived lines may not faithfully represent the primary cancer (7).

By combining the results of short hairpin RNA (shRNA) kinome screens in BTICs and neural stem cells (NSC) for genes required for progenitor expansion with a glioblastoma bionetwork created from patient molecular signatures, we identified BUB1B, a critical mitotic checkpoint kinase (17), as the top glioblastoma-specific hit. Our results

Published OnlineFirst November 15, 2012; DOI: 10.1158/2159-8290.CD-12-0353

suggest that glioblastoma tumors and genetically transformed cells have an added requirement for BUB1B to suppress lethal consequences of altered kinetochore (KT) function. Importantly, these studies show that nontransformed cells do not require BUB1B/BubR1 for chromosome alignment, nor do they require the GLE2p-binding sequence (GLEBS) domain to maintain the spindle assembly checkpoint. They further suggest that altered KT conformations, apparent in glioblastoma and genetically transformed cells, may predict cancer-specific sensitivity to BUB1B inhibition and perhaps other mitotic targets that affect KT–microtubule (KT–MT) stability.

RESULTS

An RNA Interference Kinome Screen for Genes Differentially Required for BTIC Expansion

To discover candidate therapeutic targets for glioblastoma, we conducted an shRNA screen targeting 713 human kinases to identify gene activities required for *in vitro* expansion of BTICs. To enrich for BTIC-specific hits, a parallel screen was conducted in human fetal NSC-CB660 cells (Fig. 1A; ref. 18). NSCs share molecular and phenotypic features with BTICs, including identical isolation and growth in serum-free conditions, similar doubling times, overlapping expression profiles, and similar developmental potential (18). However, they retain a normal karyotype and are not tumorigenic (18) and, thereby, represent ideal controls for BTICs.

This screening approach (see Methods for details) revealed approximately 48 candidate kinase targets with shRNAs underrepresented in BTICs relative to NSCs (Supplementary Table S1). To prioritize these hits, we examined whether hits could be parsed into distinct pathways and/or complexes using protein–protein interaction networks (19). By this analysis, most hits were connected in a single, large subnetwork, enriched for 248 gene ontology (GO) biologic processes (multiple testing adjusted $P < 0.01$), such as protein kinase cascade ($P = 5.57881e{-}085$) and protein amino acid phosphorylation ($P = 1.10068e{-}082$). This lack of specific biologic processes likely reflected the fact that these kinases are well studied and involved in many biologic processes and, thus, did not provide any useful information for prioritizing of candidate hits.

As an alternative strategy, we examined the occurrence of screen hits in a glioblastoma-specific regulatory network, constructed *de novo* from more than 421 glioblastoma samples from The Cancer Genome Atlas (TCGA; ref. 20) by integrating gene expression and DNA copy number variation data (refs. 21, 22; Supplementary data). By this analysis, 37 of 48 shRNA candidate hits appeared as nodes in the glioblastoma network. Examination of subnetworks in the glioblastoma network revealed 15 biologic processes significantly enriched (5 cell-cycle related and 9 general phosphorylation related), including the M-phase of mitotic cell cycle ($P = 1.64e{-}5$). The largest glioblastoma-specific subnetwork contained 4 screen hits, including *AURKB*, *BUB1B*, *MELK*, and PLK1 (Fig. 1B). On the basis of key driver node analysis (23), *BUB1B* scored as the top-ranked screen hit (Fig. 1C).

To control for glioblastoma network comparisons, we also examined screen hits in a normal brain network constructed from 160 nondementia human prefrontal cortex samples. Only 20 of 48 candidate hits appeared in the normal brain network and produced smaller subnetworks enriched for general phosphorylation-related GO biologic processes (data not shown). Although *BUB1B* appeared in this network, it was connected to only one gene and had no down nodes (Fig. 1B), and thus was not a key driver node.

BUB1B Is Differentially Required for BTIC Expansion

Retests of AURKB, BUB1B, MELK, and PLK1 revealed that BUB1B inhibition gave the largest differential effect on BTICs from multiple glioblastoma isolates, including common developmental subtypes (24), without observable toxicity in proliferating NSCs or astrocytes (Fig. 1A–D). In these studies, shRNA-expressing cells were subjected to short- and long-term outgrowth assays (Fig. 2D and Supplementary Fig. S1A and S1B). Knockdown of KIF11 was used as a positive control. KIF11 is a microtubule motor protein required for mitotic progression in proliferating mammalian cells (13). During short- and long-term outgrowth, shKIF11 blocked the growth of BTICs, NSCs, and astrocytes. Because shKIF11 inhibits only cycling cells entering mitosis, shKIF11-dependent growth inhibition indicates similar division rates for various cells used and shows they have comparable RNA interference (RNAi) pathway activity. However, BUB1B knockdown triggered significant growth inhibition only in BTIC lines (Fig. 2A and D). During longer term outgrowth, shBUB1B inhibited the growth of SSEA1$^+$ BTIC subpopulations, which are enriched for tumor-initiating cell activity (ref. 25 and Supplementary Fig. S1C and S1D). BUB1B knockdown was also deleterious to BTIC tumor sphere formation, which may reflect tumor-initiating cell activity (5, 6) in both BTICs and primary tumor samples (Fig. 2E). However, knockdown did not profoundly alter the expression of SSEA1 or other progenitor markers, including Sox2 and Nestin, or neural lineage markers, including GFAP and TUJ1 (data not shown).

In contrast, PLK1 knockdown had a partial effect, MELK knockdown had no effect, and inhibition of AURKB was equally toxic to BTICs and NSCs (Supplementary Fig. S2A–S2C). On the basis of these results, we further pursued BUB1B as a candidate BTIC-lethal gene.

BUB1B Is Overexpressed in Glioblastoma Isolates, and Its Checkpoint Activity Is Compromised by shBUB1B in Both BTICs and NSCs

BUB1B is a highly conserved BUB1-like kinase, BubR1, whose activity is essential for mitotic spindle checkpoint signaling (17). The mitotic spindle checkpoint monitors the attachment of kinetochores to the plus ends of spindle microtubules and prevents anaphase onset until chromosomes are aligned and kinetochores are under tension at the metaphase plate (17). Because of its role in maintaining chromosome stability, mitotic spindle checkpoint activity has been touted as a mechanism for tumor suppression (17, 26). In rare instances, partial loss-of-function mutations in checkpoint genes have been reported for certain cancers (26). However, many late-stage cancers, including glioma, exhibit high BUB1B expression (27, 28), suggestive of hyperactivity.

To begin to reconcile these observations with our results, we analyzed BUB1B expression patterns and activity in

Published OnlineFirst November 15, 2012; DOI: 10.1158/2159-8290.CD-12-0353

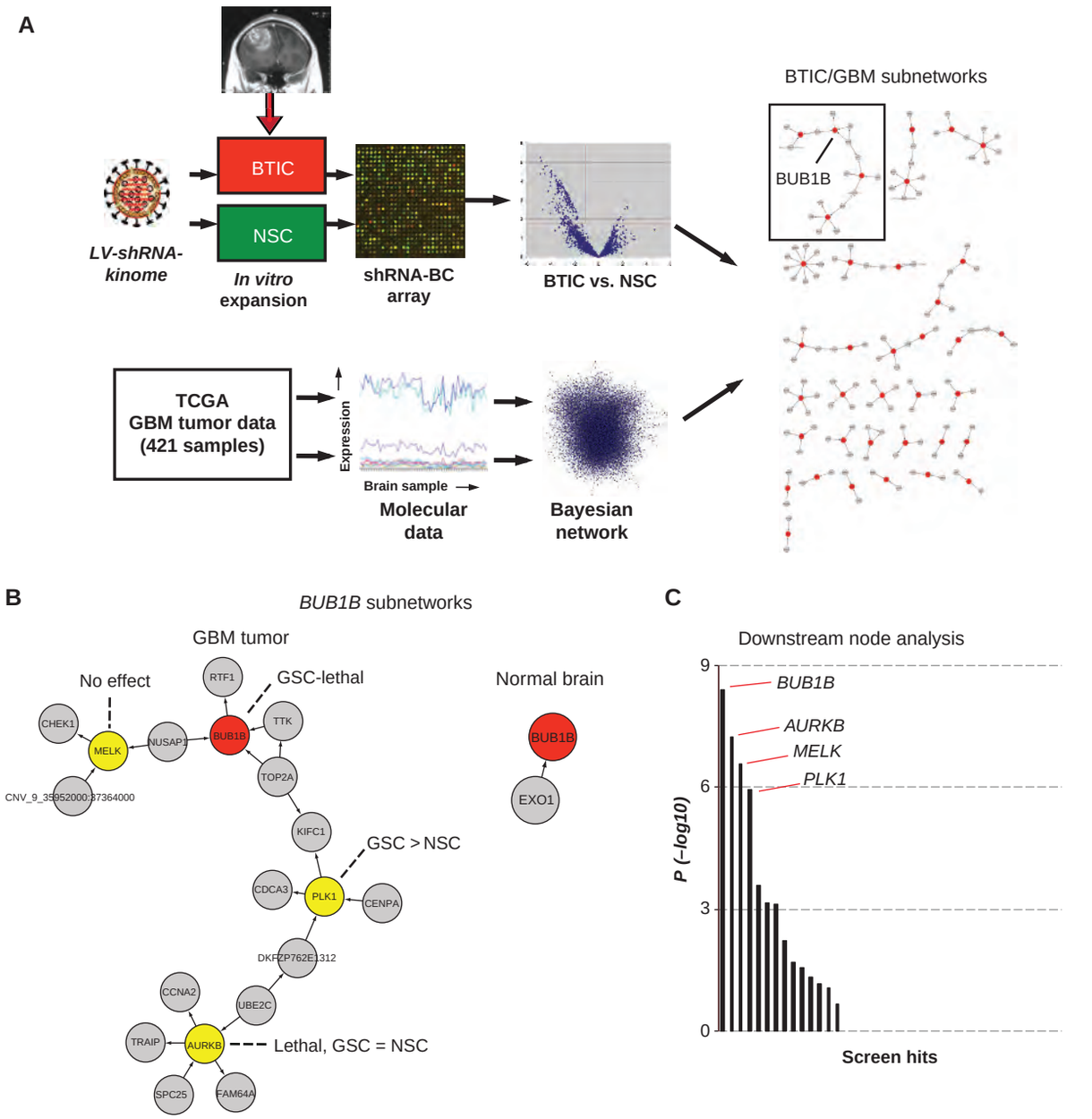

Figure 1. Integration of RNAi screens in patient-derived BTICs and glioblastoma (GBM) bionetworks. **A,** overview of shRNA screens, glioblastoma network generation, and results of seeding screen hits into the glioblastoma network (see Methods and Supplementary data for further details on glioblastoma network construction and screen comparisons). **B,** *BUB1B* subnetworks from glioblastoma tumors and also from normal brain networks. Also indicated are the node inhibition BTIC and NSC growth phenotypes. **C,** downstream node analysis, a metric that helps predict the relative importance of nodes (14, 23) of BTIC-specific screen hits that appear in the GBM Bayesian network. BC, barcode.

BTICs and NSCs. We observed that *BUB1B* and other spindle checkpoint genes were upregulated in BTIC isolates and also *RAS*-transformed astrocytes, as judged by mRNA and protein abundance (Supplementary Fig. S3A–S3C). Moreover, both BTICs and NSCs had normal mitotic spindle arrest responses after paclitaxel treatment, which were abrogated by BUB1B knockdown (Supplementary Fig. S4A–S4C). Thus, BUB1B knockdown achieves a similar level of suppression of BUB1B mRNA, protein, and activity in both BTICs and NSCs. The results suggest that BUB1B knockdown produces a hypomorphic state to which BTICs, but not NSCs or astrocytes, are sensitive. Later, we provide further evidence to support this conclusion, by addressing BUB1B's essential and nonessential functions in BTICs and in transformed and untransformed cells.

Shortened Interkinetochore Distances Are Indicative of Sensitivity to shBUB1B in BTICs and Genetically Transformed Cells

One possible explanation for BTIC's observed sensitivity to hypomorphic BUB1B activity is that KT–MT dynamics could be

Published OnlineFirst November 15, 2012; DOI: 10.1158/2159-8290.CD-12-0353

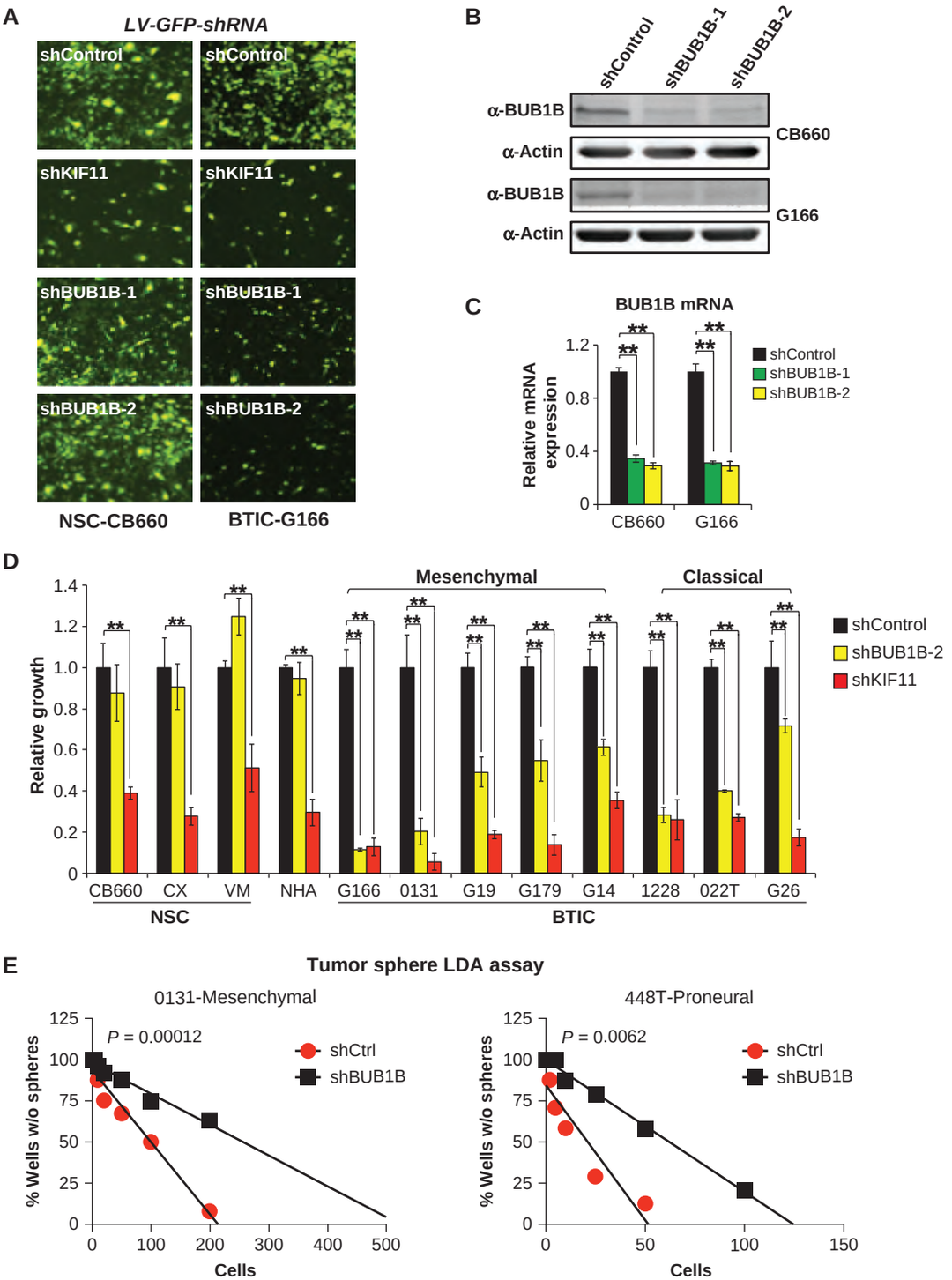

Figure 2. *BUB1B* is validated as a candidate glioblastoma-lethal gene *in vitro*. **A,** BTIC-specific effects of BUB1B knockdown, visualized using shRNA–green fluorescent protein (GFP$^+$) BTICs and NSCs 6 days after posttransduction with pGIPz-shRNA virus. Knockdown of KIF11/EG5, a microtubule motor protein critical for bipolar spindle formation during mitosis, was used as a positive control for both RNAi pathway activity and cell proliferation. **B** and **C,** examination of *BUB1B* knockdown by Western blot and quantitative real-time PCR (qRT-PCR) analysis in BTIC-G166 and NSC-CB660 cells. **D,** comparison of the effects of BUB1B knockdown on *in vitro* expansion of multiple BTIC and NSC lines and normal human astrocytes (NHA). **, Student *t* test; $P < 0.01$. See Methods for a description of how BTIC isolates were developmentally subtyped. **E,** limiting dilution assays (LDA) for *in vitro* tumor sphere formation. BTIC-0131 cells and also unpassaged primary glioblastoma tumor cells (448T) were transduced with indicated LV-GFP-shRNAs, diluted, and assayed for sphere formation after 14 days. Linear regression analysis was used to evaluate significance.

Published OnlineFirst November 15, 2012; DOI: 10.1158/2159-8290.CD-12-0353

altered to favor MT detachment. To properly segregate chromosomes during mitosis, stable attachments must occur between the "plus" end of mitotic spindle MTs and KTs, which are formed at the centromeres of each sister chromatid as cells enter mitosis (29). Early in mitosis, KT–MT attachments are unstable and dynamic, allowing chromosomes to be towed toward MT plus ends during congression and improperly attached chromosomes to be released and reattached to spindle MTs until they are bioriented and under tension (19, 29). The distance between KTs on sister chromatids can range from approximately 0.6 μm in prophase to more than 1 μm in metaphase, when sister KTs achieve stable MT attachment and are pulled toward opposing spindle poles (Fig. 3A; ref. 30). In the prevailing model, this KT movement prevents outer kinetochore proteins from being phosphorylated by Aurora B kinase, which promotes KT–MT detachment (e.g., for error correction) by physically removing them from centromere-embedded Aurora B activity (29).

To examine KT–MT dynamics, we first investigated the possibility that KT dynamics may be altered in glioblastoma cells. To this end, we measured interkinetochore distance (IKD), the maximum distance achieved between sister KTs when stable end-on MT attachment has occurred (31). We first measured IKDs for shBUB1B-insensitive NSCs (CB660) and 2 shBUB1B-sensitive BTIC isolates (G166 and 0131). The results were surprising. We found that IKDs were significantly shorter in both BTIC isolates (1.23 μm for CB660 vs. 1.13 μm for G166 and 1.09 μm for 0131; Fig. 3B and C). Thus, BTIC IKDs were shorter by 100 to 140 nm or 50 to 70 nm for each sister KT. This finding represents a significant change, as, for example, the outer kinetochore protein Hec1 moves approximately 40 nm toward the spindle pole as KTs come under tension (32, 33).

Next, we examined IKDs in 2 glioblastoma patient isolates, 0827 and 1502, which we had observed were completely insensitive to shBUB1B. These isolates were insensitive despite having similar knockdown efficiencies to shBUB1B-sensitive lines and among the fastest doubling times and tumor initiation rates (data not shown). Measuring IKDs in these cells revealed that they were indistinguishable from NSCs (1.23 μm), suggesting the possibility that IKDs may predict BUB1B sensitivity (Fig. 3B and C).

To further examine this possibility, we tested a hypothesis that shortened IKDs and added BUB1B requirement arise as a result of oncogenic transformation and, specifically, oncogenic signaling. It was recently shown that expression of activated *RAS* oncogene can lead to mitotic stress and induce chromosome instability in mammalian cells, through an as yet undefined mechanism (16). Thereby, we examined IKDs in $p53^{-/-}$ mouse embryo fibroblasts (MEF) with or without RasV12 expression. In $p53^{-/-}$ control MEFs, IKDs averaged 1.25 μm, similar to those of NSCs and 827 cells. Surprisingly, RasV12 expression converted long IKDs to short, averaging 1.13 μm, indistinguishable from those of G166 and 0131 cells (Fig. 3D). Moreover, RasV12 transformation also converted MEFs from being resistant to BUB1B inhibition to being profoundly sensitive, which was true for human astrocytes (Fig. 3D) as well (both experiments are presented below in Fig. 5 and Supplementary Fig. S8A–S8C). Importantly, all of the IKD measurements for BTICs, NSCs, and MEFs were scored blindly to avoid experimenter bias.

Because most BUB1B/BubR1 experimentation has been carried out in HeLa cells, which are derived from a cervical carcinoma (16), we next measured IKDs in these cells. As a control, we used immortalized retinal pigment epithelial (RPE-1) cells, which are untransformed. HeLa cells showed IKDs similar to other BUB1B-sensitive cells (1.11 μm), whereas RPE cells showed long IKDs, similar to those of insensitive cells (1.22 μm). In repeating the pattern above, BUB1B knockdown affected chromosome dynamics only in HeLa cells (detailed later).

These results suggest (i) that IKDs occur in discrete intervals: long (~1.24 μm) and short (~1.12 μm); (ii) that short IKDs predict sensitivity to BUB1B inhibition; and (iii) that RasV12 transformation is sufficient to induce short IKDs and sensitivity to BUB1B.

Glioblastoma Isolates with Short IKDs Require BUB1B to Suppress Severe KT–MT Attachment Defects

We next wished to determine whether BTICs with short IKDs have altered KT–MT dynamics that favor detachment. To this end, we used a metaphase chromosome alignment assay, in which KT–MT attachment defects are visualized as misaligned chromosomes during metaphase arrest induced by proteasome inhibition (34). By this assay, knockdown of BUB1B resulted in dramatic chromosome alignment defects only in BTICs with short IKDs but did not affect alignment in NSCs, 0827 cells (Fig. 4A and B; Supplementary Fig. S5A), or astrocytes (see later). The alignment defects in G166 cells were accompanied by profound loss of KT–MT attachment, as indicated by lack of colocalization of KTs with cold-resistant MTs (Supplementary Fig. S5B). Moreover, examination of phospho-Ser44-Hec1/Ndc80 at KTs revealed that after BUB1B knockdown, G166s retain Ser44 phosphorylation (ref. 35; Supplementary Fig. S5C). This phosphorylation is dependent upon centromere-embedded Aurora B kinase activity and has a KT–MT destabilizing effect (29). These results suggest that cells with short IKDs have KT–MT attachment defects, which BUB1B is required to suppress.

Consistent with this idea, G166 cells also displayed overt differences in chromosome dynamics during mitosis, with significantly more lagging chromosomes in anaphase than with NSCs (Fig. 4C). BUB1B knockdown dramatically exacerbated these defects (Fig. 4D). In control experiments in NSCs, shBUB1B did not affect lagging chromosome frequency or karyotype after extended outgrowth (Fig. 4C and Supplementary Fig. S5D), again suggesting that cells with long IKDs do not use BUB1B in the same way.

Genetic Dissection of the Added Requirement of BUB1B in RasV12-Expressing Fibroblasts and BTICs

BUB1B has multiple functional domains that have been implicated in mitotic checkpoint control, mitotic timing, and stable KT–MT attachment (17, 29). These include N- and C-terminal KEN box domains required for Cdc20 binding and anaphase-promoting complex (APC) inhibition (36–38); a C-terminal kinase domain involved in checkpoint control (39, 40); and a GLEBS-like motif necessary for KT localization during mitosis (refs. 39, 41; Fig. 5A). Although BUB1B is necessary for mammalian development (42), its essential function is contained solely within the N-terminal KEN box (36), which enables BUB1B/BubR1 to act as a pseudo-substrate inhibitor of APC/C^{Cdc20} during G_2 and preanaphase mitosis, preventing a precocious anaphase (36).

Published OnlineFirst November 15, 2012; DOI: 10.1158/2159-8290.CD-12-0353

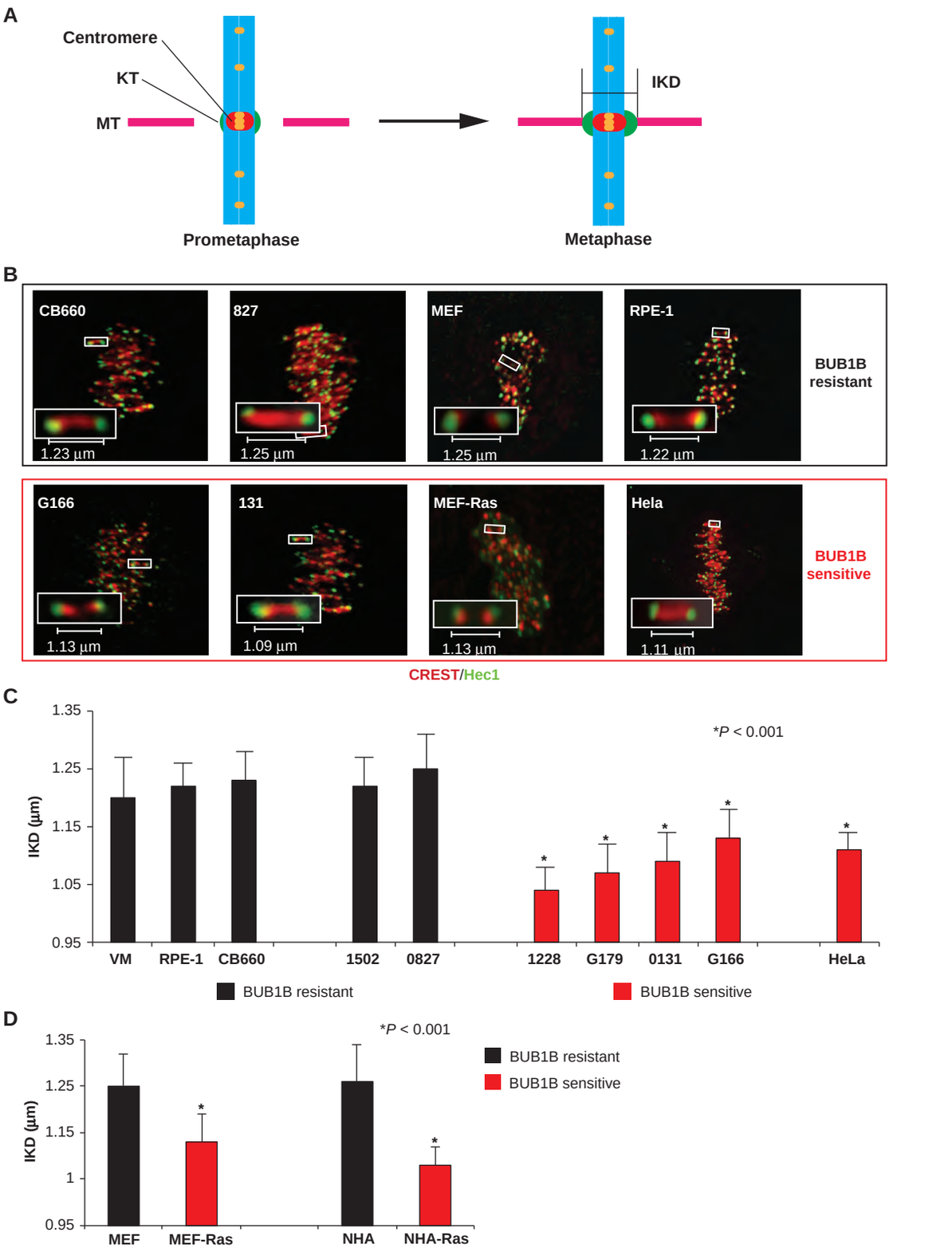

Figure 3. Measurement of IKD in BUB1B-resistant and -sensitive cells. **A,** diagram showing IKD measurement. **B,** measurement of IKDs in BTICs, NSCs, MEFs, MEF-Ras cells, RPE cells, and HeLa cells, using immunofluorescent staining of kinetochores. Constitutive centromere-associated network (CCAN/CREST) proteins (red) and outer kinetochore protein, Hec1 (green) were visualized to identify kinetochore pairs. IKDs were measured between Hec1 centroids, using Applied Precision softWoRx software package. **C** and **D,** quantification of IKDs from **B**. *, $P < 0.001$ by Student t test.

Published OnlineFirst November 15, 2012; DOI: 10.1158/2159-8290.CD-12-0353

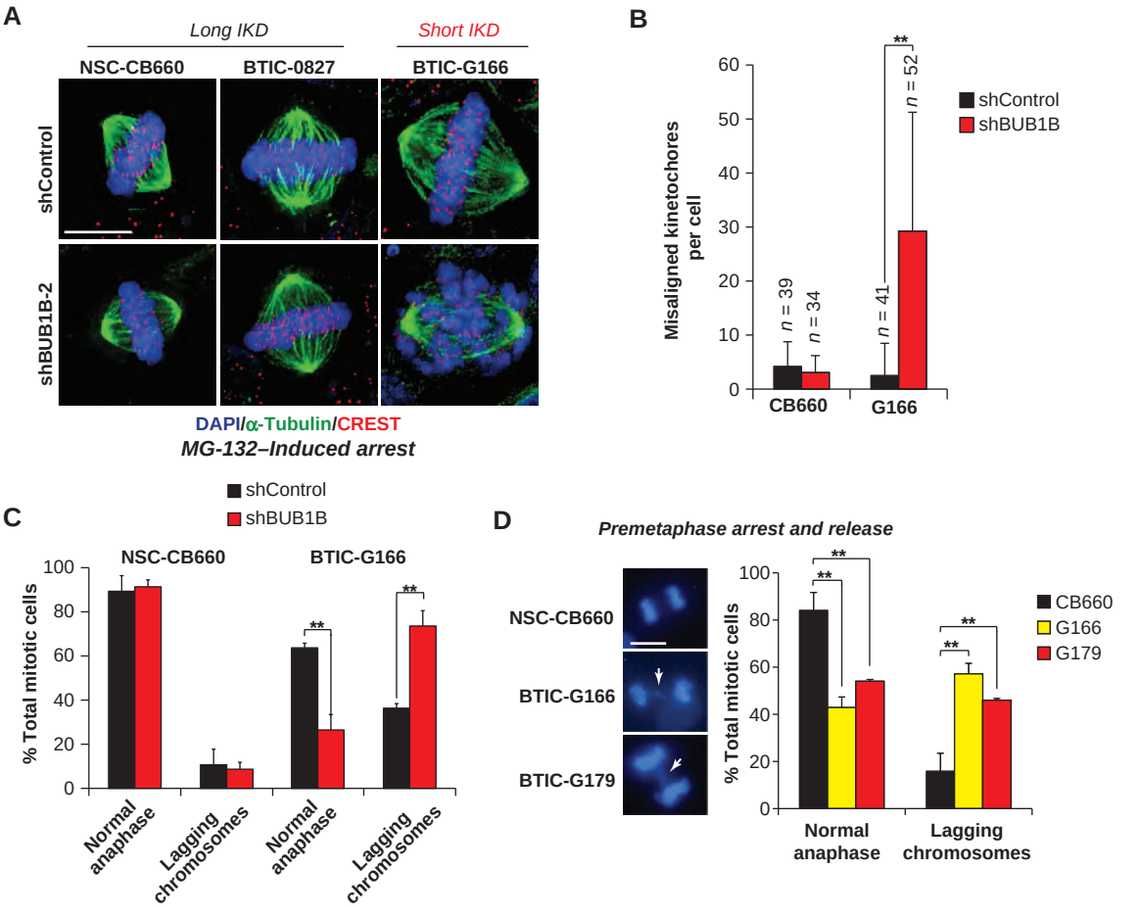

Figure 4. BTICs with short IKDs require BUB1B activity to suppress KT–MT attachment defects. **A,** chromosome alignment assays in BTICs and NSCs with BUB1B knockdown. Transduced cells were treated with 10 μmol/L MG-132 for 2 hours to arrest them at metaphase and then fixed, stained as indicated (CREST antiserum stains human kinetochores), and visualized using deconvolution microscopy. Scale bar, 10 μm. **B,** quantification of misaligned kinetochores (*n*, number of metaphase cells counted; **, $P < 0.001$ by Student *t* test). **C,** chromosome segregation defects observed in BTICs are exacerbated by BUB1B knockdown. Cells were transduced with LV-GFP-shRNA vectors; selected in puromycin; stained with an MPM-2 antibody, which marks mitotic cells, and 4′, 6-diamidino-2-phenylindole (DAPI); and examined for the appearance of lagging chromosomes in anaphase/telophase cells ($n = 3$, >40 anaphases scored). **D,** assays for lagging anaphase chromosomes were carried out by overnight arrest with the KIF11 inhibitor monastrol (100 μmol/L) followed by release for 2 hours in normal media. Lagging chromosomes were visualized by fluorescence microscopy after fixation and DAPI staining. Left, white arrows show typical examples of lagging chromosomes scored in BTICs (scale bar, 10 μm). More than 400 nuclei were counted for each trial ($n = 5$).

The above results suggested that BTICs with short IKDs have an added requirement for BUB1B that helps facilitate KT–MT attachment. The GLEBS domain of BUB1B is necessary for its KT localization and interaction with BUB3, and helps facilitate KT–MT attachment (39, 41). Maulureanu and colleagues (36) have shown that this domain is nonessential for stable end-on KT–MT attachment and viability in MEFs. Their results, however, were not consistent with previous work in HeLa cells that clearly showed that the GLEBS domain is essential for KT–MT attachment (43). Intriguingly, our datasets inform these seemingly incompatible results with the following thesis: The GLEBS domain of BUB1B is required in cells with abnormal KT conformations (e.g., HeLa cells) to suppress lethal KT–MT instability. Furthermore, as our results earlier show that RasV12 transformation can convert long IKDs to short ones, it would follow that oncogenic transformation gives rise to added BUB1B requirement.

To directly address this idea, we next conducted allelic complementation studies using mouse *Bub1b* alleles (Fig. 5A) in MEFs harboring biallelic deletion of *Bub1b* (36), which were also transformed by H-RasV12. For these experiments, we used full-length (FL) mouse *Bub1b*, the N-terminal deletion mutant, and the E406K GLEB domain–mutant allele, which cannot bind to KTs. Expression of each allele was verified by Western blotting (Supplementary Fig. S6A–S6C). For nontransformed MEFs, the viability pattern was the same as previously published (36): Both FL and E406K alleles fully complemented *Bub1b*$^{-/-}$ and only the N-terminal KEN box domain was required for *Bub1b*$^{-/-}$ cell growth (Fig. 5B). However, after *RAS*-dependent transformation of these cells, the results changed dramatically. The GLEBS domain became essential for viability, as evidenced by the complete failure of the E406K allele to complement (Fig. 5B). RasV12 activity, however, did not alter the requirement for the N-terminal KEN box domain. These results show that RasV12 transformation

Published OnlineFirst November 15, 2012; DOI: 10.1158/2159-8290.CD-12-0353

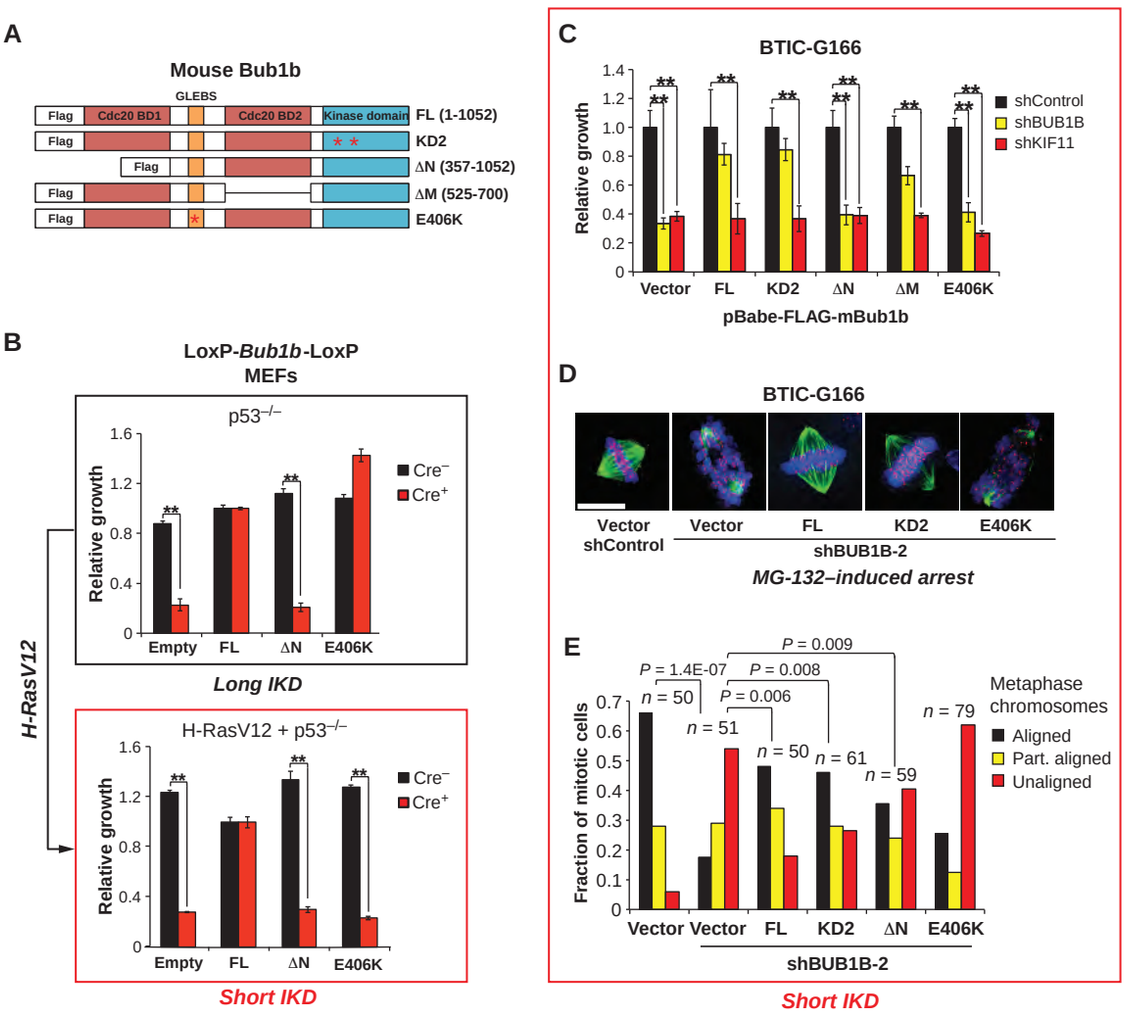

Figure 5. Allelic complementation studies with mouse *Bub1b* (mBub1b) mutants in Bub1b$^{-/-}$ MEFs and BTICs. **A,** the mouse alleles used in these studies were previously published and include FL; KD2, which harbors 2 point mutations in the kinase domain (K784>R in the ATP binding domain and K802>R in the catalytic domain); ΔN, which lacks the N-terminal Cdc20 binding domain 1; ΔM, which lacks the C-terminal Cdc20-binding domain 2; and E406K, which creates a point mutation in the GLEBS motif that interferes with kinetochore localization and Bub3 binding. **B,** viability assessment of complementation studies using p53$^{-/-}$ MEFs with floxed alleles of Bub1b, with and without transformation via H-RasV12. Knockdown of BUB1B in *RAS*-transformed NHAs phenocopies the BUB1B requirement observed in BTICs with respect to viability. MEFs were transduced with murine stem cell virus (MSCV)–GFP–mBub1b constructs, sorted for GFP^{+}, outgrown, transduced with pMSCV-Puro-Cre, selected, and seeded into microtiter growth dishes for proliferation assays. **C,** viability assessment of complementation studies using BTIC-G166 with shBUB1B (or controls) expressing each of 5 mBub1b alleles from **A**. Assays were conducted as in Fig. 1C. **D** and **E,** chromosome alignment after complementation of BUB1B knockdown with mBub1b alleles, as in Fig. 4A and B. Scale bar, 10 μm.

leads to a profound requirement for BUB1B's GLEBS domain activity.

To further examine this result, we conducted a similar set of complementation experiments in BTIC-G166 cells, using mouse Bub1b alleles to complement knockdown of endogenous human BUB1B. In this case, kinase-defective and internal KEN box deletion alleles were also included (Fig. 5C). Expression of each allele was confirmed by Western blotting (Supplementary Fig. S6A and S6B). Knockdown efficiency of endogenous BUB1B was also shown to be unaffected by the expression of mouse Bub1b (shBUB1B is not predicted to target mouse Bub1b; Supplementary Fig. S6C). As shown in Fig. 5C, expression of full-length and KD2 mBub1b alleles achieved near-complete rescue of the viability defects of BUB1B knockdown in G166 cells, indicating that the shBUB1B phenotype is due to on-target silencing of BUB1B, and that the kinase activity of BUB1B is not required in BTICs. In contrast, the ΔN and E406K alleles failed to complement viability, behaving exactly as the vector control, whereas ΔM showed a partial rescue (Fig. 5C). None of the alleles were able to complement control KIF11 knockdown. Thus, these results phenocopy those observed in RasV12-transformed MEFs.

To further investigate these results, we conducted KT–MT attachment using chromosome alignment assays as described above. All alleles showed complete or partial suppression of alignment defects, except for E406K, which failed to complement (Fig. 5D and E). This observation indicates that the

Published OnlineFirst November 15, 2012; DOI: 10.1158/2159-8290.CD-12-0353

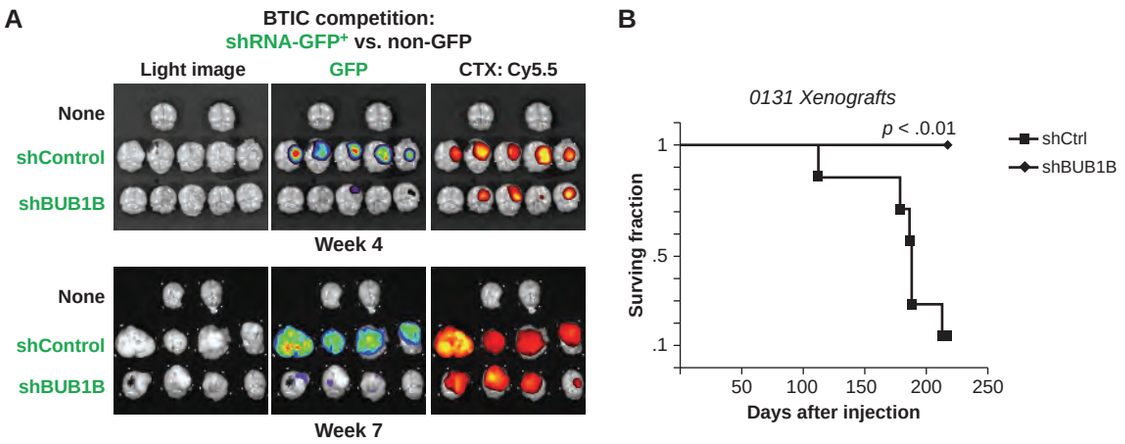

Figure 6. BUB1B knockdown inhibits BTIC-dependent tumor growth. **A,** orthotopic xenotransplants of 131 BTIC cells after stable transduction with shControl or shBUB1B. Top and bottom, experimental NSG mice 4 and 7 weeks after injection, respectively. Right, light images of brains from control. Middle, GFP+ fluorescence marking shRNA-containing cells. Left, fluorescent signal from chlorotoxin (CTX): Cy5.5 conjugate, marking bulk tumor mass. Results indicate that GFP-expressing shBUB1B cells were unable to contribute to the formation of orthotopic tumors and yielded tumor masses dominated by wild-type control cells with little to no detectable GFP expression. Quantification of GFP fluorescence in tumor 0131 orthotopic xenotransplants is shown in Supplementary Fig. S9. **B,** survival plots for mice with BTIC-0131 brain xenografts, with or without knockdown of BUB1B. Median survival for shCtrl = 178 days; shCtrl, $n = 7$; shBUB1B, $n = 6$.

GLEBS domain of BUB1B is essential for both viability and stable end-on attachment of MTs to KTs in BTICs with short IKDs.

As BUB1B's essential function is to prevent precocious anaphase through inhibiting APC^{Cdc20} activity, we also examined mitotic transit times in the same series of complementation experiments. BUB1B knockdown causes significant reduction in transit times in BTICs, which all alleles were able to complement, except for ΔN (ΔM was not determined; Supplementary Fig. S7). Because the E406K allele restored mitotic timing, but not viability or KT–MT attachment, this would suggest that the requirement for BUB1B-GLEBS domain activity is distinct from BUB1B-dependent APC regulation.

To provide additional evidence for transformation-dependent changes in BUB1B function in human cells, we examined the viability and KT–MT attachment requirements for BUB1B in normal human astrocytes with and without the expression of RasV12. Knockdown of BUB1B in RasV12-NHA, but not NHA controls, resulted in loss of viability and severe KT–MT defects (Supplementary Fig. S8A and S8B). These results were, again, consistent with the idea that oncogenic transformation leads to an added requirement for BUB1B to stabilize KT–MT attachments. A similar pattern was observed in HeLa cells and nontransformed RPE cells. Approximately 93% of HeLa cells treated with siBUB1B have severe KT–MT attachment defects ($n > 100$), compared with only 17% for control, whereas KT–MT attachment was similar regardless of siBUB1B treatment ($n > 150$; Supplementary Fig. S8C).

Several key conclusions can be drawn from these studies: (i) BUB1B is the relevant target of shBUB1B in BTICs; (ii) BUB1B's kinase activity is dispensable for added BUB1B requirement in BTICs; (iii) promotion of KT–MT attachment, rather than restoration of BTIC-mitotic delay/timing, is a key BTIC lethality-suppressing activity; (iv) glioblastoma cells differ in their requirement for the GLEBS domain of BUB1B, as compared with cells with long IKDs; and (v) oncogenic transformation drives added requirement for the GLEBS domain of BUB1B.

ShBUB1B Inhibits BTIC-Driven Tumor Formation

Finally, to ensure that the above results are applicable to tumor formation in patients, we examined the BUB1B requirement during BTIC tumor formation, for a BTIC line with short IKDs. We conducted 2 different assays. In the first, shRNA-GFP+ 0131 cells competed against non-shRNA control 0131 cells at an approximately 9:1 ratio (Fig. 6A) for injection into the cortex of immunodeficient mice. The endpoint was relative representation of shBUB1B. After 4 or 7 weeks post injection, control cells had dramatically outcompeted shBUB1B-GFP+ cells (Fig. 6A). This finding was not simply due to the inviability of injected cells at day 0, as most of the shBUB1B-GFP+ cells in the injection bolus could attach to laminin-coated dishes. For the second assay, survival was the endpoint for mice injected with either shControl or shBUB1B-expressing 0131 cells (Fig. 6B). This assay ended at 250 days after injection, when 90% of control mice had succumbed to tumors. During this time, none of the shBUB1B-0131 mice died. These results suggest that knockdown of BUB1B is deleterious to glioblastoma tumor formation and that the *in vivo* tumor environment does not suppress requirement for BUB1B.

DISCUSSION

Here, we attempted to identify kinases differentially required for the expansion of glioblastoma-derived BTICs by combining a functional genetic approach with a glioblastoma bionetwork derived from sample molecular datasets from patients (44). This approach produced BUB1B as the top-scoring screen hit. Validation studies bore out this prediction: Knockdown of BUB1B differentially blocked expansion of 9 of 11 BTIC isolates examined, without affecting

Published OnlineFirst November 15, 2012; DOI: 10.1158/2159-8290.CD-12-0353

growth of human NSCs and astrocytes, which are both candidate cell types of origin for glioblastoma (44).

BUB1B is a highly conserved BUB1-like kinase, BubR1, the activity of which is essential for mitotic spindle checkpoint signaling (17). The mitotic spindle checkpoint monitors the attachment of KTs to the plus ends of spindle MTs and prevents anaphase onset until chromosomes are aligned and kinetochores are under tension at the metaphase plate (17). To pursue the mechanism of BUB1B requirement in glioblastoma cells, we tested a hypothesis: that KT–MT dynamics are fundamentally altered in glioblastoma cells to favor KT–MT detachment, which BUB1B is required to suppress.

This hypothesis was supported by multiple observations (summarized in Fig. 7). First, in examining sister KT dynamics at metaphase, we showed that glioblastoma and other cancer cells sensitive to BUB1B inhibition have significantly shorter IKDs, indicating that KT dynamics are dramatically altered. Second, in BTICs with short IKDs, BUB1B activity is required to suppress lethal KT–MT instability and to directly or indirectly inhibit centromere-embedded Aurora B activity on outer KT proteins. Third, expression of the RasV12 oncogene is sufficient to induce the same changes in sister KTs observed in BTICs. Fourth, RasV12 also triggered requirement for the GLEBS domain of BUB1B for both viability and KT–MT attachment. Fifth, genetic dissection of BUB1B function in BTICs with short IKDs revealed the same requirement for the GLEBS domain of BUB1B to suppress lethal KT–MT instability.

These results support a model whereby oncogenic signaling alters KT regulation, resulting in short IKDs and KT–MT instability. As a direct result, BUB1B's GLEBS domain activity becomes essential for KT–MT attachment. In the absence of GLEBS domain activity, cells with short IKD undergo mitotic catastrophe and are inviable (Fig. 7). Importantly, our studies show that nontransformed cells do not require BUB1B for chromosome alignment, nor do they require the GLEBS domain to maintain the spindle assembly checkpoint or viability.

One key implication of this work is that short IKDs may be predictive of the requirement for the GLEBS domain of BUB1B and sensitivity to disruption of KT function in cancer cells. For example, we have found glioblastoma isolates (i.e., 0827 and 1502) from patients that are resistant to BUB1B knockdown and have IKDs indistinguishable from those of untransformed cells. Thus, it is conceivable that anticancer therapies targeting KT or mitotic checkpoint function (e.g., refs. 45 and 46) would benefit from using IKDs as a biomarker or companion diagnostic. However, additional studies are required to determine the extent to which IKDs are shorter in cancer cells and also the mechanisms through which KT conformations become perturbed.

One possibility is that RTK-Ras signaling directly affects KT function. Evidence has come to light that Ras effector kinases Erk1/2 can directly phosphorylate the C-terminal domain of CENPE, a key KT protein, which is predicted to decrease its MT-binding ability (47, 48). Intriguingly, we observed that in both BTIC-G166 and RasV12-transformed astrocytes, which have short IKDs, significant upregulation of Erk1/2 activity takes place in prophase and mitosis (Supplementary Fig. S9). Thus, it is conceivable that inappropriate regulation of the RTK-Ras pathway in mitosis could directly affect KT–MT attachments and/or KT conformational states. Although RasV12-transformed astrocytes may not faithfully recapitulate the mutation spectra of glioblastoma (only ~2% have mutant Ras activity; ref. 20), the Ras pathway is predicted to be inappropriately activated in a majority of glioblastoma tumors (ref. 20; e.g., by NF1 mutation or RTK activity). Future work is required to examine the relationship between Ras signaling and KT regulation.

Our results also shed light on a recent study that identified genes differentially required in cancer cell lines overexpressing the activated *KRAS* oncogene (16). Their results suggest that activated *RAS* oncogene activity triggers differential requirement for a PLK1-associated mitotic network (16), which they

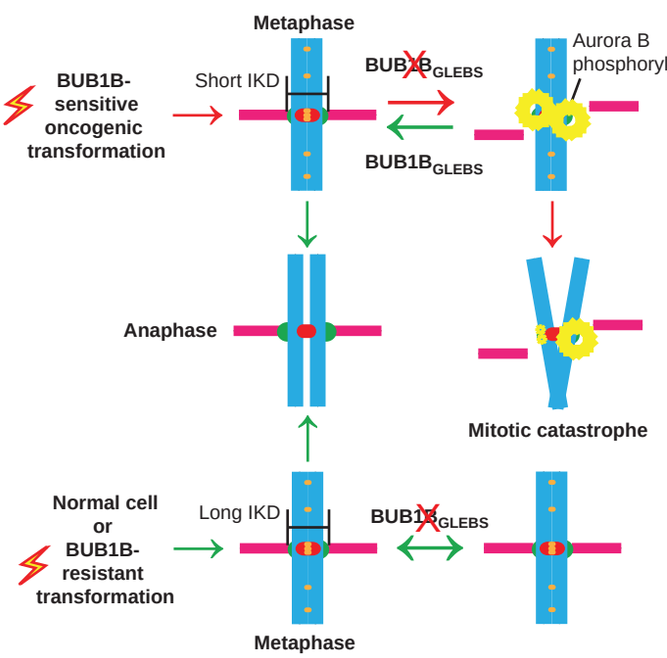

Figure 7. A model for BUB1B function in glioblastoma and genetically transformed cells.

Published OnlineFirst November 15, 2012; DOI: 10.1158/2159-8290.CD-12-0353

proposed resulted from Ras-induced "mitotic stress." Our results suggest that these phenotypes likely result from KT–MT attachment defects arising from KT conformational abnormalities.

Finally, our studies also inform the use of a large collection of cancer patient molecular signatures. We used more than 300 glioblastoma patient molecular signatures to create a Bayesian bionetwork, which, when combined with our functional genetic data, predicted BUB1B inhibition to be differentially lethal for glioblastoma cells. To our knowledge, this is the first time a bionetwork derived solely from patient data has been used to successfully predict gene activity specifically required for cancer cells. Intriguingly, integrating our BTIC kinome dataset into a bionetwork for breast cancer also yielded BUB1B as the top-scoring hit (J. Zhu; personal communication), suggesting that our results should prove useful for other cancers.

In summary, our results suggest that glioblastoma tumors and genetically transformed cells have an added requirement for BUB1B to suppress lethal consequences of altered KT function. They further suggest that IKDs may predict cancer-specific sensitivity to BUB1B inhibition and perhaps other mitotic targets that affect KT–MT stability.

METHODS

shRNA Barcode Screens and Array Analysis

For shRNA screen and barcode array analysis, cells were infected with a pool of lentiviral shRNAs targeting 713 human kinases at a representation of approximately 1,000-fold [multiplicity of infection (MOI) < 1]. At day 3 post infection, an initial day 0 sample was taken. The rest of the population was selected with puromycin (Sigma; 2 μg/mL) to remove uninfected cells. Afterwards, cells were propagated in culture for an additional 21 days and sampled for barcode array analysis at 21 days. For each passage, a minimal representation of 1,000-fold was maintained. For each corresponding sample, shRNA barcodes were PCR recovered from genomic samples, labeled with Cy5 or Cy3, and competitively hybridized to a microarray containing the corresponding probes (Agilent Technologies). Replicate array results were analyzed using the BioConductor package limma. The change in the relative abundance of each shRNA in the library over time was measured using the normalized Cy3/Cy5 ratio of its probe signal. Barcode probes depleted in the BTIC samples were considered candidate genes, using the following criteria: (i) adjusted $P \leq 0.05$ and (ii) $|\log2(\text{ratio})| \geq 0.585$.

Cell Culture

BTIC and NSC lines used in these studies have been previously published (7, 8) and were grown in N2B27 neural basal media (STEMCELL Technologies) supplemented with EGF and fibroblast growth factor 2 (FGF-2) of 20 ng/mL each (Peprotech), on laminin-coated polystyrene plates (Sigma) and passaged according to Pollard and colleagues (8). Immortalized CX cells and VM cells (Millipore) were maintained in ReNcell maintenance medium with EGF and FGF-2 (20 ng/mL each; Peprotech) and also grown on laminin-coated tissue culture–treated plates and passaged according to Pollard and colleagues (8). NHA (STEMCELL Technologies) and NHA-Ras cells (Russell Pieper, University of California San Francisco, San Francisco, CA) were grown in astrocyte growth medium (Clonetics) according to the manufacturer's instructions and published protocols (49).

RNAi

The shRNAs were obtained from the RNAi Shared Resource [Fred Hutchinson Cancer Research Center (FHCRC)] or Open Biosystems in the pGIPZ lentiviral vector. Target sequences for shRNAs are as follows: BUB1B, #1, CDS:1417, CCTACAAAGGAGACAACTA; BUB1B, #2, CDS:1547, AGGAACAACCTCATTCTAA; and KIF11, CDS:571, AAGAGAGGAGTGATAATTA. For virus production, pGIPZ-shRNA plasmids were transfected into 293T cells along with psPAX and pMD2.G packaging plasmid to produce lentivirus. Approximately 24 hours after transfection, NSC expansion medium was added to replace original growth medium. Virus was harvested 24 hours after medium change and stored at −80°C. BTICs and NSCs were infected at MOI < 1 and selected with 2 to 4 μg of puromycin for 2 to 4 days.

qRT-PCR

QuantiTect quantitative real-time PCR (qRT-PCR) primer sets and QuantiFast SYBR Green PCR Kits (Qiagen) were used according to the manufacturer's instructions with the ABI PRISM 7900 Sequence Detection System (Genomics Resource, FHCRC). Relative transcript abundance was analyzed using the $2^{-\Delta\Delta C_t}$ method. TRIzol (Invitrogen) extraction was used to collect total RNA from cells.

Western Blot Analysis

Western blots were carried out using the standard laboratory practices, except that a modified radioimmunoprecipitation assay buffer was used for protein extraction [150 mmol/L NaCl, 50 mmol/L Tris, 2 mmol/L MgCl2, 1% SDS, 4% DOC, 4% Triton-X 100, 2 mmol/L DTT, and complete protease inhibitors (Roche)] followed by a 15-minute digestion with 125 units of Benzonase (Merck) at room temperature. The following antibodies were used for detection: BUB1B (1:1,000; Sigma), Actin (1:1,000; Cell Signaling), and cleaved PARP (1:1,000; Cell Signaling). An Odyssey infrared imaging system was used to visualize blots (LI-COR) following the manufacturer's instruction.

Growth Assays

For short-term outgrowth assays, after selection, shRNA-transduced cells were harvested, counted (NucleoCounter, NBS), and plated onto a 96-well plate. After 7 days under standard growth conditions, the cell proliferative rate was measured using AlamarBlue reagent (Invitrogen). For long-term outgrowth assays, after selection, shRNA-transduced cells were mixed with nontransduced cells (9:1) and outgrown for 14 to 24 days using our standard passaging protocol. The GFP^+ fraction, which marks shRNA-containing cells, of each population was measured by fluorescence-activated cell sorting (FACS; BD LSR2 flow cytometer; FHCRC Shared Resources) at 5- to 8-day intervals.

Spindle Checkpoint Arrest

For image-based assessment, cells were plated in a 96-well plate and then treated with paclitaxel (Sigma) and nocodozole (Sigma) for various time points (6–18 hours). After treatment, cells were fixed with 2% paraformaldehyde for 30 minutes, permeabilized with 0.25% Triton X-100, and blocked in PBS containing 3% bovine serum albumin and 5% goat serum. After 3 washes with PBS, cells were stained with MPM-2 (1:300, Millipore) at room temperature for 1 hour. Next, cells were washed and incubated with Alexa Fluor 568 secondary antibody (Invitrogen) and DAPI for 1 hour in the dark. Staining was visualized by the Nikon Eclipse Ti microscope. For FACS-based assessment, cells were then collected and fixed in 70% ethanol for 1 hour at 4°C, then rinsed with ice-cold PBS + 2% fetal calf serum, and stained with anti-MPM-2 (1:300, Millipore), anti-mouse Alexa Fluor 568 (1:200, Invitrogen), and DAPI (1 μg/mL). Cells were washed, resuspended in PBS, and filtered. The mitotic index was measured by a BD LSR2 flow cytometer (FHCRC Shared Resources).

Mitotic Transit Time

NSC and BTIC cells were transduced with control and BUB1B shRNA, respectively. After selection, cells were plated into a 96-well plate for time-lapse microscopy. During imaging, the atmosphere was

Published OnlineFirst November 15, 2012; DOI: 10.1158/2159-8290.CD-12-0353

maintained at a temperature of 37°C and 5% CO_2. Imaging was conducted using a Nikon Eclipse Ti microscope equipped with a live imaging system. Nikon Elements software was used to collect and process data. Images were captured at 5.3-minute intervals for 16 hours.

Lagging Chromosome Assay

For one-step arrest in prometaphase, cells were treated overnight with the EG5 kinesin inhibitor monastrol (100 μmol/L final concentration) overnight. DAPI staining was conducted to visualize the abnormal anaphase frequency. Monastrol inhibits the mitotic kinesin EG5KIF11, a motor protein required for spindle bipolarity, and specifically arrest cells in G_2–M (26, 34). Cells were washed and released into fresh media for 2 hours and then fixed (4% PF), permeabilized, stained with DAPI, and visualized using a Nikon Eclipse E800 (Scientific Imaging, FHCRC). More than 400 nuclei were counted for each trial ($n = 5$) and the Student t test determined significance. For asynchronous populations, cells were additionally stained with an MPM-2 antibody (Millipore), which marks mitotic cells, and counterstained with DAPI (Sigma). Approximately, one-third of MPM-2–positive cells in asynchronous cultures were in anaphase/telophase, whereas the other two thirds were in prometaphase or metaphase.

Chromosome Alignment Assays

For metaphase staining, cells were treated by 10 μmol/L MG-132 (TOCRIS Bioscience) for 2 hours to arrest them at metaphase and then fixed for 20 minutes at room temperature with 4% formaldehyde in PBS and 0.2% Triton X-100. For cold-stable microtubules, cells were incubated on ice for 15 minutes before fixation. After fixation, cells were blocked and stained with α-tubulin (DM1A; 1:1,000; Sigma) and CREST anti-serum (1:1,000; Immunovision) at room temperature for 1 hour. Cells were washed and incubated with secondary antibody and DAPI for 1 hour in the dark. Immunolabeled cells were imaged on a DeltaVision RT deconvolution microscope (Applied Precision Inc.). Optical sections were acquired at 0.2-μ spacing with an Olympus ×100/1.4 NA UPLS Apo objective. Three-dimensional (3D) image stacks were deconvolved with Applied Precision's proprietary software softWoRx, using a constrained iterative algorithm. Deconvolved 3D data were loaded into the visualization software Velocity (PerkinElmer). The number of misaligned MT-attached KTs was counted on the basis of CREST staining on 3D rendered images, and confirmed by visual inspection of maximum intensity projections of whole cells. Misaligned kinetochores were defined as those with normalized distance less than 0.2 μm. At least 30 cells were analyzed for each RNAi experiment.

Xenotransplantation

BTIC isolates (0131 cells) were infected with pGIPZ-shRNA virus and selected for 3 days in puromycin (2 μg/mL), so that more than 80% of cells were GFP^+. Cells were then harvested using Accutase (Sigma), counted, resuspended in an appropriate volume of culture media, and kept on ice before immediate transplantation. Nonobese diabetic/severe combined immunodeficient (NOD/SCID) IL2Rγ-null mice (Jackson Laboratories #005557) were anesthetized by intraperitoneal injection of 0.2 mL/10 gm 1.25% Avertin solution and kept at 37°C. A small-bore hole was made in the skull, using a hand drill with a Meisinger #009 steel burr bit (Hager & Meisinger GmbH). A total of 2×10^5 cells were slowly injected by pipette into the right frontal cortex approximately 2 mm rostral to the bregma, 2 mm lateral, and 3 mm deep through a 0.2- to 10-μL disposable sterile aerosol barrier tip (Fisher Scientific #02-707-30). The burr hole was closed using SURGIFOAM (Johnson & Johnson) and the skin rejoined using TISSUMEND II (Veterinary Product Laboratories).

Brain Tumor Imaging

Seven weeks after the initial transplantation, mice were injected intravenously with 50 μL of 40 μmol/L chlorotoxin: Cy5.5 conjugate (50) 2 hours before sacrifice by CO_2 inhalation. The brain and tumor were removed from the skull and imaged for Cy5.5 and GFP fluorescence using the Xenogen IVIS Spectrum imaging system (Caliper Life Sciences).

Additional methods can be found in the Supplementary data.

Disclosure of Potential Conflicts of Interest

No potential conflicts of interest were disclosed.

Authors' Contributions

Conception and design: Y. Ding, C.G. Hubert, J.M. Olson, P.J. Paddison
Development of methodology: Y. Ding, C.G. Hubert, J.K. Risler, J.M. Olson, P.J. Paddison
Acquisition of data (provided animals, acquired and managed patients, provided facilities, etc.): Y. Ding, C.G. Hubert, J. Herman, C.M. Toledo, J.J. Delrow, J.M. Olson, P.J. Paddison
Analysis and interpretation of data (e.g., statistical analysis, biostatistics, computational analysis): Y. Ding, J. Herman, C.M. Toledo, K. Skutt-Kakaria, B. Zhang, J.J. Delrow, J. Zhu, J. DeLuca, J.M. Olson, P.J. Paddison
Writing, review, and/or revision of the manuscript: Y. Ding, J. Zhu, J. DeLuca, J.M. Olson, P.J. Paddison
Administrative, technical, or material support (i.e., reporting or organizing data, constructing databases): Y. Ding, P. Corrin, K. Skutt-Kakaria, J. Vazquez, R. Basom, D.-H. Nam, J. Lee, P.J. Paddison
Study supervision: D.-H. Nam, J.M. Olson, P.J. Paddison
Provided cell lines for study: S.M. Pollard

Acknowledgments

The authors thank Sue Biggins for critical reading of this manuscript; Jan van Deursen, Howard Fine, Russell Pieper, Xiao-Nan Li, Julian Simon, and Austin Smith for providing cell lines and/or reagents; Stacey Hansen and Sally Ditzler for technical help; Pam Lindberg and Laima Abele for administrative support; and the members of the Paddison and Olson labs for helpful discussions.

Grant Support

This work was supported by grants from the PEW Scholars Program (to P.J. Paddison), the Accelerate Brain Cancer Cure foundation (P.J. Paddison), a UK-US Stem Cell Collaboration Development Award program (to S.M. Pollard/P.J. Paddison), National Cancer Institute (NCI)/NIH CA15704 (to P.J. Paddison), NCI/NIH CA170722-01 (to P.J. Paddison), Phi Beta Psi Sorority cancer grant program (to P.J. Paddison), the Listwin Family Foundation (to P.J. Paddison), Department of Defense Translational New Investigator Award W81XWH-11-1-0756 (to P.J. Paddison), Association of American Cancer Institutes (to Y. Ding), and NIH Interdisciplinary Training in Cancer Research Program T32CA080416 (to C.G. Hubert).

Received July 25, 2012; revised November 5, 2012; accepted November 9, 2012; published OnlineFirst November 15, 2012.

REFERENCES

1. American Cancer Society. American Cancer Society: Cancer Facts and Figures 2010. [cited 2013 Jan 15]. Available from: http://www.cancer.org/research/cancerfactsfigures/cancerfactsfigures/cancer-facts-and-figures-2010.
2. Stupp R, Mason WP, van den Bent MJ, Weller M, Fisher B, Taphoorn MJ, et al. Radiotherapy plus concomitant and adjuvant temozolomide for glioblastoma. N Engl J Med 2005;352:987–96.
3. Hemmati HD, Nakano I, Lazareff JA, Masterman-Smith M, Geschwind DH, Bronner-Fraser M, et al. Cancerous stem cells can arise from pediatric brain tumors. Proc Natl Acad Sci U S A 2003;100:15178–83.

Published OnlineFirst November 15, 2012; DOI: 10.1158/2159-8290.CD-12-0353

4. Singh SK, Clarke ID, Terasaki M, Bonn VE, Hawkins C, Squire J, et al. Identification of a cancer stem cell in human brain tumors. Cancer Res 2003;63:5821–8.
5. Singh SK, Hawkins C, Clarke ID, Squire JA, Bayani J, Hide T, et al. Identification of human brain tumour initiating cells. Nature 2004; 432:396–401.
6. Galli R, Binda E, Orfanelli U, Cipelletti B, Gritti A, De Vitis S, et al. Isolation and characterization of tumorigenic, stem-like neural precursors from human glioblastoma. Cancer Res 2004;64:7011–21.
7. Lee J, Kotliarova S, Kotliarov Y, Li A, Su Q, Donin NM, et al. Tumor stem cells derived from glioblastomas cultured in bFGF and EGF more closely mirror the phenotype and genotype of primary tumors than do serum-cultured cell lines. Cancer Cell 2006;9:391–403.
8. Pollard SM, Yoshikawa K, Clarke ID, Danovi D, Stricker S, Russell R, et al. Glioma stem cell lines expanded in adherent culture have tumor-specific phenotypes and are suitable for chemical and genetic screens. Cell Stem Cell 2009;4:568–80.
9. Stiles CD, Rowitch DH. Glioma stem cells: a midterm exam. Neuron 2008;58:832–46.
10. Bao S, Wu Q, McLendon RE, Hao Y, Shi Q, Hjelmeland AB, et al. Glioma stem cells promote radioresistance by preferential activation of the DNA damage response. Nature 2006;444:756–60.
11. Bao S, Wu Q, Sathornsumetee S, Hao Y, Li Z, Hjelmeland AB, et al. Stem cell-like glioma cells promote tumor angiogenesis through vascular endothelial growth factor. Cancer Res 2006;66:7843–8.
12. Liu Q, Nguyen DH, Dong Q, Shitaku P, Chung K, Liu OY, et al. Molecular properties of CD133$^+$ glioblastoma stem cells derived from treatment-refractory recurrent brain tumors. J Neurooncol 2009; 94:1–19.
13. Sawin KE, LeGuellec K, Philippe M, Mitchison TJ. Mitotic spindle organization by a plus-end-directed microtubule motor. Nature 1992;359:540–3.
14. Hartwell LH, Szankasi P, Roberts CJ, Murray AW, Friend SH. Integrating genetic approaches into the discovery of anticancer drugs. Science 1997;278:1064–8.
15. Barbie DA, Tamayo P, Boehm JS, Kim SY, Moody SE, Dunn IF, et al. Systematic RNA interference reveals that oncogenic KRAS-driven cancers require TBK1. Nature 2009;462:108–12.
16. Luo J, Emanuele MJ, Li D, Creighton CJ, Schlabach MR, Westbrook TF, et al. A genome-wide RNAi screen identifies multiple synthetic lethal interactions with the Ras oncogene. Cell 2009;137:835–48.
17. Musacchio A, Salmon ED. The spindle-assembly checkpoint in space and time. Nat Rev Mol Cell Biol 2007;8:379–93.
18. Sun Y, Pollard S, Conti L, Toselli M, Biella G, Parkin G, et al. Long-term tripotent differentiation capacity of human neural stem (NS) cells in adherent culture. Mol Cell Neurosci 2008;38:245–58.
19. Lens SM, Voest EE, Medema RH. Shared and separate functions of polo-like kinases and aurora kinases in cancer. Nat Rev Cancer 2010; 10:825–41.
20. Cancer Genome Atlas Research Network. Comprehensive genomic characterization defines human glioblastoma genes and core pathways. Nature 2008;455:1061–8.
21. Zhu J, Zhang B, Smith EN, Drees B, Brem RB, Kruglyak L, et al. Integrating large-scale functional genomic data to dissect the complexity of yeast regulatory networks. Nat Genet 2008;40:854–61.
22. Tran LM, Zhang B, Zhang Z, Zhang C, Xie T, Lamb JR, et al. Inferring causal genomic alterations in breast cancer using gene expression data. BMC Syst Biol 2011;5:121.
23. Yang X, Deignan JL, Qi H, Zhu J, Qian S, Zhong J, et al. Validation of candidate causal genes for obesity that affect shared metabolic pathways and networks. Nat Genet 2009;41:415–23.
24. Verhaak RG, Hoadley KA, Purdom E, Wang V, Qi Y, Wilkerson MD, et al. Integrated genomic analysis identifies clinically relevant subtypes of glioblastoma characterized by abnormalities in PDGFRA, IDH1, EGFR, and NF1. Cancer Cell 2010;17:98–110.
25. Son MJ, Woolard K, Nam DH, Lee J, Fine HA. SSEA-1 is an enrichment marker for tumor-initiating cells in human glioblastoma. Cell Stem Cell 2009;4:440–52.
26. Cahill DP, Lengauer C, Yu J, Riggins GJ, Willson JK, Markowitz SD, et al. Mutations of mitotic checkpoint genes in human cancers. Nature 1998;392:300–3.
27. Bie L, Zhao G, Cheng P, Rondeau G, Porwollik S, Ju Y, et al. The accuracy of survival time prediction for patients with glioma is improved by measuring mitotic spindle checkpoint gene expression. PLoS ONE 2011;6:e25631.
28. Yuan B, Xu Y, Woo JH, Wang Y, Bae YK, Yoon DS, et al. Increased expression of mitotic checkpoint genes in breast cancer cells with chromosomal instability. Clin Cancer Res 2006;12:405–10.
29. Santaguida S, Musacchio A. The life and miracles of kinetochores. EMBO J 2009;28:2511–31.
30. DeLuca JG, Moree B, Hickey JM, Kilmartin JV, Salmon ED. hNuf2 inhibition blocks stable kinetochore-microtubule attachment and induces mitotic cell death in HeLa cells. J Cell Biol 2002;159:549–55.
31. DeLuca JG, Gall WE, Ciferri C, Cimini D, Musacchio A, Salmon ED. Kinetochore microtubule dynamics and attachment stability are regulated by Hec1. Cell 2006;127:969–82.
32. Maresca TJ, Groen AC, Gatlin JC, Ohi R, Mitchison TJ, Salmon ED. Spindle assembly in the absence of a RanGTP gradient requires localized CPC activity. Curr Biol 2009;19:1210–5.
33. Uchida KS, Takagaki K, Kumada K, Hirayama Y, Noda T, Hirota T. Kinetochore stretching inactivates the spindle assembly checkpoint. J Cell Biol 2009;184:383–90.
34. Lampson MA, Kapoor TM. The human mitotic checkpoint protein BubR1 regulates chromosome-spindle attachments. Nat Cell Biol 2005;7:93–8.
35. DeLuca KF, Lens SM, DeLuca JG. Temporal changes in Hec1 phosphorylation control kinetochore-microtubule attachment stability during mitosis. J Cell Sci 2011;124:622–34.
36. Malureanu LA, Jeganathan KB, Hamada M, Wasilewski L, Davenport J, van Deursen JM. BubR1 N terminus acts as a soluble inhibitor of cyclin B degradation by APC/C(Cdc20) in interphase. Dev Cell 2009;16:118–31.
37. Tang Z, Bharadwaj R, Li B, Yu H. Mad2-independent inhibition of APCCdc20 by the mitotic checkpoint protein BubR1. Dev Cell 2001;1:227–37.
38. Davenport J, Harris LD, Goorha R. Spindle checkpoint function requires Mad2-dependent Cdc20 binding to the Mad3 homology domain of BubR1. Exp Cell Res 2006;312:1831–42.
39. Harris L, Davenport J, Neale G, Goorha R. The mitotic checkpoint gene BubR1 has two distinct functions in mitosis. Exp Cell Res 2005; 308:85–100.
40. Mao Y, Desai A, Cleveland DW. Microtubule capture by CENP-E silences BubR1-dependent mitotic checkpoint signaling. J Cell Biol 2005;170:873–80.
41. Wang X, Babu JR, Harden JM, Jablonski SA, Gazi MH, Lingle WL, et al. The mitotic checkpoint protein hBUB3 and the mRNA export factor hRAE1 interact with GLE2p-binding sequence (GLEBS)-containing proteins. J Biol Chem 2001;276:26559–67.
42. Wang Q, Liu T, Fang Y, Xie S, Huang X, Mahmood R, et al. BUBR1 deficiency results in abnormal megakaryopoiesis. Blood 2004;103:1278–85.
43. Elowe S, Dulla K, Uldschmid A, Li X, Dou Z, Nigg EA. Uncoupling of the spindle-checkpoint and chromosome-congression functions of BubR1. J Cell Sci 2010;123:84–94.
44. Park DM, Rich JN. Biology of glioma cancer stem cells. Mol Cells 2009;28:7–12.
45. Sudakin V, Yen TJ. Targeting mitosis for anti-cancer therapy. BioDrugs 2007;21:225–33.
46. Wood KW, Lad L, Luo L, Qian X, Knight SD, Nevins N, et al. Antitumor activity of an allosteric inhibitor of centromere-associated protein-E. Proc Natl Acad Sci U S A 2010;107:5839–44.
47. Zecevic M, Catling AD, Eblen ST, Renzi L, Hittle JC, Yen TJ, et al. Active MAP kinase in mitosis: localization at kinetochores and association with the motor protein CENP-E. J Cell Biol 1998;142:1547–58.
48. Liao H, Li G, Yen TJ. Mitotic regulation of microtubule cross-linking activity of CENP-E kinetochore protein. Science 1994;265:394–8.
49. Sonoda Y, Ozawa T, Hirose Y, Aldape KD, McMahon M, Berger MS, et al. Formation of intracranial tumors by genetically modified human astrocytes defines four pathways critical in the development of human anaplastic astrocytoma. Cancer Res 2001;61:4956–60.
50. Veiseh M, Gabikian P, Bahrami SB, Veiseh O, Zhang M, Hackman RC, et al. Tumor paint: a chlorotoxin:Cy5.5 bioconjugate for intraoperative visualization of cancer foci. Cancer Res 2007;67:6882–8.

Published OnlineFirst November 15, 2012; DOI: 10.1158/2159-8290.CD-12-0353

CANCER DISCOVERY

Cancer-Specific Requirement for BUB1B/BUBR1 in Human Brain Tumor Isolates and Genetically Transformed Cells

Yu Ding, Christopher G. Hubert, Jacob Herman, et al.

Cancer Discovery 2013;3:198-211. Published OnlineFirst November 15, 2012.

Genome-wide RNAi screens in human brain tumor isolates reveal a novel viability requirement for PHF5A

Christopher G. Hubert,[1,2,3,13] Robert K. Bradley,[4,5,13] Yu Ding,[2] Chad M. Toledo,[2,3] Jacob Herman,[6] Kyobi Skutt-Kakaria,[2] Emily J. Girard,[1] Jerry Davison,[7] Jason Berndt,[8] Philip Corrin,[2] Justin Hardcastle,[2] Ryan Basom,[9] Jeffery J. Delrow,[9] Thomas Webb,[10] Steven M. Pollard,[11] Jeongwu Lee,[12] James M. Olson,[1,14] and Patrick J. Paddison[2,14]

[1]Clinical Research Division, [2]Human Biology Division, Fred Hutchinson Cancer Research Center, Seattle, Washington 98109, USA; [3]Molecular and Cellular Biology Program, University of Washington, Seattle, Washington 98195, USA; [4]Computational Biology Program, Public Health Sciences Division, [5]Basic Sciences Division, Fred Hutchinson Cancer Research Center, Seattle, Washington 98109, USA; [6]Department of Biochemistry and Molecular Biology, Colorado State University, Fort Collins, Colorado 80523, USA; [7]Computational Biology Shared Resource, Fred Hutchinson Cancer Research Center, Seattle, Washington 98109, USA; [8]Department of Pharmacology, Institute for Stem Cell and Regenerative Medicine, University of Washington, Seattle, Washington 98195, USA; [9]Genomics Shared Resource, Fred Hutchinson Cancer Research Center, Seattle, Washington 98109, USA; [10]High Throughput Chemistry Facility, St. Jude Children's Research Hospital, Memphis, Tennessee 38105, USA; [11]Cancer Institute, University College London, London WC1E 6BT, United Kingdom; [12]Stem Cell Biology and Regenerative Medicine, Lerner Research Institute, Cleveland Clinic, Cleveland, Ohio 44192, USA

To identify key regulators of human brain tumor maintenance and initiation, we performed multiple genome-wide RNAi screens in patient-derived glioblastoma multiforme (GBM) stem cells (GSCs). These screens identified the plant homeodomain (PHD)-finger domain protein PHF5A as differentially required for GSC expansion, as compared with untransformed neural stem cells (NSCs) and fibroblasts. Given PHF5A's known involvement in facilitating interactions between the U2 snRNP complex and ATP-dependent helicases, we examined cancer-specific roles in RNA splicing. We found that in GSCs, but not untransformed controls, PHF5A facilitates recognition of exons with unusual C-rich 3′ splice sites in thousands of essential genes. PHF5A knockdown in GSCs, but not untransformed NSCs, astrocytes, or fibroblasts, inhibited splicing of these genes, leading to cell cycle arrest and loss of viability. Notably, pharmacologic inhibition of U2 snRNP activity phenocopied PHF5A knockdown in GSCs and also in NSCs or fibroblasts overexpressing MYC. Furthermore, PHF5A inhibition compromised GSC tumor formation in vivo and inhibited growth of established GBM patient-derived xenograft tumors. Our results demonstrate a novel viability requirement for PHF5A to maintain proper exon recognition in brain tumor-initiating cells and may provide new inroads for novel anti-GBM therapeutic strategies.

[*Keywords*: brain tumors; RNA splicing; RNAi; cancer stem cell]

Supplemental material is available for this article.

Received December 19, 2012; revised version accepted April 4, 2013.

Malignant glioma is the most common and lethal form of brain cancer. Glioblastoma multiforme (GBM) is the most invasive and aggressive grade of glioma and is notoriously drug- and radiation-resistant. There are currently no highly effective therapies against GBM, and with standard of care treatments, including surgery, radiation, and chemotherapy, ~90% of adult patients die within 2 yr of diagnosis (Latera and Brem 2002; Central Brain Tumor Registry of the United States (CBTRUS), http://www.cbtrus.org), underscoring the need for novel therapeutic targets. The hierarchical organization of adult and pediatric brain tumors suggests a cancer stem cell origin (Hemmati et al. 2003; Singh et al. 2003, 2004; Galli et al. 2004). Consistent with this idea, tumor-initiating GBM stem cells (GSCs) isolated from patients retain the developmental potential and specific genetic alterations found in the original tumor (Hemmati et al. 2003; Singh et al. 2003; Lee et al. 2006; Pollard et al. 2009).

When isolated under serum-free monolayer conditions, GSCs can retain tumor-initiating potential and

[13]These authors contributed equally to this work.
[14]Corresponding authors
E-mail paddison@fhcrc.org
E-mail jolson@fhcrc.org
Article is online at http://www.genesdev.org/cgi/doi/10.1101/gad.212548.112.

tumor-specific genetic and epigenetic signatures over extended outgrowth periods (Lee et al. 2006; Pollard et al. 2009). In addition, they have been shown to recreate tumor cellular hierarchies when implanted into the cortex of immunocompromised mice (Lee et al. 2006; Pollard et al. 2009). Furthermore, GSC isolates also retain expression of neural progenitor molecular networks, which may contribute to the aggressive behavior of GBM tumors through enhancing self-renewal or developmental programs (Mangiola et al. 2007; Stiles and Rowitch 2008; Gangemi et al. 2009), DNA repair pathways (Bao et al. 2006a), angiogenesis (Bao et al. 2006b; Cheng et al. 2013), and/or invasiveness (Liu et al. 2009).

Recently, in order to identify new candidate therapeutic targets for GBM, we combined functional genetics and GBM network modeling to identify human kinases required for the expansion of GSCs but dispensable to proliferating neural stem cells (NSCs) (Ding et al. 2013). This approach yielded BUB1B/BUBR1, a critical mitotic spindle kinase, as a GBM-lethal gene. Our studies revealed that certain GBM tumors have an added requirement for a nonessential BUB1B activity to suppress lethal consequences of altered kinetochore function (Ding et al. 2013). Thus, these results demonstrated that patient-derived GSCs can be used to identify cancer- and patient-specific molecular vulnerabilities for GBM that are not observed in tissue-appropriate or other nontransformed control cells (e.g., NSCs and astroyctes).

Here, we expanded our search for GBM-lethal genes by performing genome-wide RNAi screens in multiple GSC patient isolates and NSCs to identify genes differentially required for GSC expansion. These studies revealed that the plant homeodomain (PHD)-finger domain protein PHF5A was differentially required for expansion and viability of multiple GSC isolates. Molecular studies demonstrated that GSCs have a novel requirement for PHF5A activity to facilitate recognition of exons with distinctive 3′ splice sites. PHF5A knockdown resulted in splicing defects in thousands of essential genes, a subset of which are predicted to affect cell division and growth (e.g., CDC20 and RAF1). Cell-based assays revealed that PHF5A/U2snRNP perturbation causes G2/M arrest in GSCs both in vitro and during cell growth in established patient-derived tumors. Importantly, sensitivity to U2snRNP perturbation could be recreated in NSCs and fibroblasts overexpressing MYC. Although MYC is not frequency amplified in GBM, MYC is coordinately activated by mutations in p53 and PTEN, two of the most common mutations in GBM (Zheng et al. 2008b), and is also essential for human GSC self-renewal (Wang et al. 2008). Our results demonstrate an unexpected role for PHF5A in maintaining proper exon recognition in GSCs, which is critical for growth and maintenance of patient-derived tumors.

Results

Functional genetic screens identify PHF5A as differentially required for GSC expansion

To identify genes necessary for the growth and survival of GSCs but likely dispensable to noncancerous neural cells and tissues, we performed functional genetic shRNA screens that targeted 1086 nucleic acid-binding factors in both primary GSC tumor isolates and human fetal NSC-CB660 cells. For these screens, we assayed genes required for GSC and NSC in vitro expansion in serum-free monolayer culture (Fig. 1A; Pollard et al. 2009; Ding et al. 2013).

Cells were infected with pools of shRNAs (Paddison et al. 2004; Luo et al. 2009) and expanded in triplicate screening populations under normal conditions for 21 d. Comparisons of shRNA representation in GSCs or NSCs over time using microarrays or deep sequencing revealed a subset of shRNAs that became significantly under- or overrepresented during expansion. Candidate GSC-specific lethal genes were defined as those shRNAs that were significantly underrepresented in GSC cultures relative to NSC control cultures.

The nucleic acid-binding gene screen, which was performed in a single GBM isolate (G166 cells) along with NSC controls, yielded 27 genes as candidate GBM-lethal hits. Retests of each screen hit were performed using multiple single-shRNA viral clones. Seven genes (26% of candidates) met our validation criteria of two or more single hairpin clones that produced a growth ratio of <0.65 in GSCs cells compared with NSCs with a *P*-value <0.05 after 7 d of outgrowth (Fig. 1B; Supplemental Fig. 1a). Significantly, knockdown of the gene PHF5A was strongly indicated as the top hit affecting in vitro expansion of GSC-G166 cells (Fig. 1B; Supplemental Fig. 1a). To ensure that the results were applicable to other GBM tumors and that hits would score similarly when comparing the entire genome, we also performed genome-wide shRNA screens in multiple GSC isolates from three different GBM patients that represented two developmental subtypes (G166, mesenchymal; 0131, mesenchymal; 0827, proneural), again in triplicate with NSCs as controls. This approach yielded GSC screen hits that were mainly isolate-specific, likely owing to different tumor backgrounds and heterogeneity in cell populations during expansion (Fig. 1C). However, there were 17 candidate lethal genes shared by each GSC isolate that did not score in NSCs; PHF5A was among these genes (Fig. 1C).

It should be noted that identifying genes that, when inhibited, affect growth of GSCs more than NSCs is unusual. We found that most perturbations in pathways required for cell growth or cell cycle progression (e.g., PI3K pathway, Aurora A and B kinases, heat-shock protein 90, and the microtubule motor protein KIF11/Eg5) (Ding et al. 2013; data not shown) either show no differential effect between NSCs and GSCs or affect NSCs more than GSCs.

PHF5A is a highly conserved PHD-zinc finger domain protein that facilitates interactions between the U2 snRNP complex and DNA/RNA helicases (Rzymski et al. 2008). PHF5A may also bind to chromatin through its PHD domain (Trappe et al. 2002), which, in other PHD family members, can facilitate interactions with specific histone marks on chromatin-bound nucleosomes (Mellor 2006; Musselman and Kutateladze 2009). Consistent with this

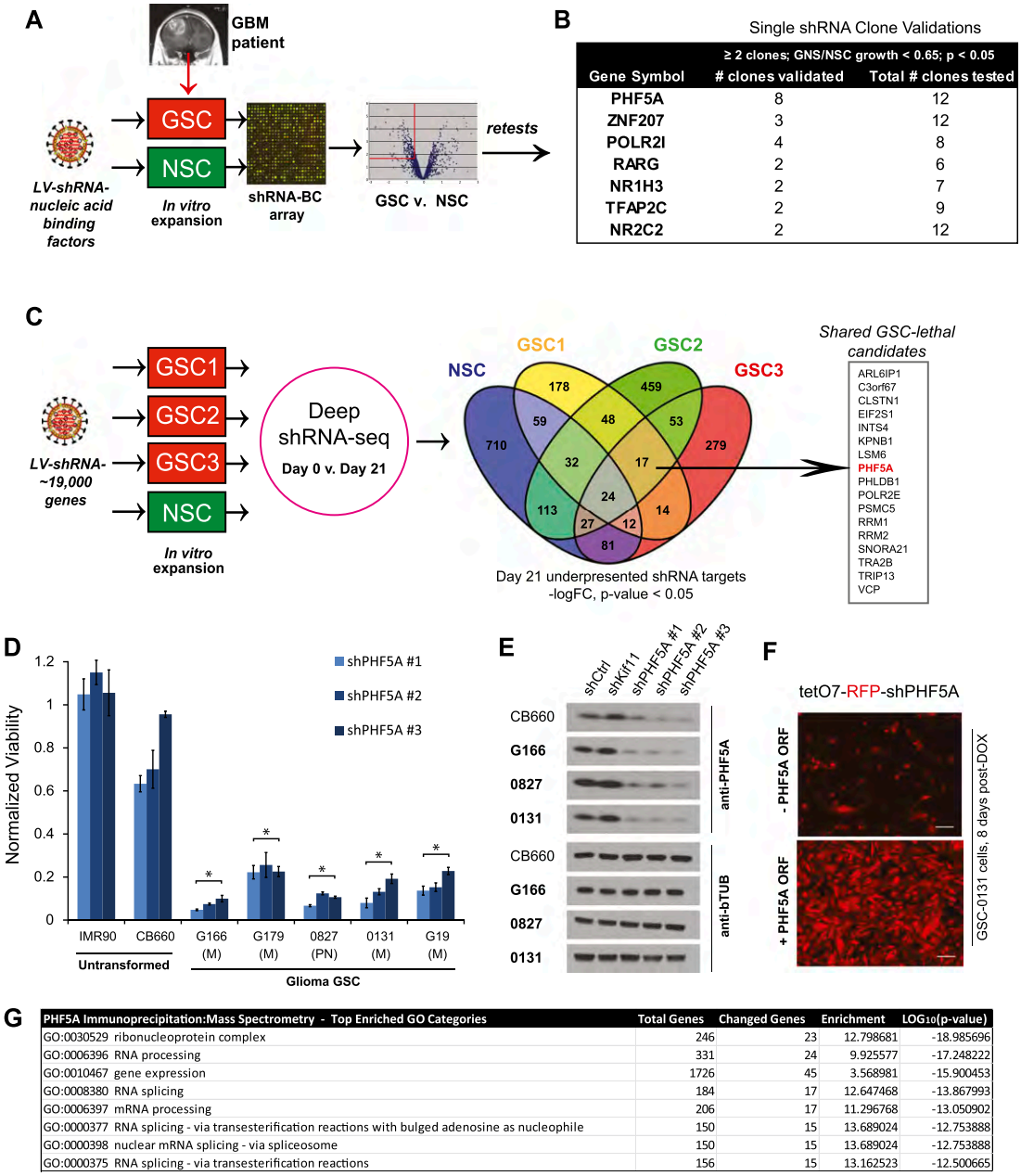

G

PHF5A Immunoprecipitation:Mass Spectrometry - Top Enriched GO Categories	Total Genes	Changed Genes	Enrichment	LOG10(p-value)
GO:0030529 ribonucleoprotein complex	246	23	12.798681	-18.985696
GO:0006396 RNA processing	331	24	9.925577	-17.248222
GO:0010467 gene expression	1726	45	3.568981	-15.900453
GO:0008380 RNA splicing	184	17	12.647468	-13.867993
GO:0006397 mRNA processing	206	17	11.296768	-13.050902
GO:0000377 RNA splicing - via transesterification reactions with bulged adenosine as nucleophile	150	15	13.689024	-12.753888
GO:0000398 nuclear mRNA splicing - via spliceosome	150	15	13.689024	-12.753888
GO:0000375 RNA splicing - via transesterification reactions	156	15	13.162523	-12.500665

Figure 1. Functional genetic screens identify PHF5A as differentially required for GSC expansion. (*A*) The shRNA screening approach used to initially identify PHF5A as differentially required for GSC expansion. Pooled viruses targeting nucleic acid-binding factors were used in outgrowth screens in human GSC-G166 and NSC-CB660 cells. Candidate genes differentially required for GSC expansion over 21 d of outgrowth were identified through hybridization of viral DNA barcodes to custom microarrays. (*B*) Average differential between GSCs and NSCs for shRNA clones targeting candidate screen hits by in vitro competition assay. Cells infected with single shRNA clones (GFP^+) were mixed with uninfected cells and outgrown for 10 d, and the change in GFP^+ cells in each culture was quantified by FACS analysis. (*C*) Our genome-wide shRNA screening strategy used in NSC-CB660 and three primary GSC isolates. Viral shRNA pools targeting ~19,000 human genes were infected into cells prior to 21 d of outgrowth in vitro. The change in viral shRNA representation in each cell population was quantified by sequencing. Gene targets statistically underrepresented at the end of the culture period are shown. (*D*) Viability of NSCs and five GSC isolates infected with three independent shRNA viral clones targeting PHF5A. (M) Mesenchymal subgroup; (PN) proneural subgroup; (*) *P*-value < 0.002 vs. CB660. (*E*) Western blot analysis of PHF5A protein expression in NSCs and GSCs after PHF5A knockdown. (*F*) Images of GSC-0131 cell clones expressing an inducible shRNA construct targeting the endogenous 3′ UTR of PHF5A, with or without rescue by exogenous expression of full length PHF5A. Bar, 50 μm. (*G*) PHF5A was immunoprecipitated from cellular lysates, and associated binding proteins were analyzed by mass spectrometry. The gene ontology (GO) categories most enriched among PHF5A-bound proteins are presented. See also Supplemental Figure S1.

latter notion, PHF5A protein was found to be an enhancer of estrogen-mediated transcription of the Connexin 43 gene (Oltra et al. 2003). PHF5A has also been characterized as a member of the SF3b component of the U2 snRNP splicing complex (Will et al. 2002). Since PHF5A was a highly reproducible GSC-specific screen hit, yet nothing is known about a cancer-specific role for PHF5A, we further pursued it as a GBM-lethal target.

PHF5A is differentially required for GSC in vitro expansion

To further confirm differential effects of PHF5A knockdown, we performed short-term outgrowth assays in five primary GSC cultures using multiple shRNAs. In each case, PHF5A knockdown showed a strong, GSC-specific loss of viability (Fig. 1D). Next, we examined the effects of PHF5A knockdown on $SSEA1^+$ GSC subpopulations, which are enriched for tumor-initiating cell activity (Son et al. 2009). In the three different GSC isolates examined, PHF5A knockdown compromised outgrowth of $SSEA1^+$ populations over the course of several weeks (Supplemental Fig. S1b). This indicates that PHF5A suppression blocks gross expansion of GSC isolates, including both the bulk cell population and tumor-initiating GSC subpopulations.

GSCs and NSCs express PHF5A at relatively similar levels, and knockdown is equivalently effective in each cell type at both the RNA and protein levels (Fig. 1E; Supplemental Fig. S1c), indicating that the lack of phenotype in NSCs is not due to inefficient knockdown or major differences in expression. Moreover, PHF5A expression levels were similar in GSCs, NSCs, and other tissues, indicating that GSCs do not abnormally overexpress the gene (Supplemental Fig. S1c). We further performed a complementation assay in which a validated, inducible shPHF5A sequence targeting the PHF5A endogenous 3′ untranslated region (UTR) was coexpressed with the PHF5A ORF lacking its endogenous 3′ UTR. Expression of the PHF5A ORF rescued the growth defect observed in PHF5A knockdown GSCs (Fig. 1F; Supplemental Fig. S1d), indicating that the phenotypic effects are PHF5A-specific.

Furthermore, to query what key roles PHF5A might play in our cells, we examined PHF5A-interacting proteins by coimmunoprecipitation (co-IP) mass spectrometry. This yielded a strong enrichment for candidate interacting proteins involved in splicing (GO:0008380 RNA splicing, $P = 10^{-14}$) as well as gene expression (GO: 0010467 gene expression, $P = 10^{-16}$) (Fig. 1G; Supplemental Table S1).

PHF5A is specifically required for normal exon recognition in GSCs but not NSCs

Because PHF5A has been characterized as both a splicing factor (Will et al. 2002; Rzymski et al. 2008) and a transcriptional regulator (Oltra et al. 2003), we next wished to define which of these activities was most relevant for GBM-specific survival. Recently, Paulsen et al. (2009) found that knockdown of multiple spliceosomal genes in HeLa cells resulted in dsDNA breaks and H2AX phosphorylation. We therefore first examined whether PHF5A knockdown might similarly give rise to DNA damage in GSCs, thereby triggering arrest and growth inhibition. However, upon PHF5A knockdown in GSCs, we did not see an increase in pH2AX levels, phosphorylation of the DNA damage signaling proteins CHK1 and CHK2, or activation of the mitotic spindle checkpoint (Supplemental Fig. S2a). These results suggest that the shPHF5A growth inhibition does not simply arise from a DNA damage response or alterations in the mitotic spindle.

We next hypothesized that PHF5A knockdown might induce GSC-specific aberrant splicing of genes required for cell cycle progression or cell growth. To directly test this hypothesis, we asked whether splicing was globally dysregulated following PHF5A knockdown by performing deep RNA sequencing (RNA-seq) in control NSCs (CB660 cells) and GSCs (G166 and 0827 cells) treated with control or PHF5A-targeting shRNAs. We quantified changes in isoform ratios using only reads that crossed splice sites, an approach that treats all splicing events with equivalent statistical power (Bradley et al. 2012).

This analysis revealed that PHF5A knockdown results in dramatic GSC-specific exon skipping and intron retention events (Figs. 2A; Supplemental Fig. S2b) in hundreds of genes. Other forms of splicing regulation, including selection of competing 5′ and 3′ splice sites and mutually exclusive exon selection, were unaffected (Supplemental Fig. S2b) in both GSCs and NSCs. Most of the resulting GSC-specific splicing changes introduced in-frame stop codons into the mRNAs, strongly suggesting that the splicing changes are aberrant, rather than functionally relevant, splicing (Fig. 2B). Furthermore, the overall expression of GSC mRNAs harboring in-frame stop codons was decreased, consistent with triggering nonsense-mediated mRNA decay (NMD) (Fig. 2B; Amrani et al. 2006).

Only a relatively small subset of splice junctions was affected by PHF5A depletion in GSCs, indicating that the requirement for PHF5A is not universal across exons. To gain mechanistic insight into the origins of the observed splicing dysregulation, we identified specific features characteristic of 5′ and 3′ splice sites susceptible to PHF5A knockdown in GSCs. We could not detect differences in the 5′ splice site features of affected genes (data not shown). 3′ Splice sites associated with abnormal splicing of constitutive junctions had slightly shorter, but otherwise normal, polypyrimidine tracts relative to unaffected 3′ splice sites. In contrast, 3′ splice sites associated with retained constitutive introns had unusual C-rich tracts (Fig. 2C). The retained constitutive introns were short (Fig. 2D) and had unusually proximal branch points (Fig. 2E). While PHF5A is known as a core component of the spliceosome, it appears to be most important for the recognition of an unusual class of exons with distinctive 3′ splice sites. These data suggested that PHF5A primarily functions to facilitate exon recognition rather than regulate alternative splicing, which is consistent with its characterization as a core component of the spliceosome (Will et al. 2002).

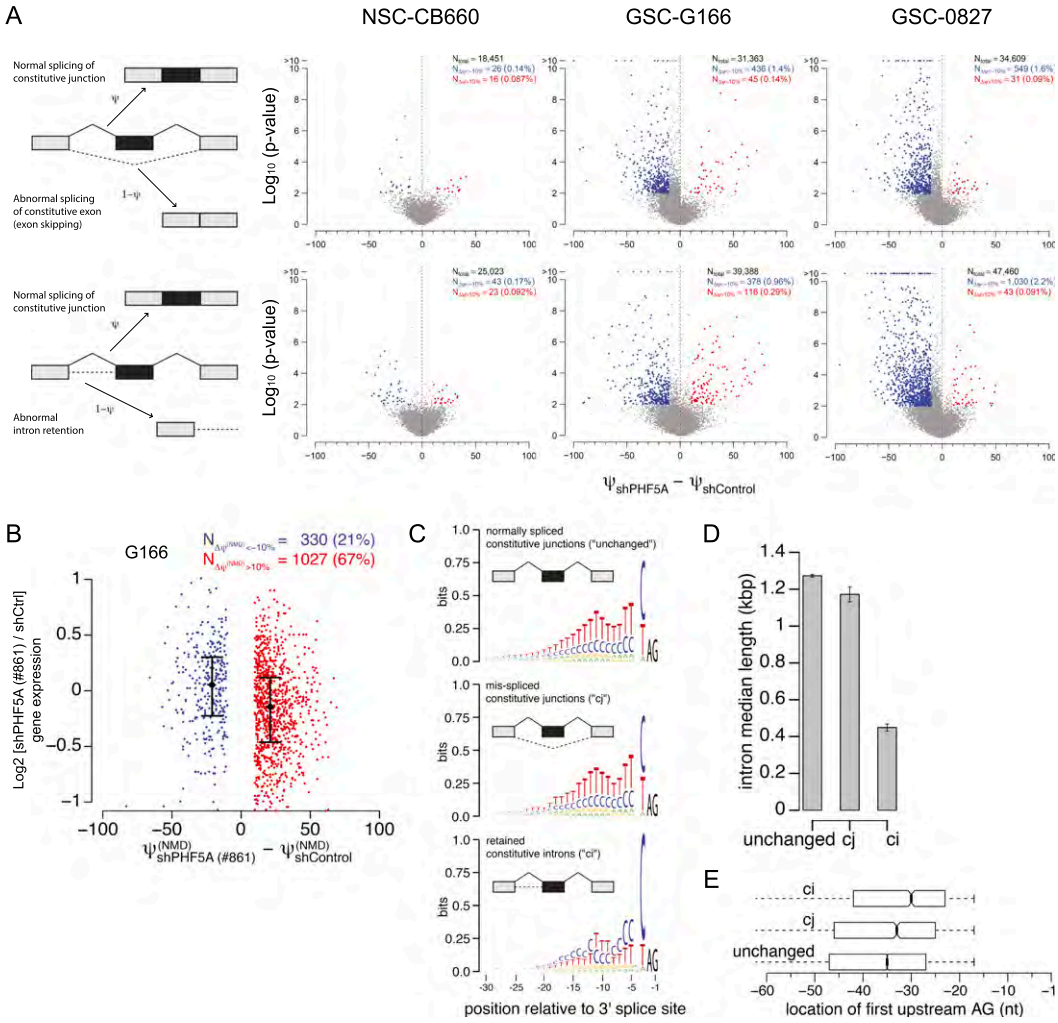

Figure 2. PHF5A is globally required by GSCs for proper recognition of an unusual class of exons. (*A*) In GSCs but not NSCs, PHF5A knockdown causes a dramatic increase in missplicing of constitutive junctions (*top* row) as well as retention of constitutive introns (*bottom* row). (*B*) Many of the splicing changes induced by PHF5A knockdown in GSCs introduce in-frame stop codons, suggesting that the resulting transcripts will be degraded by NMD. Gene expression values were computed with RSEM (Li and Dewey 2011) and normalized with the TMM method (Robinson and Oshlack 2010). Confidence intervals indicate the first and third quartiles of expression. (*C*) Constitutive junctions that are misspliced following PHF5A knockdown in GSCs (*center*) have slightly shorter polypyrimidine tracts than do unaffected constitutive junctions (*top*); in contrast, retained constitutive introns have unusually C-rich polypyrimidine tracts (*bottom*). (*D*) Retained constitutive introns are much shorter. Plot illustrates the median intron length, and error bars indicate the standard error estimated by bootstrapping. (*E*) Retained constitutive introns have branch points that are unusually proximal to the 3′ splice site. Box plots indicate the first and third quartiles of the first upstream AG, a proxy for the branch point location (Gooding et al. 2006). See also Supplemental Figure S2.

Consistent with the GSC-specific growth defect caused by PHF5A knockdown, we observed severe RNA processing defects in many genes important for cell cycle progression, including CDC16, CDC20, CDC25C, CDC37, CDC45, and RCC2, in GSCs (G166 or 0827 cells) but not NSCs (CB660). For example, the 3′-most constitutive exons of CDC20 (Fig. 3A) and many constitutive exons in RCC2 (Supplemental Fig. S3a) were frequently skipped following PHF5A knockdown in GSCs but not in NSCs. In addition, after PHF5A knockdown, multiple constitutive exons of the well-characterized RTK/Ras signaling effector RAF1 and the cancer-associated deacetylase HDAC6 were skipped in GSCs but not in normal NSCs (Fig. 3B).

To further substantiate these results, we examined the effects of two candidate small molecule inhibitors of the U2 snRNP complex: spliceostatin A (SSA) and sudemycin C1 (SudC1). SSA binds to and inhibits the U2 snRNP subunit SF3b, which contains PHF5A, resulting in a reduction in the fidelity of branch point recognition and a down-regulation of genes important for cell division. (Kaida et al. 2007; Corrionero et al. 2011). SudC1 shares the consensus pharmacophore of SSA and pladienolide (Kotake et al. 2007) and also modulates RNA splicing (Lagisetti et al. 2008, 2009; Fan et al. 2011). We reasoned that if the most relevant GSC-specific function of PHF5A is its function in the splicing activity of the U2 snRNP,

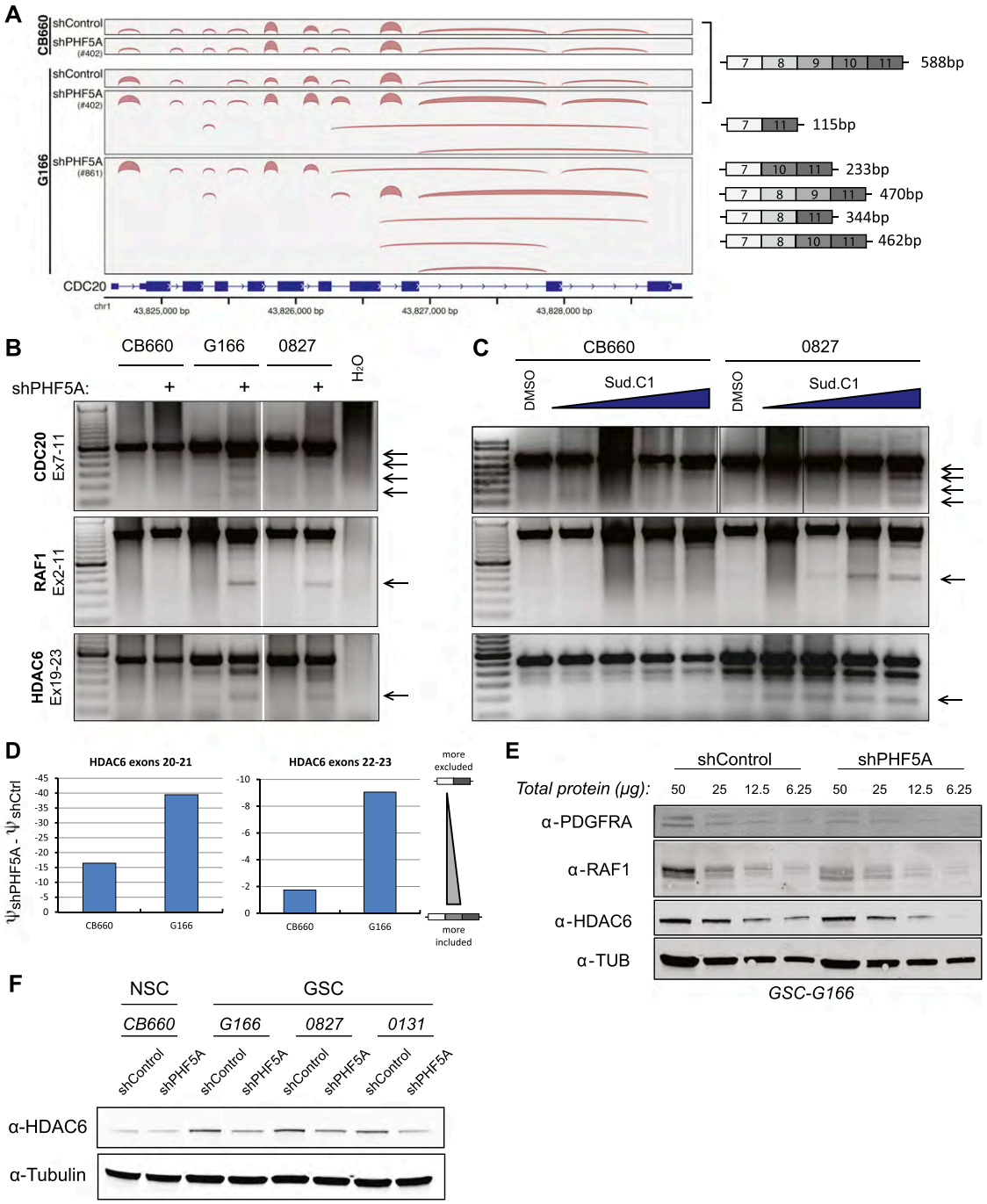

Figure 3. Loss of PHF5A results in splicing defects in GSCs but not NSCs. (*A*) Select genes important for cell cycle progression, such as CDC20, display broad splicing defects following PHF5A knockdown. Plot illustrates the density of RNA-seq reads crossing splice junctions and was created with IGV (Robinson et al. 2011). Aberrant isoforms lacking constitutive exons appear following knockdown of PHF5A with two distinct shRNAs. cDNA base pair sizes indicate the expected product size of each isoform using the cdc20 primers indicated in *C* and *D*. (*B*) RT–PCR of RNA isoforms of example genes after PHF5A knockdown. PCR products were generated using primers in the indicated exons of each gene. Arrows indicate splicing products specifically induced in GSCs after PHF5A knockdown. (*C*) RT–PCR as in *B* using RNA from cells treated for 24 h with 0.5, 1, 2, or 4 μM SudC1. (*D*) qRT–PCR using primers designed to specifically recognize the splice junctions between consecutive and nonconsecutive exons was performed to determine ψ-values for inclusion of potentially skipped exons in HDAC6 identified *above*. The change in inclusion rate after PHF5A knockdown is presented. (*E*) Serial dilutions of GSC lysate with or without PHF5A knockdown were run as Western blots and probed with antibodies specific to example genes with predicted missplicing events. (*F*) Western blot of GSCs and NSCs with or without PHF5A knockdown probed for levels of the frequently misspliced protein HDAC6. See also Supplemental Figure S3.

then these drugs should show a similar pattern of effects on RNA splicing in GSCs and NSCs. This was indeed the case. Treatment of GSCs with SudC1 resulted in dose-dependent GSC-specific splicing defects (Fig. 3C). Finally, we compared the changes in inclusion of identified skipped exons in the example gene HDAC6 after PHF5A knockdown using quantitative RT–PCR (qRT–PCR) primers designed to span potential consecutive and nonconsecutive exon splice junctions in the mature RNA isoforms. As predicted by the data above, this quantitatively demonstrated greater exclusion of tested exons from mature RNA transcripts in GSCs compared with normal NSCs (Fig. 3D).

If these aberrant mRNAs are translated, they would produce C-terminally truncated proteins. We therefore investigated the effects of PHF5A knockdown on the protein levels of these example genes. As predicted, the protein level of PDGFRA, RAF1, and HDAC6 decreased in knockdown cells (Fig. 3E,F), likely due to effects of NMD (Fig. 2B) and altered protein stability. This severe dysregulation of multiple growth regulatory and essential cell cycle genes in GSCs, but not NSCs, suggests that aberrant splicing in GSCs following PHF5A knockdown may give rise to GBM-specific growth defects and inviability.

Taken together, these results indicate that PHF5A is important for proper recognition of a specific, relatively small class of exons in GSCs. Knockdown of PHF5A causes defective RNA processing of thousands of genes, a subset of which are essential for cell cycle progression. Given the broad splicing dysregulation that we observed, there are likely to be numerous cellular defects induced by PHF5A knockdown that contribute to the observed GSC inviability. This model is consistent with our observation that multiple methods of inhibiting U2 snRNP activity—including knockdown of other spliceosomal genes (below) as well as SudC1 treatment—mimic the effects of PHF5A knockdown even though these distinct perturbations are unlikely to lead to identical defects in RNA processing.

PHF5A-binding partners involved in RNA splicing are also differentially required by GSCs and, when inhibited, trigger GSC-specific G2/M cell cycle arrest

Because PHF5A may play multiple cellular roles (Will et al. 2002; Oltra et al. 2003; Rzymski et al. 2008) and its cellular functions are poorly characterized, we next wished to define whether its splicing role was its critical function in GBM cell survival. To this end, we analyzed knockdown of two PHF5A-binding partners in the spliceosome, U2AF1 and DDX1, which interact with the PHF5A C-terminal and N-terminal domains, respectively (Rzymski et al. 2008). U2AF1 is a key member of the U2 snRNP, which is required for RNA branch point recognition (Kramer 1996; Jurica and Moore 2003), and DDX1 is an ATP-dependent DEAD-box RNA helicase (Fang et al. 2005). Knockdown of either U2AF1 or DDX1 phenocopied PHF5A knockdown in GSCs (Fig. 4A). Moreover, a comprehensive examination of multiple shRNAs against PHF5A and U2AF1 in short-term growth assays showed the same strong trend of requirement of these genes in GSCs but not NSCs (Fig. 4B). These results suggest that the PHF5A function most relevant for GSC-specific viability is associated with its role in splicing and the U2 snRNP complex. Supporting this hypothesis, our examination of PHF5A-interacting proteins by co-IP mass spectrometry yielded a strong enrichment for candidate interacting proteins involved in splicing, especially the U2 snRNP complex, including U2AF1, U2AF2, and multiple DDX/DHX helicase family members (Fig. 1G; Supplemental Table S1).

A striking feature of PHF5A depletion in GSCs was that, preceding widespread GSC cell death, PHF5A knockdown triggered a dramatic cell cycle arrest that resembled the rounded-up phenotype of kinesin motor protein KIF11 knockdown (Sawin et al. 1992), our nonspecific cell-lethal control (Fig. 4C). MPM-2 staining, indicative of CyclinB/CDK activity, dramatically increased in PHF5A knockdown GSCs, confirming mitotic arrest (Fig. 4C [inset], D). Moreover, DNA content analysis showed a pronounced increase in the percentage of G2/M cells in GSCs, but not NSCs or normal fibroblasts, with PHF5A knockdown (Fig. 4E).

Further examination of GSC PHF5A knockdown G2/M-arrested cells showed condensed chromatin and monopolar or multipolar spindles (Supplemental Fig. S4a). Along with high MPM-2 staining and little or no phophosphorylated BubR1, this is consistent with a preanaphase arrest in which the mitotic checkpoint has not been triggered. Consistent with the requirement for U2snRNP activity, treatment of GSCs with SSA or SudC1 resulted in a greater dose-dependent viability loss in GSCs relative to NSCs (Fig. 4F; Supplemental Fig. S4b) and also resulted in the characteristic cell cycle arrest in GSCs but not NSCs at doses within this efficacy window (Fig. 4G).

To better characterize GSC-specific G2/M arrest, we performed metaphase capture assays in H2B-GFP-expressing GSCs treated with the proteasome inhibitor MG132, which arrests mitotic cells at metaphase, blocking APC^{Cdc20}-dependent degradation of Cyclin B (Lampson and Kapoor 2005). After overnight exposure to SudC1 or SSA, cells were treated with MG132 for 2 h. Control cells displayed proper enrichment for metaphase cells, with chromosomes aligned along the metaphase plate (Fig. 4H). However, SSA- or SudC1-treated cells were unable to properly arrest, further suggesting a premetaphase arrest (Fig. 4H). Similarly, live-cell imaging of GSC-H2B-GFP cells treated with SudC1 or SSA showed mitotic arrest premetaphase (Supplemental Movies 1–3). We also observed that the viability loss in drug-treated GSC cultures results from the death of previously arrested mitotic cells and not interphase GSCs, identifying the cancer-specific mitotic arrest as a causative event in cancer cell death due to splicing inhibition. A fraction of arrested GSCs were able to survive by progressing through mitosis after arresting, but these cells displayed disorganized, multilobed nuclei and were not observed to successfully divide again (Supplemental Movies 2, 3).

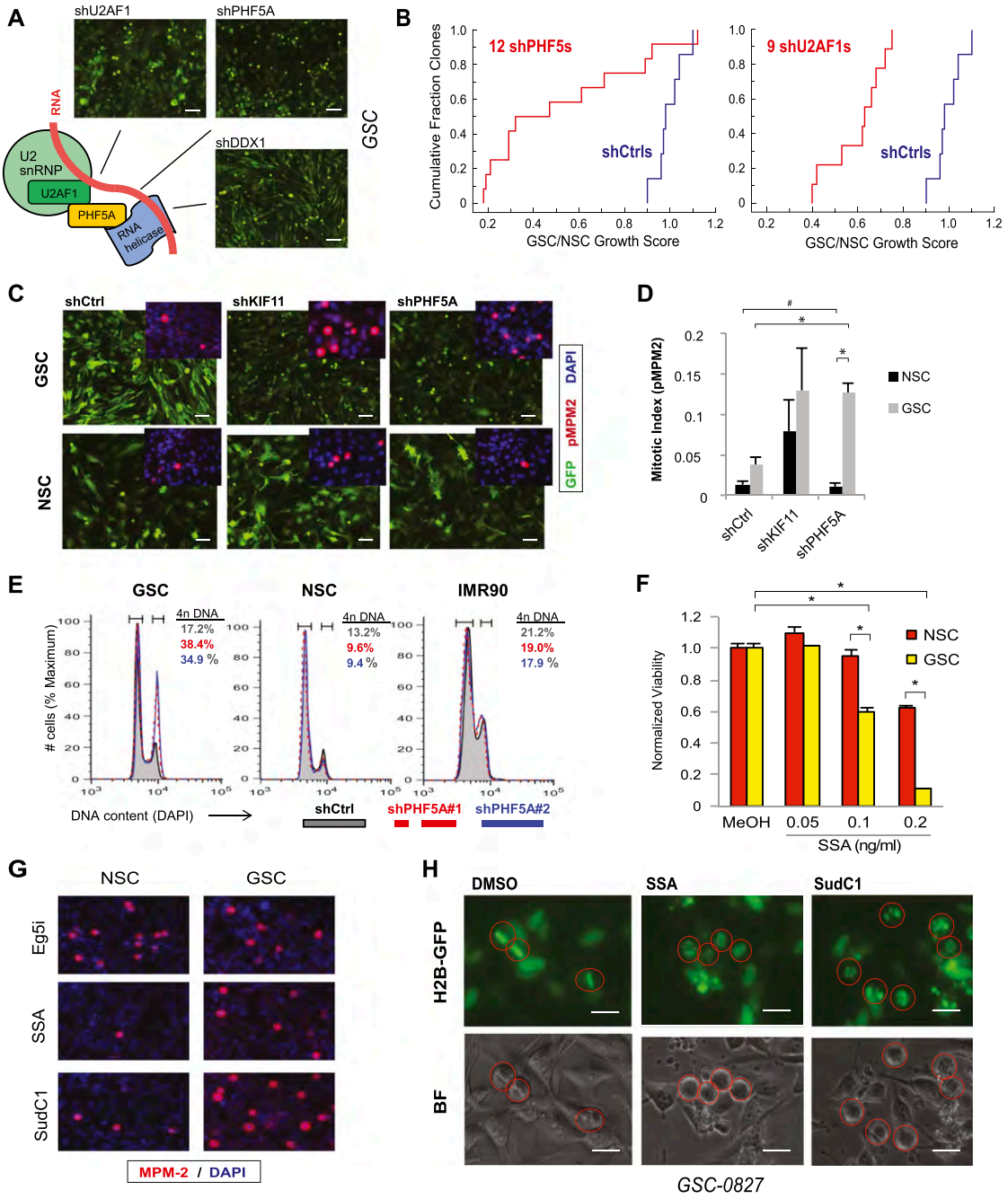

Figure 4. PHF5A and its binding partners are differentially required for GSC expansion, and their inhibition triggers G2/M cell cycle arrest in GSCs but not NSCs. (*A*) Model of PHF5A splicing interactions based on previous research. Knockdown of known PHF5A-binding partners in the spliceosome recapitulates the PHF5A knockdown phenotype, shown. Bar, 50 µm. (*B*) Cumulative probability plot of multiple shRNAs scoring as cell-lethal versus their GSC to NSC viability ratio. (*C*) Fluorescence microscopy images of GSCs or NSCs expressing constitutive GFP and PHF5A knockdown or control constructs. (*Inset*) Immunofluorescent images of phospho-MPM2, indicative of mitotic activity, in GSCs and NSCs depleted for PHF5A. Bar, 100 µm. (*D*) Quantification of phospho-MPM2 staining in GSCs and NSCs infected with control or shPHF5A virus. (*) *P*-value < 0.001; (#) insignificant *P*-value = 0.5. (*E*) Cellular DNA content as measured by DAPI staining and FACS analysis in GSC, NSC, and IMR90 normal fibroblast cultures with or without PHF5A knockdown. The percentage of cells in each sample with 4n DNA content is shown, indicative of cells that have completed DNA replication in S phase. (*F*) Viability of GSCs or NSCs treated with increasing doses of SSA. (*) *P*-value < 0.0003. (*G*) Immunofluorescent images of phospho-MPM2 in GSCs and NSCs treated with SSA or SudC1. (*H*) Fluorescent and light images of GSCs expressing Histone 2B-GFP fusion protein, which marks DNA. Cells were pretreated with SSA or SudC1 for 22 h before addition of MG132 for an additional 2 h to arrest dividing cells in metaphase. Circles mark the same cell in corresponding images. See also Supplemental Figure 4 and Supplemental Movies S1–S3.

Taken together, the above results establish that PHF5A and U2 snRNP complex activity are differentially required for GSC viability compared with NSCs, and their activity is necessary for GSC but not NSC transit through premetaphase mitosis. Moreover, because treatment of GSCs with SSA or SudC1 did not affect the timing of mitoses for several hours after drug treatment (Supplemental Movies 2, 3), it is unlikely that PHF5A and U2 snRNP activity are directly required for mitotic progression.

Overexpression of MYC recapitulates GSC sensitivity to splicing inhibition

We next wished to determine the possible mechanism by which GSCs become differentially sensitive to inhibition of PHF5A and U2 snRNP activity. One possibility was that the process of cellular immortalization or oncogenic transformation itself resulted in splicing dysregulation. To test this possibility in the context of our normal NSCs, we investigated the expression of multiple human genes known to be involved in cellular transformation (Kendall et al. 2005) and that mimic pathway aberrations frequently found in GBM (Parsons et al. 2008; The Cancer Genome Atlas Research Network 2008). Specifically, we used expression of hTERT, dominant-negative $p53^{DD}$, CyclinD1, $CDK4^{R24C}$ (p16-resistant), H-RasV12, and MYC either alone or in combination in NSC-CB660 cells and tested the sensitivity of the resulting cell lines to the SF3b inhibitors pladienolide B (Kotake et al. 2007) and SudC1. That the p53 pathway (i.e., $p53^{DD}$) and the Rb axis (i.e., CyclinD1 and $CDK4^{R24C}$) were functionally impacted was noted by virtue of the fact that only combined expression of $p53^{DD}$, CyclinD1, and $CDK4^{R24C}$ was sufficient to bypass RasV12-induced senescence in human NSCs (Supplemental Fig. S5a; data not shown).

Using this platform, we found that expression of MYC alone in NSCs is sufficient to induce sensitivity to U2snRNP perturbation observed in primary GSC cultures

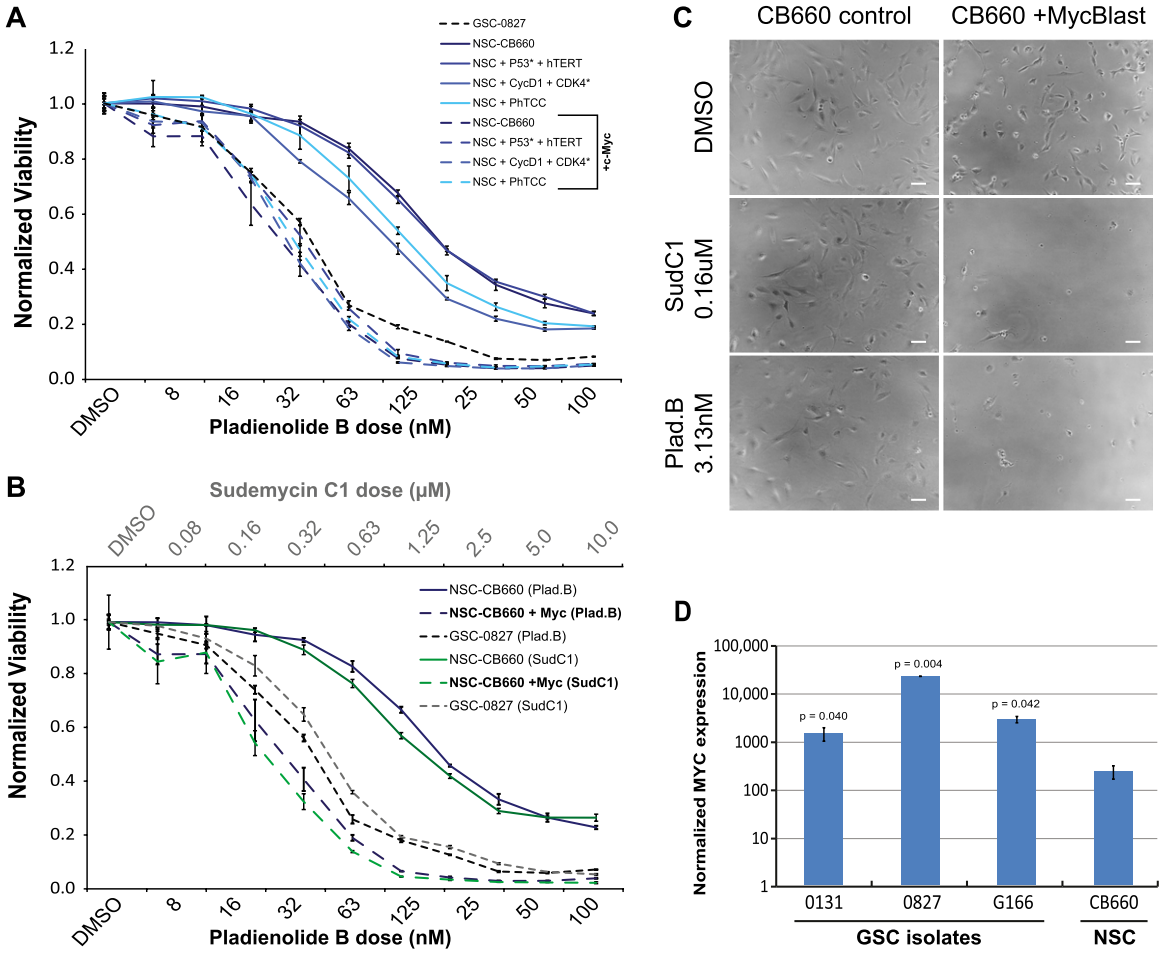

Figure 5. MYC expression in NSCs recapitulates GSC sensitivity to splicing inhibition. (*A*) Viability of NSCs with or without expression of hTERT, $p53^{DD}$, CyclinD1, $CDK4^{R24C}$, and/or MYC after treatment with pladienolide B. (*B*) Viability of NSCs with or without MYC expression after treatment with SudC1 (*top X*-axis) or pladienolide B (*bottom X*-axis). (*C*) Micrographs of normal CB660 NSCs with or without MYC expression after treatment with the indicated splicing inhibitors. Bar, 64 μm. (*D*) Log graph of MYC levels in GSCs and NSCs as determined by RNA-seq (fragments per kilobase of exon per million reads mapped [FPKM] normalized; $n = 3$) (Ding et al. 2013). *P*-values were determined by Student's *t*-test. See also Supplemental Figures S5 and S6.

(Fig. 5A,B). In each experiment, dramatic cell death was observed at doses not lethal to the parent CB660 cells (Fig. 5C). We further validated this effect in fibroblasts (Supplemental Fig. S5d) and also using two NSC lines immortalized through MYC expression (CX and VM) (Donato et al. 2007) versus two primary NSCs (one embryonic and one adult-derived) without exogenous MYC (Supplemental Fig. S5e). Moreover, we observed that our GSC isolates show higher expression of MYC mRNA than NSCs (Fig. 5D).

In addition, we found that RasV12 expression alone could also sensitize NSCs, normal human astrocytes, or fibroblasts to PHF5A/U2snRNP perturbation (Supplemental Figs. S5c,e, S6) but did not synergize with MYC expression (Supplemental Fig. S5c). Moreover, the activated MEK allele could partially sensitize cells (Supplemental Fig. S5e). Both results are consistent with the notion that MYC is a downstream target of the Ras pathway by multiple pathways, including ERK and GSK-3 (Sears et al. 2000). Taken together, these results are consistent with recent observations regarding brain tumor-associated MYC activity. For example, concomitant loss of PTEN and p53, two of the most frequently mutated genes in GBM tumors, activates MYC (Zheng et al. 2008a,b), and MYC activity contributes to maintenance of tumor-initiating capacity in mouse and human models of GBM (Wang et al. 2008; Zheng et al. 2008b). The results suggest that inappropriate MYC activity in GBM tumors can give rise to molecular vulnerabilities in PHF5/U2snRNP function. However, future work will need to determine just how MYC function can impact the integrity of 3′ splice site recognition. However, these results raise the possibility that a wide range of MYC- and/or Ras-driven cancer may be vulnerable to PHF5A/U2snRNP inhibition.

Suppression of PHF5A expression compromises GBM tumor formation and maintenance in vivo

Finally, we wished to test whether PHF5A expression was required for GBM tumor formation and maintenance in vivo. To examine tumor formation, we devised an in vivo competition experiment to directly test the proliferative effects of PHF5A suppression in an orthotopic xenograft model of glioblastoma. GSCs were infected with GFP-expressing shPHF5A or shCtrl virus and then mixed with 10% ChFP-expressing control cells. This cell mixture was then either grown in adherent culture or xenografted into the cortex of immunocompromised mice (Supplemental Fig. S7a). Whereas shCtrl cells were able to proliferate and maintain their representation in culture, shPHF5A cells began to exhibit characteristic cell cycle arrest within 2 d of xenograft and were almost completely replaced by ChFP$^+$ control cells within 2 wk (Supplemental Fig. S7b). Likewise, orthotopically xenografted GFP$^+$ shCtrl GSCs were able to proliferate in vivo, whereas GFP$^+$ shPHF5A GSCs were unable to proliferate and meaningfully contribute to in vivo tumor growth (Fig. 6A). The small fraction of coinjected ChFP$^+$ control GSCs were able to engraft and give rise to tumors in every case, and ChFP expression mirrored bulk tumor mass as marked by the Chlorotoxin:Cy5.5 conjugate Tumor Paint (CTX:Cy5.5) (Veiseh et al. 2007). This underscores that expression of PHF5A shRNA was the key determinant in whether GSCs could contribute to tumor growth.

We next wished to examine whether PHF5A inhibition in established tumors could compromise tumor maintenance, a key metric in evaluating potential therapeutic avenues. To this end, we generated xenograft mice bearing GSC tumors with doxycycline (Dox)-inducible PHF5A shRNA (Fig. 1F; Supplemental Fig. S1d) or control shRNAs. Tumors were allowed to grow to ~75 mm^3 in size prior to the start of continuous Dox treatment. Whereas control shRNA tumors showed no measurable difference in growth rate upon Dox treatment (Fig. 6B), shPHF5A tumor growth arrested upon Dox administration, and tumors diminished until they were nearly undetectable (Fig. 6C). The onset of this growth arrest corresponded to greatly increased phosphorylation of Histone H3-S10 (Supplemental Fig. S7c,d) indicating a G2/M cell cycle arrest similar to that seen in vitro for shPHF5A-treated GSCs.

Since the above tumor studies were carried out in mouse flanks rather than the brain where GBM arises, we finally asked whether brain-derived, GSC-driven tumors would respond to PHF5A suppression as well. To test this, we xenografted GSCs bearing Dox-inducible PHF5A shRNA into the right cortex of immunocompromised mice. After 52 d, the first mouse showed initial mild symptoms of a brain tumor. CTX:Cy5.5 imaging after sacrifice confirmed a tumor signal in the right cortex (Fig. 6D, inset). We therefore randomized the remaining mice into Dox-treated and vehicle control cohorts and followed their survival over time. Survival was significantly improved by PHF5A suppression in the Dox-treated cohort (P = 0.0006), to the point where, at the conclusion of the study, when all vehicle-treated mice had succumbed to their tumors, 100% of Dox-treated mice were alive and free of symptoms (Fig. 6D). We conclude that PHF5A inhibition compromises both GBM tumor formation and maintenance, suggesting that PHF5A/U2snRNP inhibition may be an effective therapy for GBM.

Discussion

Here, we performed parallel shRNA screens during in vitro expansion of human GSCs and NSCs to identify novel gene activities required for growth and viability of patient-derived GSCs but not normal NSCs. Despite observing a high degree of GSC isolate-specific variation in the screening results, we identified PHF5A as differentially required for expansion of all GSCs examined. PHF5A is a highly conserved PHD-zinc finger domain protein that facilitates interactions between the U2 snRNP complex and ATP-dependent helicases (Rzymski et al. 2008). In vitro assays established that PHF5A activity was required for G2/M progression in GSCs but not NSCs. Consistent with a role in GSC-specific splicing phenomena, knockdown of other U2 snRNP complex members or pharmacological inhibition of U2 snRNP

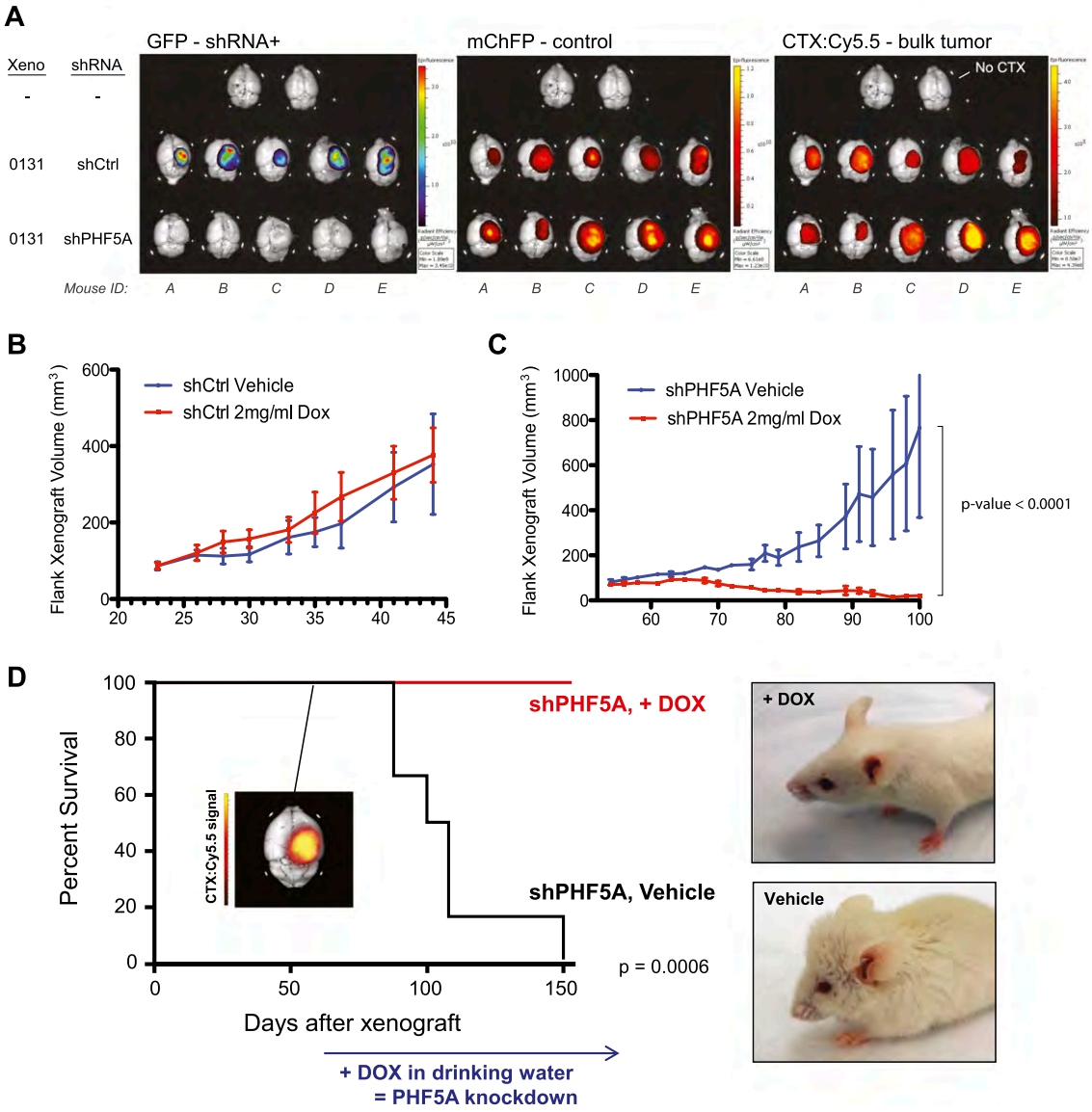

Figure 6. Suppression of PHF5A expression compromises GBM tumor formation and maintenance in vivo. (*A*) Fluorescence overlay images of in vivo competition mouse brains 5 wk after xenograft. In addition to GFP and ChFP signal, CTX:Cy5.5 (Tumor Paint) was used to mark total tumor mass. (*B*,*C*) Flank xenograft volume over time of GSC-0131 clones expressing Dox-inducible PHF5A shRNA or control (Ctrl) shRNA. Tumors were allowed to progress in the absence of Dox until the tumor volume of each cohort averaged ~75 mm^3. Mice were then randomized onto continuous Dox or vehicle treatment, and tumor volume was monitored over time. (*D*) Kaplan-Meier analysis of mice bearing brain xenografts of Dox-inducible PHF5A knockdown GSCs. (*Inset*) At the first sign of symptoms in the first mouse (day 52; CTX:Cy5.5 image) mice were randomized onto continuous Dox or vehicle treatment, and survival was monitored over time. Photographs of representative mice from each cohort are shown. See also Supplemental Figure S7.

activity both phenocopied PHF5A knockdown. Furthermore, PHF5A knockdown triggered defective splicing of thousands of essential genes, including many important for mitotic progression (e.g., CDC20). Examination of affected splice sites revealed a specific requirement for PHF5A in recognition of 3′ splice sites with C-rich polypyrimidine tracts in GSCs. Moreover, modeling experiments in MYC- and RasV12-expressing NSCs and fibroblasts suggested that oncogenic signaling gives rise to the added requirement for PHF5A and U2 snRNP activity. Finally, in vivo tumor experiments suggested that PHF5A is required for generation and, more importantly, maintenance of GBM tumors. Taken together, our results support a model whereby oncogenic signaling leading to increased MYC activity triggers enhanced reliance on PHF5A/U2snRNP to properly recognize a subclass of 3′ splice sites.

Our results provide new insight into cancer-specific RNA splicing phenomena. Oncogene-associated activities (e.g., MYC, AKT, and Ras) can alter splicing of select genes, including pyruvate kinase (Clower et al. 2010; David et al. 2010), caspases (Shultz et al. 2010), and CD44

(Weg-Remers et al. 2001), to promote tumor formation or growth. Our results provide two important contrasts to these findings. First, while previous examples of cancer-associated splicing events can be largely explained by the activity of canonical splicing regulators on individual substrates, our results indicate that fundamental aspects of 3′ splice site recognition are modulated by transformation. In particular, the GSC-specific reliance on PHF5A suggests that basal spliceosome composition may differ between normal and transformed cells. Therefore, many cancer-associated changes in splicing may be inherently global, rather than specific, phenomena. Second, the many reports of cancer-promoting protein isoforms suggest that splicing can confer tumor robustness. However, our findings suggest a different model, wherein splicing is a source of tumor vulnerability due to "fragile" recognition of specific subclasses of exons.

Future studies are required to define just how this vulnerability might arise in GBM and other transformed cells. One possibility is that oncogenic signaling leads to direct perturbation of U2 snRNP activity by affecting complex assembly, activity, turnover, nuclear localization, and/or coordination with transcription (for review, see Heyd and Lynch 2011). As many splicing factors have complementary or compensatory activity and also participate in feedback loops to maintain cellular homeostasis, one attractive model is that transformation disrupts expression of spliceosomal proteins that normally complement PHF5A's role. A related question is how MYC activity gives rise to PHF5A/U2snRNP sensitivity. MYC is known to affect the expression of specific splicing factors (David et al. 2010; Das et al. 2012), which can alter ratios of spliced isoforms of genes such as pyruvate kinase (David et al. 2010). However, with regard to 3′ splice site recognition and U2snRNP function, it is unclear whether MYC activity has a direct role in causing a perturbation or does so indirectly, for example, by perturbing regulatory pathways that in turn might affect splicing fidelity (e.g., protein turnover/degradation).

Another key question arising from our studies is whether PHF5A and U2 snRNP represent reasonable therapeutic targets for GBM. One notable benefit of targeting their activity is that partial inhibition simultaneously affects the splicing of thousands of essential genes. For the vast majority of affected genes, the resulting isoforms contain in-frame stop codons, resulting in either degradation by NMD or translation of aberrant truncated proteins. Therefore, targeting PHF5A or U2 snRNP leads to partial or complete loss of function for many essential genes, collectively causing loss of viability. For example, the observed arrest phenotype is likely due to simultaneous dysregulation of many genes required for cell cycle progression (CDC16, CDC20, CDC25C, CDC37, CDC45, RCC2, etc.) rather than abrogation of a single "target" gene's activity. In contrast to the yeast *cef1-13* example—where the arrest phenotype was rescued by removal of a single misspliced intron in α-tubulin (Burns et al. 2002)—mutations affecting just one of the thousands of dysregulated splice sites are highly unlikely to rescue GSCs. As a result, targeting PHF5A/U2 snRNP may have an advantage over current targeted therapeutic strategies focused on inhibiting the activities of single oncogenic drivers (e.g., EGFR, RAF1, AKT, etc.), which cancer cells can circumvent through mutation or up-regulation of parallel or downstream pathway components. Moreover, classes of synthetic and natural compounds already exist that inhibit U2 snRNP activity (e.g., Pladienolide B, SudC1, and SSA). The natural product splicing modulators were originally identified on the basis of anti-cancer activity in vitro and in vivo (Nakajima et al. 1996; Mizui et al. 2004; Kaida et al. 2007; Kotake et al. 2007), and at least one derivative has entered clinical trials for solid tumors (NCT00499499). Our results suggest that further investigation of this family of compounds may be beneficial for GBM as well as a variety of other MYC- and Ras-driven cancers.

In summary, this study establishes that patient-derived GSCs are vulnerable to perturbation in recognition of a subclass of 3′ splice sites, which results in a reduction in GSC viability and loss of GBM tumor maintenance. Since standard of care therapies are ineffective against GBM, we proffer that targeting PHF5A and/or U2 snRNP activity may offer a new therapeutic inroad for this cancer.

Materials and methods

Pooled shRNA barcode screens and analysis

For both the focused and genome-wide RNAi screens, GSCs or NSCs were infected with pooled GIPZ lentivirus (Open Biosystems) at a multiplicity of infection (MOI) <1 and selected with puromycin (Sigma) to remove uninfected cells. Cells were propagated in culture for an additional 21 d, during which time a minimal representation of 1000-fold per replicate was maintained. For each corresponding sample, shRNA barcodes (for microarray or one-half hairpin for deep shRNA sequencing) were PCR-recovered from genomic DNA samples. The change in the relative abundance of each shRNA in the library over time was measured using the normalized Cy3/Cy5 ratio of its probe signal or sequence counts. Barcode probes depleted in the GSC samples were considered candidate screen hits. Hits from the genome-wide screens were further filtered based on cellular expression as measured by RNA-seq.

Additional methods can be found in the Supplemental Material.

Acknowledgments

We thank Stephen Tapscott, Bruce Clurman, and Valeri Vasioukhin for critical reading of this manuscript; Minoru Yoshida, Howard Fine, Russell Pieper, Do-Hyun Nam, Yoshihiko Kotake, and Austin Smith for providing cell lines and/or reagents; Stacey Hansen, Kyle Pedro, and Sally Ditzler for technical help; Pam Lindberg and Laima Abele for administrative support; and members of the Paddison and Olson laboratories for helpful discussions. This work was supported by Fred Hutchinson Cancer Research Center institutional funds (P.J.P. and R.K.B.) and grants from AACI Translational Cancer Research Fellowship (to Y.D.), Accelerate Brain Cancer Cure (to P.J.P.), Damon Runyon Cancer Research Foundation (DFS 04-12 to R.K.B.), Department of Defense Translational New Investigator Award CA100735 (to P.J.P.), National Cancer Institute/National Institutes of Health (NCI/NIH) (R21CA170722-01 and P30CA15704 to P.J.P.; and R01CA155360 , R01 CA135491, and 5R01 CA114567 to J.M.O.),

NIH Interdisciplinary Training in Cancer Research Program (no. T32CA080416 to C.G.H.), the Pew Biomedical Scholars Program (to P.J. P.), a Phi Beta Psi Sorority Cancer Research Grant (to P.J.P.), and U.K.-U.S. Stem Cell Collaboration Development Award (to S.M.P. and P.J.P.).

References

Amrani N, Sachs MS, Jacobson A. 2006. Early nonsense: mRNA decay solves a translational problem. *Nat Rev Mol Cell Biol* **7:** 415–425.

Bao S, Wu Q, McLendon RE, Hao Y, Shi Q, Hjelmeland AB, Dewhirst MW, Bigner DD, Rich JN. 2006a. Glioma stem cells promote radioresistance by preferential activation of the DNA damage response. *Nature* **444:** 756–760.

Bao S, Wu Q, Sathornsumetee S, Hao Y, Li Z, Hjelmeland AB, Shi Q, McLendon RE, Bigner DD, Rich JN. 2006b. Stem cell-like glioma cells promote tumor angiogenesis through vascular endothelial growth factor. *Cancer Res* **66:** 7843–7848.

Bradley RK, Merkin J, Lambert NJ, Burge CB. 2012. Alternative splicing of RNA triplets is often regulated and accelerates proteome evolution. *PLoS Biol* **10:** e1001229.

Burns CG, Ohi R, Mehta S, O'Toole ET, Winey M, Clark TA, Sugnet CW, Ares M Jr, Gould KL. 2002. Removal of a single α-tubulin gene intron suppresses cell cycle arrest phenotypes of splicing factor mutations in *Saccharomyces cerevisiae*. *Mol Cell Biol* **22:** 801–815.

The Cancer Genome Atlas Research Network. 2008. Comprehensive genomic characterization defines human glioblastoma genes and core pathways. *Nature* **455:** 1061–1068.

Cheng L, Huang Z, Zhou W, Wu Q, Donnola S, Liu JK, Fang X, Sloan AE, Mao Y, Lathia JD, et al. 2013. Glioblastoma stem cells generate vascular pericytes to support vessel function and tumor growth. *Cell* **153:** 139–152.

Clower CV, Chatterjee D, Wang Z, Cantley LC, Vander Heiden MG, Krainer AR. 2010. The alternative splicing repressors hnRNP A1/A2 and PTB influence pyruvate kinase isoform expression and cell metabolism. *Proc Natl Acad Sci* **107:** 1894–1899.

Corrionero A, Minana B, Valcarcel J. 2011. Reduced fidelity of branch point recognition and alternative splicing induced by the anti-tumor drug spliceostatin A. *Genes Dev* **25:** 445–459.

Das S, Anczukow O, Akerman M, Krainer AR. 2012. Oncogenic splicing factor SRSF1 is a critical transcriptional target of MYC. *Cell Rep* **1:** 110–117.

David CJ, Chen M, Assanah M, Canoll P, Manley JL. 2010. HnRNP proteins controlled by c-Myc deregulate pyruvate kinase mRNA splicing in cancer. *Nature* **463:** 364–368.

Ding Y, Hubert CG, Herman J, Corrin P, Toledo CM, Skutt-Kakaria K, Vazquez J, Basom R, Zhang B, Risler JK, et al. 2013. Cancer-specific requirement for BUB1B/BUBR1 in human brain tumor isolates and genetically transformed cells. *Cancer Discov* **3:** 198–211.

Donato R, Miljan EA, Hines SJ, Aouabdi S, Pollock K, Patel S, Edwards FA, Sinden JD. 2007. Differential development of neuronal physiological responsiveness in two human neural stem cell lines. *BMC Neurosci* **8:** 36.

Fan L, Lagisetti C, Edwards CC, Webb TR, Potter PM. 2011. Sudemycins, novel small molecule analogues of FR901464, induce alternative gene splicing. *ACS Chem Biol* **6:** 582–589.

Fang J, Acheampong E, Dave R, Wang F, Mukhtar M, Pomerantz RJ. 2005. The RNA helicase DDX1 is involved in restricted HIV-1 Rev function in human astrocytes. *Virology* **336:** 299–307.

Galli R, Binda E, Orfanelli U, Cipelletti B, Gritti A, De Vitis S, Fiocco R, Foroni C, Dimeco F, Vescovi A. 2004. Isolation and characterization of tumorigenic, stem-like neural precursors from human glioblastoma. *Cancer Res* **64:** 7011–7021.

Gangemi RM, Griffero F, Marubbi D, Perera M, Capra MC, Malatesta P, Ravetti GL, Zona GL, Daga A, Corte G. 2009. SOX2 silencing in glioblastoma tumor-initiating cells causes stop of proliferation and loss of tumorigenicity. *Stem Cells* **27:** 40–48.

Gooding C, Clark F, Wollerton MC, Grellscheid SN, Groom H, Smith CW. 2006. A class of human exons with predicted distant branch points revealed by analysis of AG dinucleotide exclusion zones. *Genome Biol* **7:** R1.

Hemmati HD, Nakano I, Lazareff JA, Masterman-Smith M, Geschwind DH, Bronner-Fraser M, Kornblum HI. 2003. Cancerous stem cells can arise from pediatric brain tumors. *Proc Natl Acad Sci* **100:** 15178–15183.

Heyd F, Lynch KW. 2011. Degrade, move, regroup: Signaling control of splicing proteins. *Trends Biochem Sci* **36:** 397–404.

Jurica MS, Moore MJ. 2003. Pre-mRNA splicing: Awash in a sea of proteins. *Mol Cell* **12:** 5–14.

Kaida D, Motoyoshi H, Tashiro E, Nojima T, Hagiwara M, Ishigami K, Watanabe H, Kitahara T, Yoshida T, Nakajima H, et al. 2007. Spliceostatin A targets SF3b and inhibits both splicing and nuclear retention of pre-mRNA. *Nat Chem Biol* **3:** 576–583.

Kendall SD, Linardic CM, Adam SJ, Counter CM. 2005. A network of genetic events sufficient to convert normal human cells to a tumorigenic state. *Cancer Res* **65:** 9824–9828.

Kotake Y, Sagane K, Owa T, Mimori-Kiyosue Y, Shimizu H, Uesugi M, Ishihama Y, Iwata M, Mizui Y. 2007. Splicing factor SF3b as a target of the antitumor natural product pladienolide. *Nat Chem Biol* **3:** 570–575.

Kramer A. 1996. The structure and function of proteins involved in mammalian pre-mRNA splicing. *Annu Rev Biochem* **65:** 367–409.

Lagisetti C, Pourpak A, Goronga T, Jiang Q, Cui X, Hyle J, Lahti JM, Morris SW, Webb TR. 2009. Synthetic mRNA splicing modulator compounds with in vivo antitumor activity. *J Med Chem* **52:** 6979–6990.

Lagisetti C, Pourpak A, Jiang Q, Cui X, Goronga T, Morris SW, Webb TR. 2008. Antitumor compounds based on a natural product consensus pharmacophore. *J Med Chem* **51:** 6220–6224.

Lampson MA, Kapoor TM. 2005. The human mitotic checkpoint protein BubR1 regulates chromosome-spindle attachments. *Nat Cell Biol* **7:** 93–98.

Latera J, Brem H. 2002. Primary brain tumors in adults. In *Diseases of the nervous system: Clinical neuroscience and theraputic principals* (ed. A Asbury, et al.), pp. 1431–1466 Cambridge University Press, Cambridge, UK.

Lee J, Kotliarova S, Kotliarov Y, Li A, Su Q, Donin NM, Pastorino S, Purow BW, Christopher N, Zhang W, et al. 2006. Tumor stem cells derived from glioblastomas cultured in bFGF and EGF more closely mirror the phenotype and genotype of primary tumors than do serum-cultured cell lines. *Cancer Cell* **9:** 391–403.

Li B, Dewey CN. 2011. RSEM: Accurate transcript quantification from RNA-seq data with or without a reference genome. *BMC Bioinformatics* **12:** 323.

Liu Q, Nguyen DH, Dong Q, Shitaku P, Chung K, Liu OY, Tso JL, Liu JY, Konkankit V, Cloughesy TF, et al. 2009. Molecular properties of $CD133^+$ glioblastoma stem cells derived from treatment-refractory recurrent brain tumors. *J Neurooncol* **94:** 1–19.

Luo J, Emanuele MJ, Li D, Creighton CJ, Schlabach MR, Westbrook TF, Wong KK, Elledge SJ. 2009. A genome-wide RNAi screen identifies multiple synthetic lethal interactions with the Ras oncogene. *Cell* **137:** 835–848.

Mangiola A, Lama G, Giannitelli C, De Bonis P, Anile C, Lauriola L, La Torre G, Sabatino G, Maira G, Jhanwar-Uniyal M, et al. 2007. Stem cell marker nestin and c-Jun NH2-terminal kinases in tumor and peritumor areas of glioblastoma multiforme: Possible prognostic implications. *Clin Cancer Res* **13:** 6970–6977.

Mellor J. 2006. It takes a PHD to read the histone code. *Cell* **126:** 22–24.

Mizui Y, Sakai T, Iwata M, Uenaka T, Okamoto K, Shimizu H, Yamori T, Yoshimatsu K, Asada M. 2004. Pladienolides, new substances from culture of *Streptomyces platensis* Mer-11107. III. In vitro and in vivo antitumor activities. *J Antibiot (Tokyo)* **57:** 188–196.

Musselman CA, Kutateladze TG. 2009. PHD fingers: Epigenetic effectors and potential drug targets. *Mol Interv* **9:** 314–323.

Nakajima H, Hori Y, Terano H, Okuhara M, Manda T, Matsumoto S, Shimomura K. 1996. New antitumor substances, FR901463, FR901464 and FR901465. II. Activities against experimental tumors in mice and mechanism of action. *J Antibiot (Tokyo)* **49:** 1204–1211.

Oltra E, Pfeifer I, Werner R. 2003. Ini, a small nuclear protein that enhances the response of the connexin43 gene to estrogen. *Endocrinology* **144:** 3148–3158.

Paddison PJ, Silva JM, Conklin DS, Schlabach M, Li M, Aruleba S, Balija V, O'Shaughnessy A, Gnoj L, Scobie K, et al. 2004. A resource for large-scale RNA-interference-based screens in mammals. *Nature* **428:** 427–431.

Parsons DW, Jones S, Zhang X, Lin JC, Leary RJ, Angenendt P, Mankoo P, Carter H, Siu IM, Gallia GL, et al. 2008. An integrated genomic analysis of human glioblastoma multiforme. *Science* **321:** 1807–1812.

Paulsen RD, Soni DV, Wollman R, Hahn AT, Yee MC, Guan A, Hesley JA, Miller SC, Cromwell EF, Solow-Cordero DE, et al. 2009. A genome-wide siRNA screen reveals diverse cellular processes and pathways that mediate genome stability. *Mol Cell* **35:** 228–239.

Pollard SM, Yoshikawa K, Clarke ID, Danovi D, Stricker S, Russell R, Bayani J, Head R, Lee M, Bernstein M, et al. 2009. Glioma stem cell lines expanded in adherent culture have tumor-specific phenotypes and are suitable for chemical and genetic screens. *Cell Stem Cell* **4:** 568–580.

Robinson MD, Oshlack A. 2010. A scaling normalization method for differential expression analysis of RNA-seq data. *Genome Biol* **11:** R25.

Robinson JT, Thorvaldsdottir H, Winckler W, Guttman M, Lander ES, Getz G, Mesirov JP. 2011. Integrative genomics viewer. *Nat Biotechnol* **29:** 24–26.

Rzymski T, Grzmil P, Meinhardt A, Wolf S, Burfeind P. 2008. PHF5A represents a bridge protein between splicing proteins and ATP-dependent helicases and is differentially expressed during mouse spermatogenesis. *Cytogenet Genome Res* **121:** 232–244.

Sawin KE, LeGuellec K, Philippe M, Mitchison TJ. 1992. Mitotic spindle organization by a plus-end-directed microtubule motor. *Nature* **359:** 540–543.

Sears R, Nuckolls F, Haura E, Taya Y, Tamai K, Nevins JR. 2000. Multiple Ras-dependent phosphorylation pathways regulate Myc protein stability. *Genes Dev* **14:** 2501–2514.

Shultz JC, Goehe RW, Wijesinghe DS, Murudkar C, Hawkins AJ, Shay JW, Minna JD, Chalfant CE. 2010. Alternative splicing of caspase 9 is modulated by the phosphoinositide 3-kinase/Akt pathway via phosphorylation of SRp30a. *Cancer Res* **70:** 9185–9196.

Singh SK, Clarke ID, Terasaki M, Bonn VE, Hawkins C, Squire J, Dirks PB. 2003. Identification of a cancer stem cell in human brain tumors. *Cancer Res* **63:** 5821–5828.

Singh SK, Hawkins C, Clarke ID, Squire JA, Bayani J, Hide T, Henkelman RM, Cusimano MD, Dirks PB. 2004. Identification of human brain tumour initiating cells. *Nature* **432:** 396–401.

Son MJ, Woolard K, Nam DH, Lee J, Fine HA. 2009. SSEA-1 is an enrichment marker for tumor-initiating cells in human glioblastoma. *Cell Stem Cell* **4:** 440–452.

Stiles CD, Rowitch DH. 2008. Glioma stem cells: A midterm exam. *Neuron* **58:** 832–846.

Trappe R, Ahmed M, Glaser B, Vogel C, Tascou S, Burfeind P, Engel W. 2002. Identification and characterization of a novel murine multigene family containing a PHD-finger-like motif. *Biochem Biophys Res Commun* **293:** 816–826.

Veiseh M, Gabikian P, Bahrami SB, Veiseh O, Zhang M, Hackman RC, Ravanpay AC, Stroud MR, Kusuma Y, Hansen SJ, et al. 2007. Tumor paint: A chlorotoxin:Cy5.5 bioconjugate for intraoperative visualization of cancer foci. *Cancer Res* **67:** 6882–6888.

Wang J, Wang H, Li Z, Wu Q, Lathia JD, McLendon RE, Hjelmeland AB, Rich JN. 2008. c-Myc is required for maintenance of glioma cancer stem cells. *PLoS ONE* **3:** e3769.

Weg-Remers S, Ponta H, Herrlich P, Konig H. 2001. Regulation of alternative pre-mRNA splicing by the ERK MAP-kinase pathway. *EMBO J* **20:** 4194–4203.

Will CL, Urlaub H, Achsel T, Gentzel M, Wilm M, Luhrmann R. 2002. Characterization of novel SF3b and 17S U2 snRNP proteins, including a human Prp5p homologue and an SF3b DEAD-box protein. *EMBO J* **21:** 4978–4988.

Zheng H, Ying H, Yan H, Kimmelman AC, Hiller DJ, Chen AJ, Perry SR, Tonon G, Chu GC, Ding Z, et al. 2008a. p53 and Pten control neural and glioma stem/progenitor cell renewal and differentiation. *Nature* **455:** 1129–1133.

Zheng H, Ying H, Yan H, Kimmelman AC, Hiller DJ, Chen AJ, Perry SR, Tonon G, Chu GC, Ding Z, et al. 2008b. Pten and p53 converge on c-Myc to control differentiation, self-renewal, and transformation of normal and neoplastic stem cells in glioblastoma. *Cold Spring Harb Symp Quant Biol* **73:** 427–437.

Developmental Cell
Article

BuGZ Is Required for Bub3 Stability, Bub1 Kinetochore Function, and Chromosome Alignment

Chad M. Toledo,[1,3,6] Jacob A. Herman,[4,6] Jonathan B. Olsen,[5] Yu Ding,[1] Philip Corrin,[1] Emily J. Girard,[2] James M. Olson,[2] Andrew Emili,[5] Jennifer G. DeLuca,[4,*] and Patrick J. Paddison[1,3,*]
[1]Human Biology Division, Fred Hutchinson Cancer Research Center, Seattle, WA 98109, USA
[2]Clinical Research Division, Fred Hutchinson Cancer Research Center, Seattle, WA 98109, USA
[3]Molecular and Cellular Biology Program, University of Washington, Seattle, WA 98195, USA
[4]Department of Biochemistry and Molecular Biology, Colorado State University, Fort Collins, CO 80523, USA
[5]Donnelly Centre for Cellular and Biomolecular Research, University of Toronto, Toronto, ON M5S 3E1, Canada
[6]These authors contributed equally to this work
*Correspondence: jennifer.deluca@colostate.edu (J.G.D.), paddison@fhcrc.org (P.J.P.)
http://dx.doi.org/10.1016/j.devcel.2013.12.014

SUMMARY

During mitosis, the spindle assembly checkpoint (SAC) monitors the attachment of kinetochores (KTs) to the plus ends of spindle microtubules (MTs) and prevents anaphase onset until chromosomes are aligned and KTs are under proper tension. Here, we identify a SAC component, BuGZ/ZNF207, from an RNAi viability screen in human glioblastoma multiforme (GBM) brain tumor stem cells. BuGZ binds to and stabilizes Bub3 during interphase and mitosis through a highly conserved GLE2p-binding sequence (GLEBS) domain. Inhibition of BuGZ results in loss of both Bub3 and its binding partner Bub1 from KTs, reduction of Bub1-dependent phosphorylation of centromeric histone H2A, attenuation of KT-based Aurora B kinase activity, and lethal chromosome congression defects in cancer cells. Phylogenetic analysis indicates that BuGZ orthologs are highly conserved among eukaryotes, but are conspicuously absent from budding and fission yeasts. These findings suggest that BuGZ has evolved to facilitate Bub3 activity and chromosome congression in higher eukaryotes.

INTRODUCTION

During mitosis, the spindle assembly checkpoint (SAC) monitors the attachment of kinetochores (KTs) to the plus ends of spindle microtubules (MTs) and prevents anaphase onset until chromosomes are aligned and KTs are under proper tension (Lara-Gonzalez et al., 2012; Santaguida and Musacchio, 2009). The SAC machinery contains multiple KT proteins (i.e., Bub1, BubR1, Bub3, Mad1, Mad2, and Mps1) that monitor MT attachment and regulate anaphase progression (Lara-Gonzalez et al., 2012; Santaguida and Musacchio, 2009). The SAC proteins Mad2, BubR1, and Bub3 comprise the soluble Mitotic Checkpoint Complex (MCC) and prevent activation of the ubiquitin ligase anaphase-promoting complex/cyclosome (APC/C) by targeting APC/C's cofactor, Cdc20 (Musacchio and Salmon, 2007). Following proper chromosome alignment and tension at the KT, Cdc20 inhibition is released to activate the APC/C, which begins the cascade of events that lead to anaphase (Musacchio and Salmon, 2007).

In addition, Bub1, BubR1, and Bub3 have been implicated in promoting chromosome alignment through regulation of Aurora B kinase (ABK) activity at KTs during chromosome congression (Lampson and Kapoor, 2005; Logarinho et al., 2008; Meraldi and Sorger, 2005). In prometaphase, Bub1 kinase phosphorylates threonine 120 of centromere-bound Histone 2A (pH2A-T120), which facilitates recruitment of ABK to the KT (Ricke et al., 2012; Taylor et al., 1998; Yamagishi et al., 2010). ABK, in turn, phosphorylates KT-MT attachment proteins, which reduces their binding affinity for MTs and prevents the premature stabilization of KT-MT attachments (Cheeseman et al., 2006; DeLuca et al., 2006, 2011; Welburn et al., 2010). In contrast to Bub1, BubR1 activity opposes ABK-dependent phosphorylation of KT-binding factors by recruiting PP2A phosphatase to the KT (Kruse et al., 2013; Suijkerbuijk et al., 2012). The interplay between these opposing activities regulates the formation of stable end-on KT-MT attachments (Kruse et al., 2013; Lampson and Kapoor, 2005; Suijkerbuijk et al., 2012). Bub3 is required to recruit both Bub1 and BubR1 to KTs (Harris et al., 2005; Wang et al., 2001), and Bub3 inhibition results in chromosome congression defects consistent with loss of Bub1 function at KTs (Logarinho et al., 2008).

Bub1 and BubR1 both interact with Bub3 through highly conserved GLEBS domains (Bailer et al., 1998; Taylor et al., 1998; Wang et al., 2001). These are short, disordered regions of about 40 amino acids that form a series of salt bridges between the WD40 domains of Bub3 and two glutamate residues in the GLEBS domain (Larsen et al., 2007). As a result of Bub3 binding, the GLEBS domain undergoes a conformational shift from a disordered to a well-ordered structure with fixed interaction points on the top face of Bub3's WD40 propeller (Larsen et al., 2007). This interaction is critical for Bub3-dependent recruitment of Bub1 and BubR1 to KTs (Harris et al., 2005; Taylor et al., 1998; Wang et al., 2001). For example, a

single amino-acid change in BubR1's GLEBS domain (E406K) is sufficient to prevent Bub3 interaction and BubR1's KT localization (Harris et al., 2005).

We previously found that human glioblastoma multiforme (GBM) brain tumors, the most common and lethal form of brain cancer, differentially require BubR1's GLEBS domain to suppress the lethal consequences of altered KT function by promoting attachment of MTs to KTs (Ding et al., 2013). Removal of BubR1 from KTs of GBM stem cells (GSCs) or transformed fibroblasts results in lethality due to a lack of KT-MT attachments, whereas nontransformed cells are unaffected (Ding et al., 2013; Malureanu et al., 2009). Thus, GBM isolates appear to be more sensitive to perturbation of certain activities of SAC proteins than nontransformed cells. This added sensitivity in GSCs led us to isolate a facilitator of Bub3 function, ZNF207, an uncharacterized C2–H2 zinc-finger domain gene (Hubert et al., 2013; Pahl et al., 1998). Because we implicate ZNF207 below as a key effector of Bub3 function, we rename the gene *BuGZ* (Bub3 interacting GLEBS and Zinc finger domain containing protein). Here, we report that the human *BuGZ/ZNF207* gene encodes a GLEBS-domain-containing and KT-binding protein that is required for Bub3 stability, Bub1 KT function, and chromosome alignment.

RESULTS

BuGZ was isolated from an RNAi screen targeting putative human transcription factors to identify key regulators of the expansion and survival of GSCs. As in our previous studies (Ding et al., 2013; Hubert et al., 2013), we compared the GSC screen results with those obtained from nontransformed human neural stem cells (NSCs), a candidate cell of origin for GBM, to identify GBM-specific lethality hits (Figure 1A). We found *BuGZ* short hairpin RNAs (shRNAs) in this category. Thus, we set out to validate *BuGZ* as a candidate cancer lethal gene and then attempted to ascertain its cellular function.

Figures 1A–1D show that, consistent with the screen data, *BuGZ* knockdown results in differential growth inhibition of GSCs when compared with proliferating human NSCs. Multiple shRNAs provided robust GSC-specific growth inhibition and penetrant knockdown in both GSCs and NSCs (see also Figure S1A available online). Knockdown of KIF11/Eg5 was used as a positive proliferation control. Its inhibition blocks the growth of cultured cells regardless of transformation status (Figures 1B and 1F; Ding et al., 2013; Hubert et al., 2013).

BuGZ knockdown also inhibited the growth of SSEA1+ GSC subpopulations, which are enriched for tumor-initiating cell activity (Son et al., 2009; Figure 1E), and inhibited tumor sphere formation, a surrogate assay for stem cell self-renewal (Galli et al., 2004; Singh et al., 2004; Figure S1B). However, *BuGZ* knockdown did not alter expression of SSEA1 or other progenitor markers, including SOX2 and NESTIN, or neural lineage markers, including GFAP and TUJ1 (data not shown). Moreover, *BuGZ*-knockdown-insensitive NSCs could be made sensitive by genetic transformation with hTERT, dominant-negative $p53^{DD}$, CyclinD1, $CDK4^{R24C}$, H-RasV12, and MYC (Hubert et al., 2013; Kendall et al., 2005; Figure 1F). Other GSC patient isolates also showed sensitivity to *BuGZ* knockdown, demonstrating that the effect is not patient specific (Figure 1F). Finally, we performed an in vivo competition experiment to directly test the effects of *BuGZ* suppression in an orthotropic xenograft model of GBM by mixing GSCs containing GFP-expressing *shBuGZ* or shControl with non-shRNA control GSCs at an approximate 9:1 ratio, respectively (Hubert et al., 2013). We found that 17 days postinjection, the non-shRNA control GSCs drastically outcompeted the *shBuGZ* GSCs, and the shControl GSCs comprised the bulk tumor mass (Figures 1G and S1C). Thus, *BuGZ* expression is required for GBM tumor formation in vivo. Taken together, these results suggest that GSCs have a differential requirement for *BuGZ*, which is likely driven by oncogenic activity.

To gain insight into the molecular function of BuGZ, we next performed affinity purification mass spectrometry to identify candidate protein-binding partners (see Supplemental Experimental Procedures for details). This analysis revealed Bub3 as the top-scoring hit (Figure 2A; Table S1). We confirmed this interaction in reciprocal coimmunoprecipitation experiments. BuGZ was able to pull down Bub3, and vice versa in GSCs (Figure 2B) and 293T cells (Figure S2), demonstrating that the proteins interact in cells.

Because SAC signaling is an essential and highly conserved process, we performed phylogenetic analysis to identify *BuGZ* orthologs and examine available data regarding their function in model genetic systems. *BuGZ* shows strong conservation among eukaryotes, with the exception of budding and fission yeasts, where no orthologs could be identified (Figure 2C; Powell et al., 2012). This is in contrast to Bub3, which is highly conserved in all eukaryotes, including budding and fission yeasts, where it was first identified (Hoyt et al., 1991). Additionally, examination of protein-protein interaction databases available for humans, worms, flies, and plants revealed additional evidence for *BuGZ* ortholog interaction with Bub3 from genome-scale yeast two-hybrid screens or mass-spectrometry analysis (Table S2). However, other candidate proteins identified in our mass-spectrometry analysis were not found. This suggests that BuGZ-Bub3 interactions are highly conserved among higher eukaryotes.

We next examined whether BuGZ interacts with Bub3 through a GLEBS domain similarly to Bub1 and BubR1. We observed that *BuGZ* orthologs also harbor a single conserved GLEBS domain motif (AA 344–376 for human), which contains the characteristic two glutamate residues found in all GLEBS domains (AA 358 and 359 for human *BuGZ*; Figure 2D). Furthermore, mutational analysis of human *BuGZ* followed by immunoprecipitations revealed that BuGZ's GLEBS domain is required for interaction with Bub3, whereas its zinc finger domains are dispensable (Figures 2E and 2F). Thus, similarly to Bub1 and BubR1, BuGZ interacts with Bub3 through a GLEBS domain.

To further explore the role of BuGZ-Bub3 binding, we evaluated the protein levels of each binding partner after RNAi depletion. We found that depletion of BuGZ led to an ~2-fold depletion of Bub3 protein in GSCs, NSCs, and HeLa cells, whereas other SAC and KT proteins (including Bub1, BubR1, Mad2L1, Hec1, and Cdc20) were unaffected (Figures 3A, 3B, and S3A–S3C). However, mRNA levels of *BUB3* remain unchanged with *BuGZ* knockdown (Figure 3C), suggesting the effects are not due to transcriptional regulation or to off-target RNAi. In addition, Bub3 loss due to BuGZ depletion can be rescued by overexpressing a *BuGZ* allele that is resistant to the *shBuGZ* (Figure 3D). Moreover, mutational analysis revealed that the glutamic acid

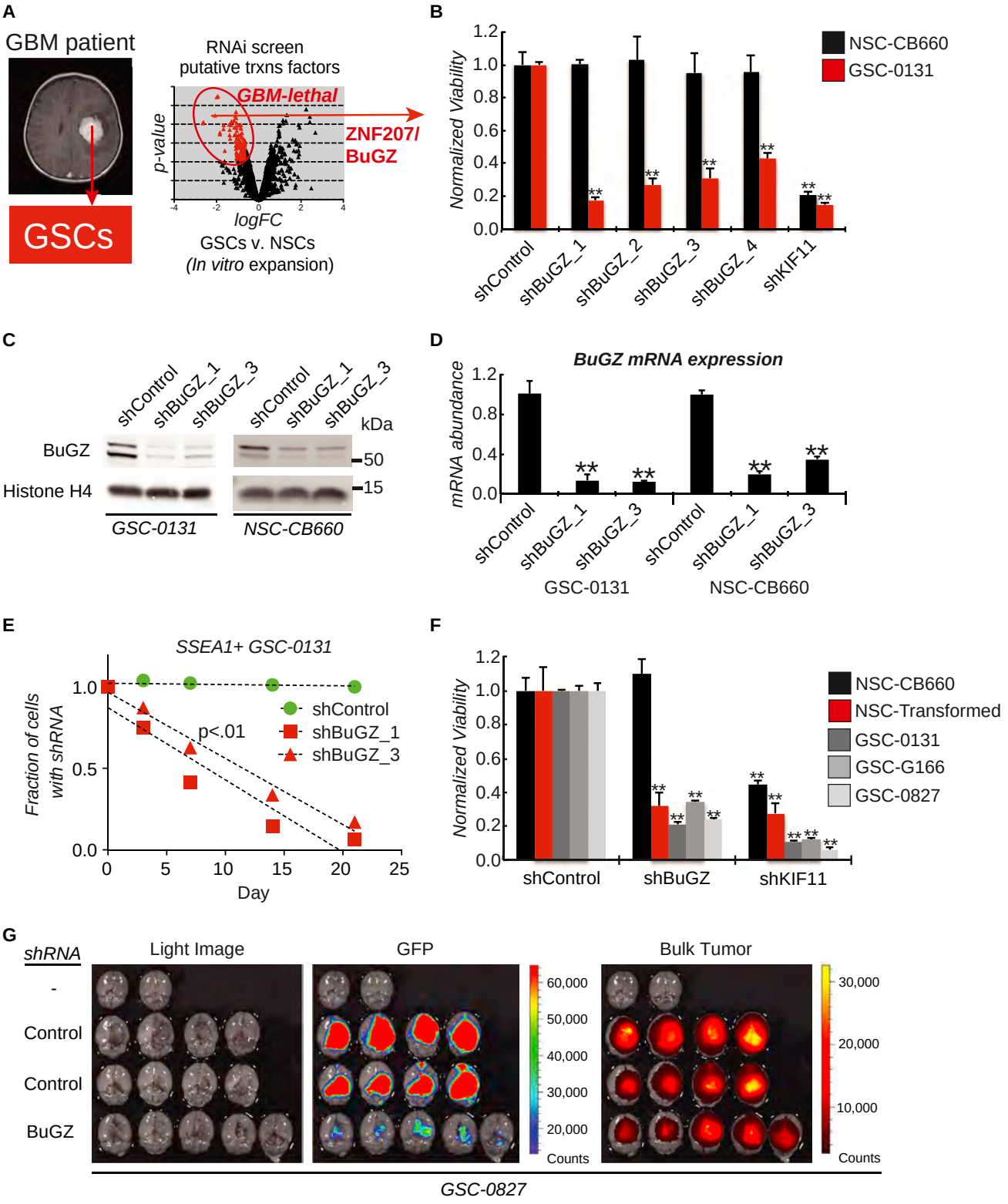

Figure 1. *BuGZ* Is a Candidate GBM-Lethal Gene

(A) An RNAi screen of putative transcription factors revealed that *ZNF207/BuGZ* is differentially required for GSC expansion as compared with NSCs.

(B) *BuGZ* knockdown causes loss of viability in GSCs, but not NSCs. Cells were infected with lentiviruses expressing *BuGZ*, KIF11, or control shRNAs, outgrown for 7 days, and assayed for growth. Knockdown of KIF11 was used as a positive control for both RNAi knockdown and cell proliferation. All viral clones were normalized to their respective shControl. **Student's t test, $p < 0.01$, +SD.

(legend continued on next page)

residues E358 and E359 of BuGZ's GLEBS domain are critical for Bub3 stability (Figure 3D). These two glutamic acid residues are invariant among consensus residues for Bub1, BubR1, and Nup98 GLEBS domains (Figure 2D) and are essential for their binding to Bub3 or Rae1 (Bailer et al., 1998; Larsen et al., 2007; Pritchard et al., 1999; Ren et al., 2010; Taylor et al., 1998; Wang et al., 2001). These results suggest that the BuGZ-Bub3 GLEBS-mediated interaction decreases protein turnover of Bub3.

We next addressed whether BuGZ and Bub3 have overlapping localization patterns in cells. Similar to reports for Bub3 (Taylor et al., 1998), we found that a BuGZ-GFP fusion localized primarily to the nucleus in interphase, concentrated at KTs prior to nuclear envelope breakdown and during early prometaphase, and disappeared from KTs upon MT binding (Figure 3E). Immunostaining of BuGZ revealed a similar localization pattern (Figure S4A). We next determined colocalization patterns of BuGZ and Bub3 in HeLa cells. Just like BuGZ, Bub3 maximally localized to KTs prior to nuclear envelope breakdown and remained bound throughout prometaphase as previously described (Howell et al., 2004; Figure 4A). However, unlike BuGZ, Bub3 persisted in low levels at metaphase KTs.

In contrast to BuGZ and Bub3 KT localization, Bub1 and BubR1, which also associate with Bub3 via GLEBS domains, concentrated at KTs after nuclear envelope breakdown (Figure S4B), consistent with previously published results (Jablonski et al., 1998; Taylor and McKeon, 1997). Similar to what was observed for these proteins, BuGZ's GLEBS domain was required for KT localization (Figure 4B), whereas its zinc finger motifs were dispensable (Figure 4B). In addition, depletion of Bub3 using RNAi prevented BuGZ localization to the KT (Figure 4C). Previous reports demonstrated that Bub3, Bub1, and BubR1 all require KNL-1 in order to bind KTs (Kiyomitsu et al., 2007; London et al., 2012; Primorac and Musacchio, 2013; Yamagishi et al., 2012). We found that KNL-1 depletion also resulted in a loss of BuGZ from KTs (Figure 4D). Moreover, when cells were treated with nocodazole, causing spindle MTs to depolymerize, unattached KTs reaccumulated BuGZ (Figure 4E). Conversely, treating cells with taxol, which stabilizes KT-MT attachments, did not recruit BuGZ to MT-attached KTs (Figure 4E). This behavior is similar to those previously observed for Bub3 and other SAC proteins (Hoffman et al., 2001). Together, these results indicate that BuGZ localizes to KTs by binding to Bub3 through its GLEBS domain, and BuGZ's KT localization is regulated by attachment of MTs.

Previous studies reported that Bub3 and its binding partners Bub1 and BubR1 exhibit interdependencies for KT localization (Lara-Gonzalez et al., 2012; Santaguida and Musacchio, 2009). We therefore analyzed KT localization of Bub3, Bub1, and BubR1 in BuGZ-depleted HeLa cells. After BuGZ depletion, Bub3 levels were reduced at KTs, which is not unexpected due to the decrease in total protein (Figure 4F). Bub1 KT localization was also significantly decreased (Figure 5A), which is likely due to loss of its obligate KT recruitment factor Bub3 (Taylor et al., 1998; Taylor and McKeon, 1997; Vanoosthuyse et al., 2004). Intriguingly, BubR1 KT association was not affected after BuGZ depletion (Figure 5A), though previous studies have demonstrated that BubR1 KT recruitment relies on Bub3 (Logarinho et al., 2008; Meraldi et al., 2004). It is possible that BubR1 outcompetes Bub1 to limit the Bub3-binding sites that remain after BuGZ depletion, or alternatively, that BuGZ plays a more direct role in Bub1 KT recruitment.

In addition to their well-known roles in SAC signaling, Bub1, BubR1, and Bub3 have also been implicated in facilitating chromosome alignment during mitosis (Lampson and Kapoor, 2005; Logarinho et al., 2008; Meraldi and Sorger, 2005). We therefore examined chromosome alignment in BuGZ-depleted HeLa cells treated with the proteasome inhibitor MG132 (to prevent precocious anaphase entry), and found that this process was significantly compromised (Figure 5B). In control populations, >95% of cells were able to fully align chromosomes, whereas proper chromosome alignment was observed in <55% of BuGZ-depleted cells (Figure 5B). We also detected similar chromosome alignment defects in GSC-0131 and transformed NSC-CB660 cells upon BuGZ depletion and MG132 treatment (Figure 5C). However, nontransformed NSC-CB660 cells were able to fully align chromosomes following BuGZ loss (Figure 5C). In addition, codepleting both BuGZ and Bub3 in GSC-0131 resulted in partial to severe chromosome alignment defects similar to what was found with BuGZ and Bub3 depletion alone (Figure 5D). The chromosome alignment defects in GSC-131 following depletion of endogenous BuGZ could be rescued by ectopic expression of the *BuGZ* ORF (Figure 5E), which further demonstrates that the chromosome alignment defects are due to BuGZ depletion and not to off-target RNAi. However, BuGZ GLEBS domain mutations (E358K and E359K) failed to rescue the chromosome alignment defects (Figure 5E). The alignment defects were also observed in live BuGZ-depleted cells, which exhibited significantly extended mitotic transit times (120 min compared with 60 min in control cells; Figures 5F and S5). Together, these results suggest that oncogenic stress alters KT function, which leads to a differential requirement for BuGZ's GLEBS domain in cancer cells for chromosome congression.

(C and D) Western blot analysis and quantitative RT-PCR (qRT-PCR) for BuGZ protein and mRNA expression, respectively, of whole-cell extracts from GSC-0131 and NSC-CB660 following shRNA knockdown. **Student's t test, $p < 0.01$, +SD.

(E) *BuGZ* knockdown compromises the growth of SSEA1+ GSC subpopulations. Flow-cytometry analysis of SSEA1+ GSC-0131 cells infected with *shBuGZ*-GFP+ or shControl-GFP+, mixed with untreated cells, and followed for 21 days in vitro under self-renewing conditions.

(F) *BuGZ* knockdown compromises the growth of transformed NSCs and multiple GSC isolates, but not NSCs (assay same as in B). **Student's t test, $p < 0.01$, +SD.

(G) Suppression of *BuGZ* expression compromises GBM tumor formation in vivo. Images of in vivo competition mouse brains 17 days after orthotopic xenograft of GSC-0827 cells expressing GFP-shControl or GFP-*shBuGZ* mixed with non-shRNA GSC-0827 cells. Right: light images of brains. Middle: GFP+ fluorescence marking shRNA-containing cells. Left: fluorescent signal from Tumor Paint (chlorotoxin:indocyanine green) to identify the total tumor mass. The first mouse brain in the top row did not receive GSC-0827 cells or Tumor Paint, whereas the second mouse brain in the top row did not receive GSC-0827 cells, but received Tumor Paint. Quantification of GFP fluorescence is shown in Figure S1C. **Student's t test, $p < 0.01$.

See also Figure S1.

A

Affinity Purification Mass. Spec.

		GFP		BuGZ-GFP	
GENE	kDa	Rep1	Rep2	Rep1	Rep2
BUB3	37.2	0	0	92	154
GFP	26.9	32	53	59	73
BuGZ	50.8	0	0	32	45
TCOF	152.1	0	0	31	33
SNUT1	90.3	0	0	12	17
PRDM13	74	0	0	10	11

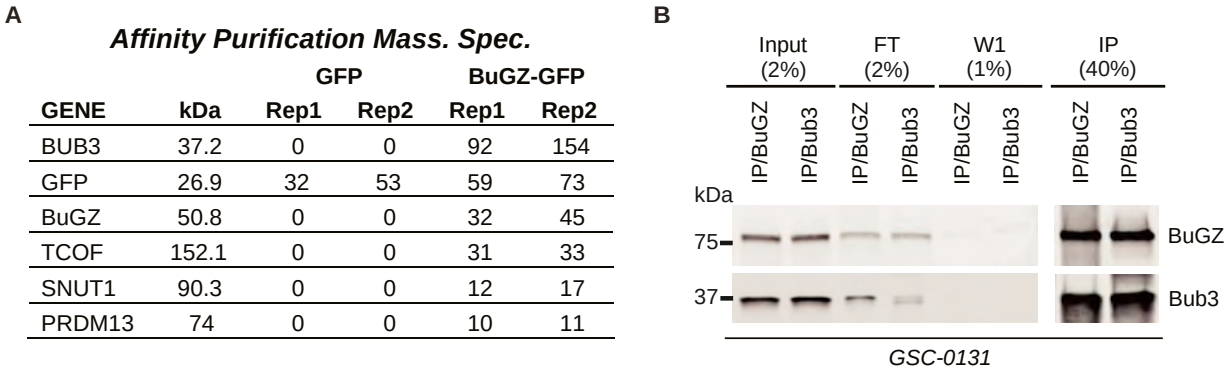

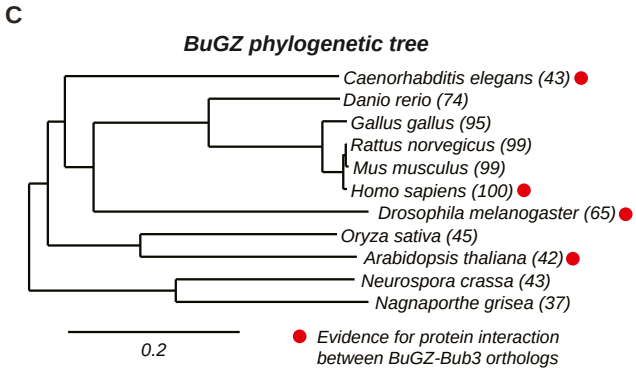

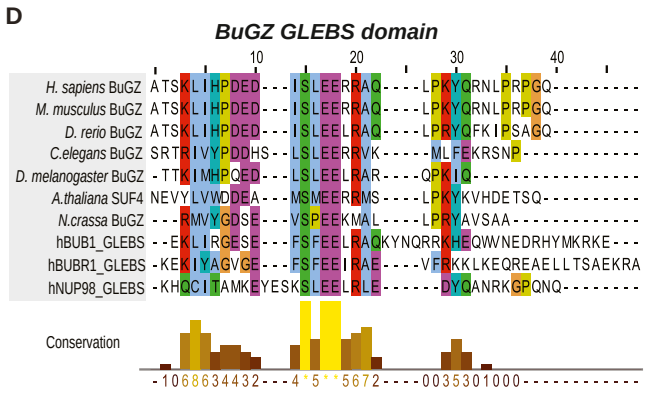

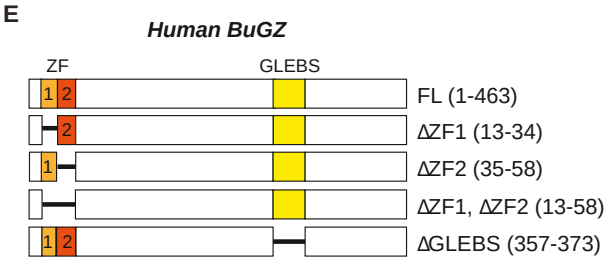

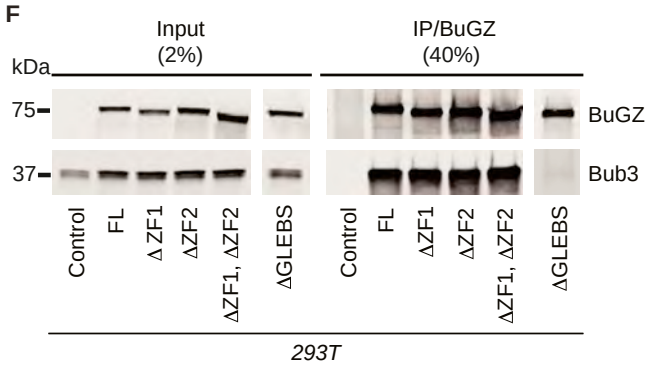

Figure 2. BuGZ Binds to Bub3 through a Highly Conserved GLEBS Domain

(A) Results of affinity purification mass spectrometry of 293T cell extracts transfected with GFP-tagged ZNF207 open reading frame (ORF). Bub3 was identified as the top candidate protein to interact with BuGZ. GFP control ORF was used to identify nonspecific protein interactions. Total results are presented in Table S1.

(B) BuGZ binds to Bub3 and vice versa. Western blot analysis with anti-turboGFP (BuGZ) and anti-Bub3 of immunoprecipitates with the turboGFP antibody (BuGZ) or V5 antibody (Bub3) from GSC-0131 cells infected with V5-Bub3 and turboGFP-BuGZ constructs. FT, flowthrough; IP, immunoprecipitation; W1, wash 1.

(C) Evolutionary distance between orthologs of ZNF207/BuGZ sampled from major phyla. Percent protein identity to human BuGZ from pairwise protein alignments is indicated in parentheses (NCBI, HomoloGene database). Red dot indicates evidence for BuGZ-Bub3 interactions from protein-protein interaction databases (Table S2).

(D) BuGZ orthologs contain a highly conserved GLEBS domain. GLEBS domains from hBub1 (AA240–280), hBubR1 (AA400–440), and hNup98 (157–213) (Larsen et al., 2007; Wang et al., 2001) were used to create pairwise alignments of the indicated BuGZ orthologs using CLUSTALW.

(E) Human *BuGZ* alleles generated and used in these studies. FL, full-length *BuGZ* ORF; ΔZF1, deletion of the first zinc finger motif; ΔZF2, deletion of the second zinc finger motif; ΔZF1, ΔZF2, deletion of the two zinc finger motifs; ΔGLEBS, deletion of a portion of the GLEBS motif.

(F) BuGZ binds to Bub3 through its GLEBS domain. Western blot analysis with anti-turboGFP and anti-Bub3 of immunoprecipitates with the turboGFP antibody (BuGZ) from 293T cells transfected with the mutant alleles in (E) or the control (V5-Bub3).

See also Figure S2 and Tables S1 and S2.

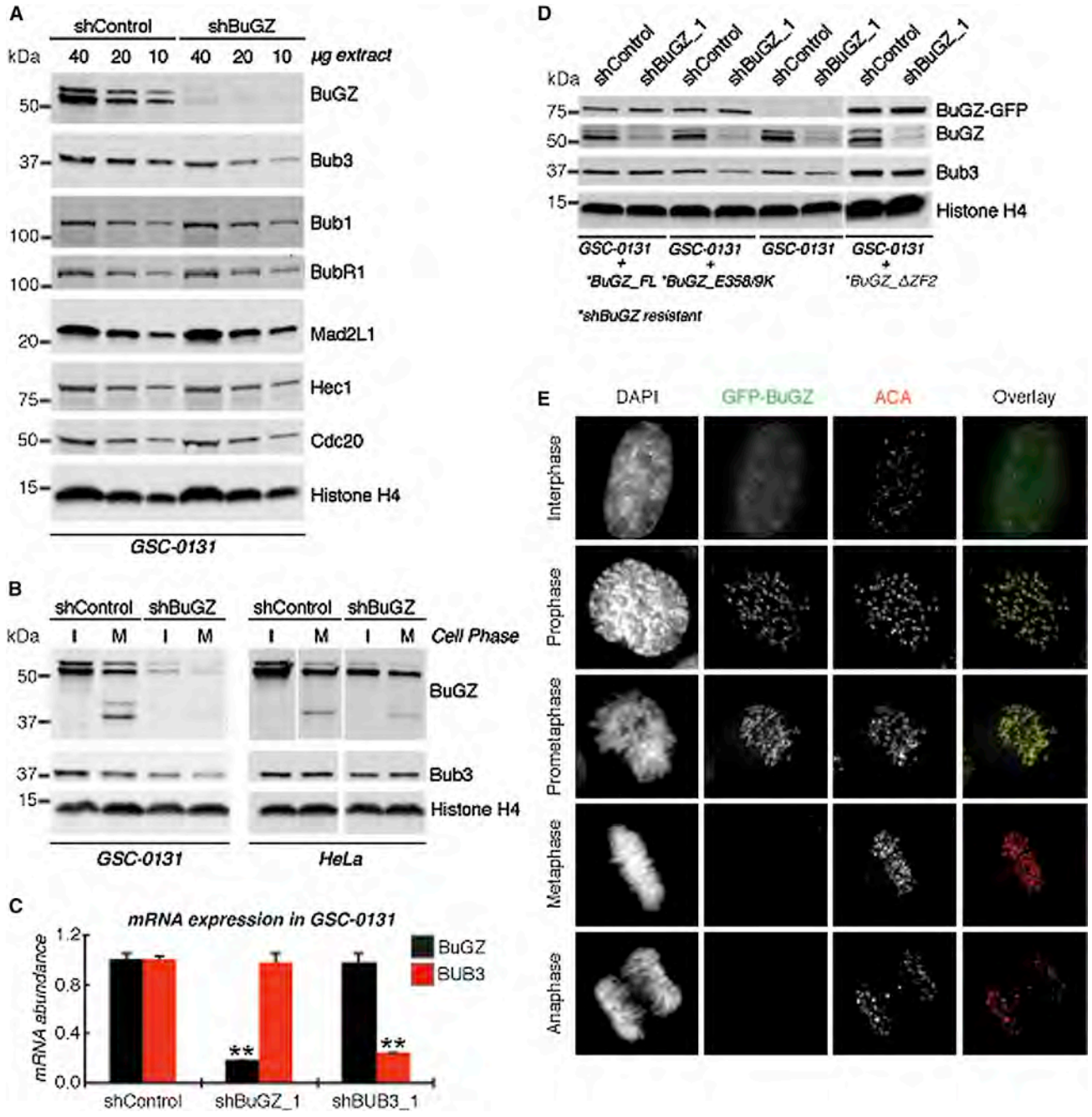

Figure 3. BuGZ Stabilizes Bub3 Expression and Localizes to the KT

(A) BuGZ stabilizes Bub3 expression. Western blot analysis of GSC-0131 whole-cell extracts infected with shControl or *shBuGZ* virus for antibodies to multiple KT-associated proteins and to the loading control anti-Histone H4.

(B) BuGZ stabilizes Bub3 expression in interphase and mitotic cells. Western blot analysis of GSC-0131 and HeLa interphase or mitotic cell extracts for anti-BuGZ, anti-Bub3, and loading control anti-Histone H4 antibodies. GSC-0131 cells were infected with shControl or *shBuGZ* virus and treated with the proteasome inhibitor MG-132 for 18.5 hr. HeLa cells were not treated with MG-132. Interphase and mitotic cells were collected by shake-off for both GSC-0131 and HeLa cells. *Mitotic extracts contain additional lower-molecular-weight species of BuGZ, which could represent a cleavage or degradation product.

(C) Knockdown of *BuGZ* does not alter *BUB3* mRNA levels and vice versa. qRT-PCR was used to access *BuGZ* and *BUB3* mRNA expression after shRNA viral infection with shControl, *shBuGZ*, and *shBUB3*. **Student's t test, $p < 0.01$, +SD.

(D) Expression of BuGZ in BuGZ-depleted GSCs rescues Bub3 expression, but BuGZ-GLEBS domain mutants (E358K E359K) do not. Western blot analysis of GSC-0131 cell extracts for anti-turboGFP, anti-BuGZ, anti-Bub3, and loading control anti-Histone H4 antibodies. GSC-0131 cells were first infected with *BuGZ*

(legend continued on next page)

To understand the source of these attachment errors, we assayed Bub1 kinase activity, which is implicated in mediating proper chromosome alignment through localization and activation of ABK (Kawashima et al., 2007; Tsukahara et al., 2010; Yamagishi et al., 2010). We measured Bub1 kinase activity in cells by immunostaining its substrate, histone H2AT120. Consistent with loss of Bub1 at KTs, pH2A levels were significantly lower after BuGZ depletion (Figure 6A). Consistent with loss of ABK activity at KTs after BuGZ depletion, we also observed significant loss of phosphorylation of Hec1S44, a critical downstream KT substrate of ABK that is involved in the regulation of KT-MT attachments (Figure 6A; DeLuca et al., 2011). Thus, BuGZ affects chromosome alignment by ensuring Bub3-mediated recruitment of Bub1, which in turn ensures appropriate ABK-mediated phospho-regulation of KT-MT attachments.

However, unlike Bub1 and BubR1, BuGZ-depleted cells retained a functional SAC response and elicited a significant mitotic delay in response to MT poisons, albeit at diminished levels (Figures 6B and S6). BuGZ- and Bub3-codepleted cells did not sustain a checkpoint arrest under these same conditions, which was similar to the behavior of cells depleted of Bub3 alone (Figure 6C). These results suggest that BuGZ-depleted cells have enough residual Bub1 and Bub3 to activate the SAC.

DISCUSSION

Here, we report that the human *BuGZ/ZNF207* gene encodes a GLEBS-domain-containing and KT-binding protein that is required for Bub3 stability, Bub1 KT function, and chromosome alignment. A model for BuGZ function is presented in Figure 6D. We propose that BuGZ activity is required for Bub3 stability during interphase and mitosis. BuGZ depletion, therefore, results in a reduction of Bub3 protein levels during interphase and decreased binding to KTs during mitosis. As a consequence, Bub3-dependent Bub1 recruitment to KTs is compromised. This, in turn, compromises Bub1-dependent recruitment of ABK, which causes lethal chromosome congression defects in cancer cells. Importantly, viability defects and chromosome alignment defects resulting from BuGZ depletion were recreated in nonsensitive cells through oncogenic transformation. This suggests that oncogenic stress can drive an added requirement for BuGZ function in our GBM isolates and other cancer lines.

We previously established that GSCs differentially require BubR1's GLEBS domain to suppress the lethal consequences of altered KT function by promoting attachment of MTs to KTs (Ding et al., 2013). Similar to the case with BuGZ, the BubR1-GLEBS viability requirement can be reproduced in nonsensitive cells through genetic transformation with RasV12. However, the phenotypes associated with the BubR1-GLEBS-domain requirement appear to be distinct from those observed for BuGZ. For example, BubR1 knockdown results in severe defects in KT-MT attachment in GBM isolates with short inter-KT distances at metaphase, whereas BuGZ knockdown results in alignment defects similar to those produced by Bub3 depletion in all GSC isolates (Figure 5E). We postulate that GBM isolates and transformed NSCs have an added requirement for BuGZ due to oncogenic signaling that leads to changes in either KT protein activity (e.g., through changes in stoichiometry) or feedback regulation of genes involved in chromosome congression (e.g., ABK). Based on these studies, the RTK/Ras pathway is a likely candidate for triggering a BuGZ requirement. The RTK/Ras pathway is overactivated in many cancers, including GBM, and there is evidence that the Ras downstream effectors Erk1/2 can directly phosphorylate the C-terminal domain of CENPE, a key KT protein, which is predicted to decrease its MT-binding ability (Benanti and Galloway, 2004).

The functional dichotomy between BuGZ and BubR1 is also observed in the SAC. BubR1's essential function is to maintain an intact mitotic checkpoint until all chromosomes are properly aligned and KTs are under proper tension. We observed a significant mitotic delay in cancer cells following depletion of BuGZ despite a significant loss of both Bub1 and Bub3 at the KTs (Figures 6B and S6). This mitotic delay is checkpoint dependent, as codepletion of BuGZ and Bub3 prevented mitotic arrest (Figure 6C). Thus, it is likely that unattached KTs present in BuGZ-depleted cells are able to generate a functional SAC signal. It is known that Bub1 must be depleted >95% to cause checkpoint abrogation (Meraldi and Sorger, 2005). Therefore, the >40% of Bub3 and Bub1 present in BuGZ-depleted cells is likely sufficient for SAC activation. However, we cannot preclude the possibility that BuGZ is also involved in SAC silencing, which would contribute to the observed mitotic delay.

Our studies raise a key question: Is BuGZ essential in nontransformed cells? Bub1, Bub3, and BubR1 are all essential for mouse development, because null mutations of these genes cause early embryo lethality (Kalitsis et al., 2000; Malureanu et al., 2009; Perera et al., 2007; Wang et al., 2004). However, the heterozygous state is permissive for normal development, albeit with increases in mitotic abnormalities. Consistent with being nonessential, BubR1's GLEBS domain is not required for mouse embryo fibroblast proliferation or KT-MT attachment (Ding et al., 2013; Malureanu et al., 2009). Our knockdown studies suggest that the hypomorphic BuGZ state is permissive for viability of nontransformed cells, where Bub3 expression is probably equivalent to that in Bub3 heterozygous cells. However, we do not know whether complete removal of BuGZ would reduce Bub3 levels further, or whether BuGZ has other essential functions not revealed by our studies (e.g., in its zinc finger domains). It will also be interesting to see whether GLEBS domains are essential for mammalian development, given that our findings suggest that targeting GLEBS-domain interactions with Bub3 might represent a precision therapy for GBM.

Our findings also raise a critical question regarding BuGZ's role in facilitating Bub3's function: How does BuGZ regulate Bub3's stability? One possibility is that upon Bub3 binding,

ΔZF2 (*shBuGZ*_1 targets the second zinc finger motif), *shBuGZ*-resistant (denoted by *) full-length (FL) *BuGZ*, or *shBuGZ*-resistant *BuGZ* E358K E359K. Following selection, these cells were virally transduced with shControl or *shBuGZ*.

(E) BuGZ localizes to KTs in prophase and prometaphase, but diminishes during metaphase. HeLa cells were transfected with GFP-*BuGZ* fusions and imaged for DAPI, GFP, and KTs (anticentromere antibody [ACA]). Representative images are shown.

See also Figure S3.

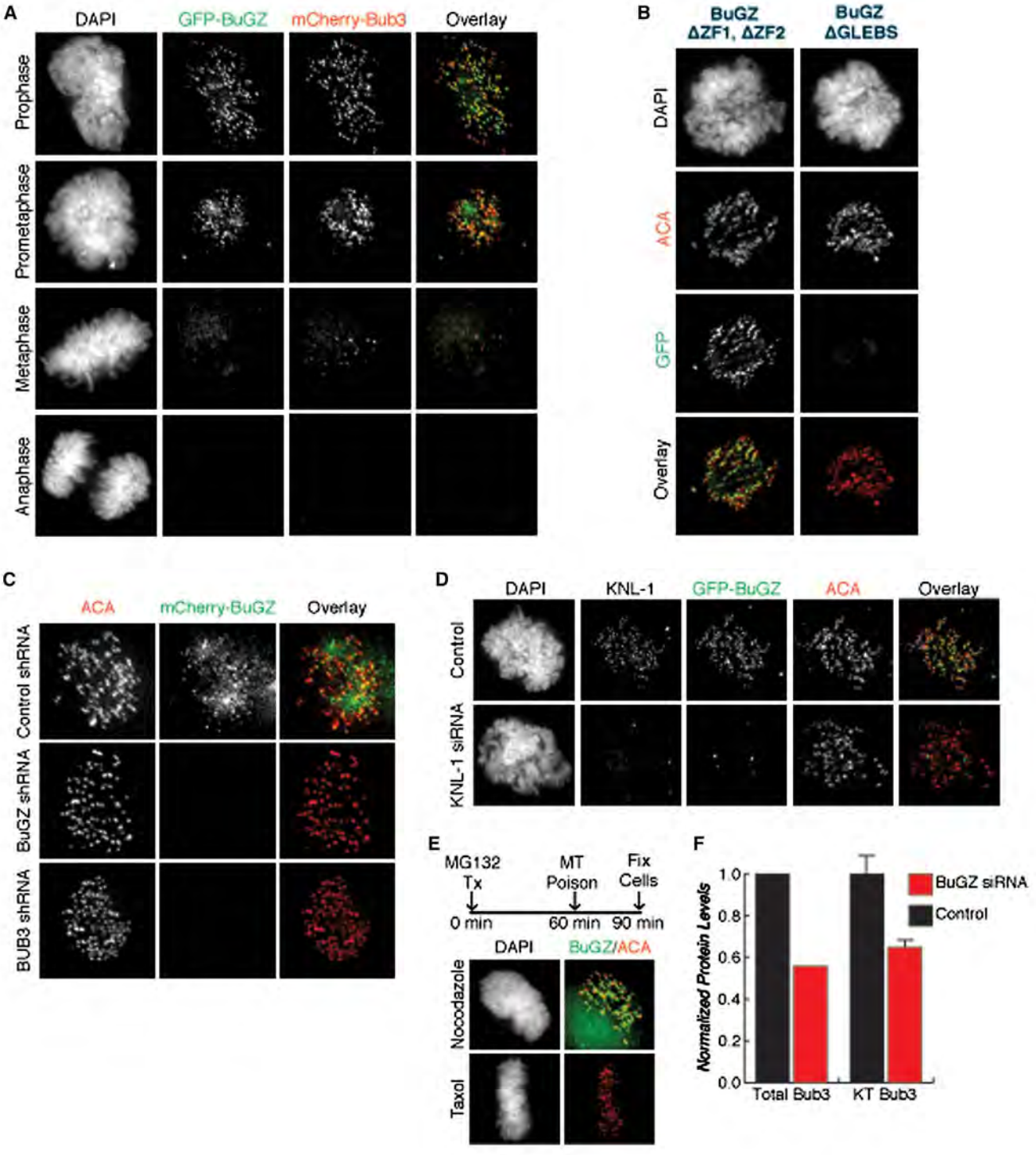

Figure 4. BuGZ Colocalizes with Bub3 at KTs during Early Mitosis by Virtue of its GLEBS Domain and Reduces Bub3 Levels at KTs when Inhibited

(A) BuGZ and Bub3 colocalization in HeLa cells transfected with GFP-*BuGZ* and mCherry-BUB3 expression constructs. BuGZ and Bub3 colocalize during prophase and prometaphase. Representative images are shown.

(B) BuGZ localization in HeLa cells infected with GFP-*BuGZ* ΔZF1, ΔZF2, or *BuGZ* ΔGLEBS mutants. BuGZ ΔZF1, ΔZF2 localizes to the KTs, whereas BuGZ ΔGLEBS does not. KTs are stained with ACA.

(C) BuGZ localization is Bub3 dependent. HeLa cells stably expressing BuGZ-mCherry were infected with shControl, *shBuGZ*, or *shBUB3*, selected, and stained with ACA.

(legend continued on next page)

BuGZ's GLEBS domain masks posttranslational modifications of Bub3, such as phosphorylation, ubiquitination, or sumoylation, which prevent its degradation. However, we were unable to detect increases in Bub3 expression from BuGZ-depleted cells treated with the proteasome inhibitor MG132 (Figure 3B) or the sumoylation inhibitor ginkgolic acid (data not shown). Another possibility is that BuGZ acts as a molecular chaperone for Bub3 by converting an unfolded or partially folded Bub3 into its final compact and stable confirmation (Larsen et al., 2007), which, for example, might prevent specific proteases from recognizing and degrading unfolded Bub3. Overexpression of BuGZ increases the steady-state levels of both ectopically expressed and endogenous Bub3 (Figures 2F and 3D), suggesting that BuGZ expression is rate limiting for Bub3 stability. Thus, further experimentation is warranted to determine the nature of the change in Bub3 turnover following BuGZ depletion.

Another question is, how does BuGZ-dependent Bub3 regulation affect Bub1 and BubR1 function at KTs? Bub3 and its binding partners Bub1 and BubR1 exhibit interdependencies for KT localization (Lara-Gonzalez et al., 2012; Santaguida and Musacchio, 2009). Our results suggest that BuGZ loss preferentially depletes Bub1 recruitment to the KT, leaving BubR1 levels unchanged (Figure 5A). This appears to contradict previous studies that have established roles for Bub1 and Bub3 in recruiting BubR1 to KTs (Klebig et al., 2009; Liu et al., 2006; Logarinho et al., 2008; Perera et al., 2007; Primorac and Musacchio, 2013; Taylor et al., 1998). However, these studies produced knockdowns of >90% of Bub1 or Bub3. Our studies produced more modest changes in Bub3 levels after BuGZ knockdown (Figure 4F) and only partial loss of recruitment of Bub1 to KTs (Figure 5A). This suggests that BubR1 might outcompete Bub1 at KTs for residual Bub3 (e.g., BubR1 could have a higher affinity for Bub3 than for Bub1). Alternatively, BuGZ could act as an exchange factor in facilitating Bub3-Bub1 interactions.

Further, it was recently found that Bub3 KT recruitment is driven by Mps1/TTK-dependent phosphorylation of KNL1's MELT motifs (Kiyomitsu et al., 2007; London et al., 2012; Primorac and Musacchio, 2013; Yamagishi et al., 2012). Consistent with this result, we found that BuGZ KT localization is KNL1 dependent (Figure 4D). Interestingly, Bub3 binding of phosphorylated MELT motifs is ~10-fold greater when Bub1 is present (Primorac et al., 2013). Future work will be required to determine whether BuGZ, Bub1, and BubR1 have similar effects on KNL1-dependent Bub3 KT localization.

In summary, we find that BuGZ is a GLEBS-domain-containing and KT-binding protein that is required for Bub3 stability and KT function. In transformed cells, BuGZ knockdown results in defects in KT-MT attachments and chromosome congression. For cancer biology, these results raise the possibility that inhibiting GLEBS domain interactions with Bub3 might be a therapeutic strategy for refractory cancers like GBM, which suffer from lethal KT-MT instability brought about by oncogenic stress (Ding et al., 2013). For evolutionary biology, these results suggest that BuGZ function might have arisen in higher eukaryotes to facilitate Bub3 function and chromosome congression.

EXPERIMENTAL PROCEDURES

Western blotting, affinity purification, mass spectrometry, and immunoprecipitations were performed according to standard protocols. Refer to the Supplemental Experimental Procedures for details.

Cell Culture and Drug Treatment

GSC and NSC lines were grown in N2B27 neural basal media (StemCell Technologies) supplemented with epidermal growth factor (EGF) and fibroblast growth factor 2 (FGF-2; 20 ng/ml each; Peprotech) on laminin (Sigma) coated polystyrene plates and passaged as described previously (Ding et al., 2013; Hubert et al., 2013). Specifically, cells were detached from their plates using Accutase (Millipore), centrifuged, and resuspended with the appropriate media every 3–4 days. 293T and HeLa cells (ATCC) were grown in 10% fetal bovine serum (FBS)/Dulbecco's modified Eagle's medium (Invitrogen). Cells were incubated with 800 nM or 10 μM nocodazole (Sigma) for 24 hr or 1 hr, respectively. Taxol (Sigma) was used at 10 μM for 24 hr, and MG132 (Tocris) was also used at a final concentration of 10 μM. Live-cell imaging was performed in Leibovitz's L-15 media (Invitrogen) supplemented with 10% FBS, 7 mM HEPES pH 7.0, and 4.5 g/l glucose.

Growth Assays

For short-term single clone validation assays, cells were infected with lentivirus containing a single shRNA to the respective gene. Following selection, cells were harvested, counted (NucleoCounter; NBS), and plated in triplicate onto 96-well plates coated with laminin (Ding et al., 2013; Hubert et al., 2013). After 7 days under standard growth conditions with 0.5 μg/ml of puromycin to maintain selection and prevent outgrowth of residual uninfected cells, cell-proliferation rates were measured using Alamar blue reagent (Invitrogen) according to the manufacturer's instructions. For analysis, shRNA-containing samples were normalized to their respective shControl samples.

Western Blotting

Western blots were carried out according to standard laboratory practices (http://www.cshprotocols.org), except that cells were lysed in a modified RIPA buffer (150 mM NaCl, 50 mM Tris, pH 7.5, 2 mM $MgCl_2$, 0.1% SDS, 2 mM dichlorodiphenyltrichloroethane, 0.4% deoxycholate, 0.4% Triton X-100, 1× complete protease inhibitor cocktail [complete Mini EDTA-free; Roche], and 1 U/μl benzonase nuclease [Novagen]) at room temperature for 15 min (Chen et al., 2012; Ding et al., 2013; Hubert et al., 2013). Additionally, some cells were subjected to treatment with the protease inhibitor MG-132 (EMD Millipore) at 10 μM for 18.5 hr following the infection/selection process. After a shake-off, cells in suspension (mitotic cells) were harvested. Cells that remained attached to the culture plate were washed with PBS to remove the remaining mitotic cells in culture and detached (interphase/asynchronous cells). Attached cells were then washed with PBS and lysed using the modified RIPA buffer.

Immunofluorescence

Cells were grown on sterile acid-washed coverslips in 35 mm cell-culture dishes. The cells were rinsed with PHEM (60 mM PIPES, 25 nM HEPES, 10 mM EGTA, 4 mM $MgSO_4$) and either immediately treated with 4% paraformaldehyde (PFA) for 20 min at room temperature or (for phosphorylation-specific antibodies) treated with lysis buffer (PHEM + 1.0% Triton X-100) for 5 min at 37°C and then PFA fixed for 20 min at room temperature. Fixed cells were washed and then blocked for 1 hr at room temperature in PHEM + 10% boiled donkey serum

(D) BuGZ KT localization requires KNL1. HeLa cells stably expressing BuGZ-GFP were transfected with siControl or siKNL1 and stained with ACA.
(E) BuGZ KT binding is regulated by KT-MT attachment. GFP-BuGZ stable HeLa cells were treated as shown with nocodazole or taxol and imaged.
(F) Bub3 total and KT-associated protein decreases after BuGZ depletion. Normalized protein levels were determined by western blot (left) and immunofluorescence (right) (n = 2; error bars represent cellular deviation [control] and experimental deviation [*BuGZ* siRNA]).
See also Figure S4.

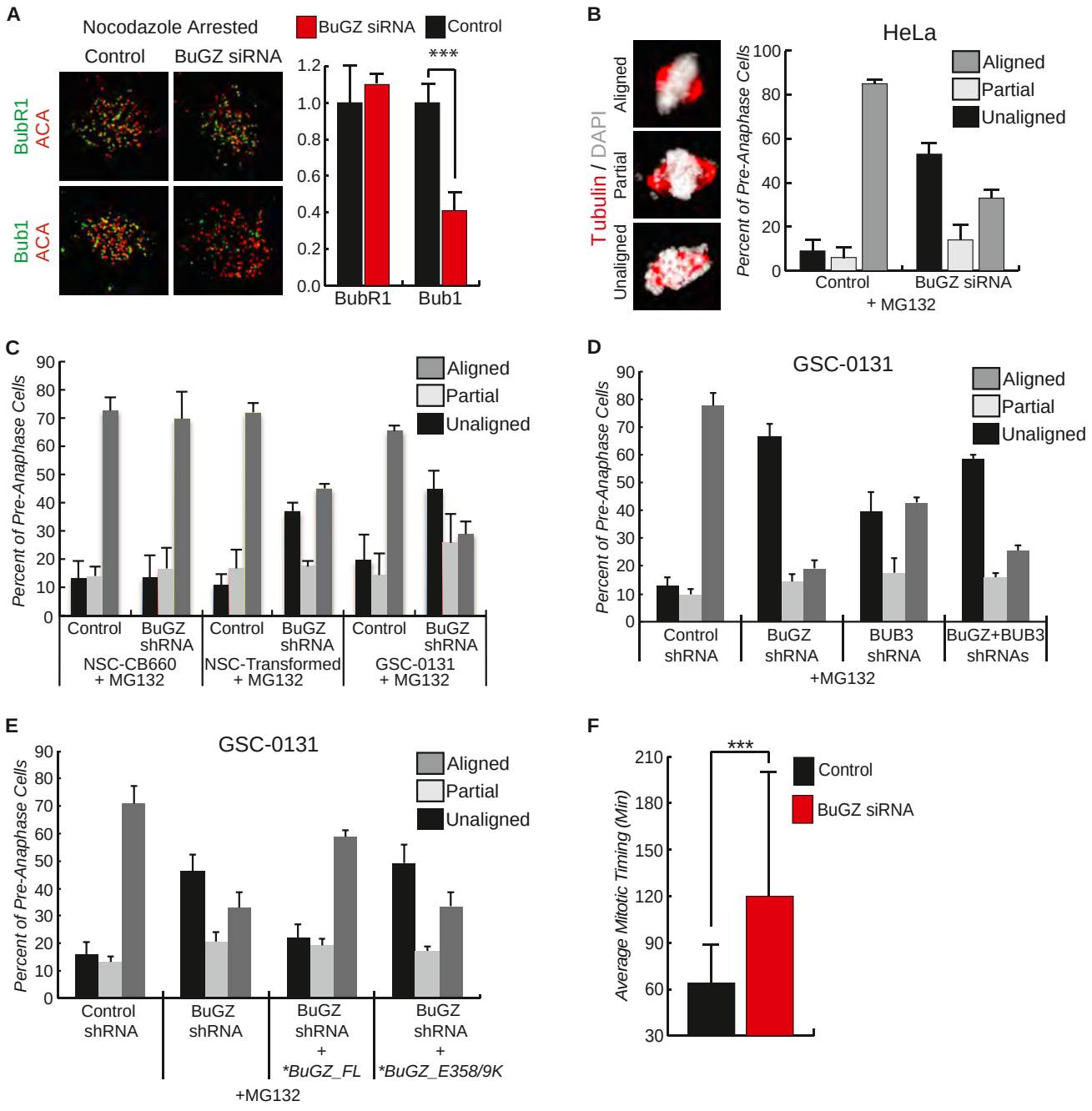

Figure 5. BuGZ Activity Is Required for Proper Chromosome Alignment

(A) Immunofluorescence analysis of BubR1 and Bub1 KT association. Representative images (left) and quantitative analysis (right) show that BuGZ depletion does not alter BubR1 levels, but Bub1 localization is significantly reduced (Student's t test $p < 0.001$). The total protein levels of both BubR1 and Bub1 are unaltered (Figure 3; n = 2; error bars represent cellular deviation [control] and experimental deviation [*BuGZ* siRNA]).

(B) BuGZ depletion causes chromosome alignment defects in HeLa cells. After MG132 treatment, 35% of BuGZ-depleted cells align chromosomes, compared with 85% of control cells (>800 cells counted/condition; +SD).

(C) BuGZ depletion causes chromosome alignment defects in transformed NSC-CB660 and GSC-0131 cells, but not in nontransformed NSC-CB660 cells. After 2 hr of MG132 treatment, 70% of BuGZ-depleted NSC-CB660 cells align chromosomes, compared with 45% of BuGZ-depleted transformed NSC-CB660 cells (>395 cells counted/condition; +SD).

(D) In GSC-0131 cells, BuGZ and Bub3 codepletion causes chromosome alignment defects similar to those observed with BuGZ and Bub3 depletion alone. After 2 hr of MG132 treatment, 26% of BuGZ/Bub3-codepleted GSC-0131 cells align chromosomes, compared with 19% of BuGZ-depleted cells and 43% of Bub3-depleted cells (>535 cells counted/condition; +SD).

(E) Ectopic expression of wild-type BuGZ, but not BuGZ GLEBS-domain mutants (E358K E359K), rescues chromosome alignment defects in GSCs depleted for endogenous BuGZ. After 2 hr of MG132 treatment, 59% of BuGZ-depleted GSCs expressing *shBuGZ*-resistant (denoted by *) full-length

(legend continued on next page)

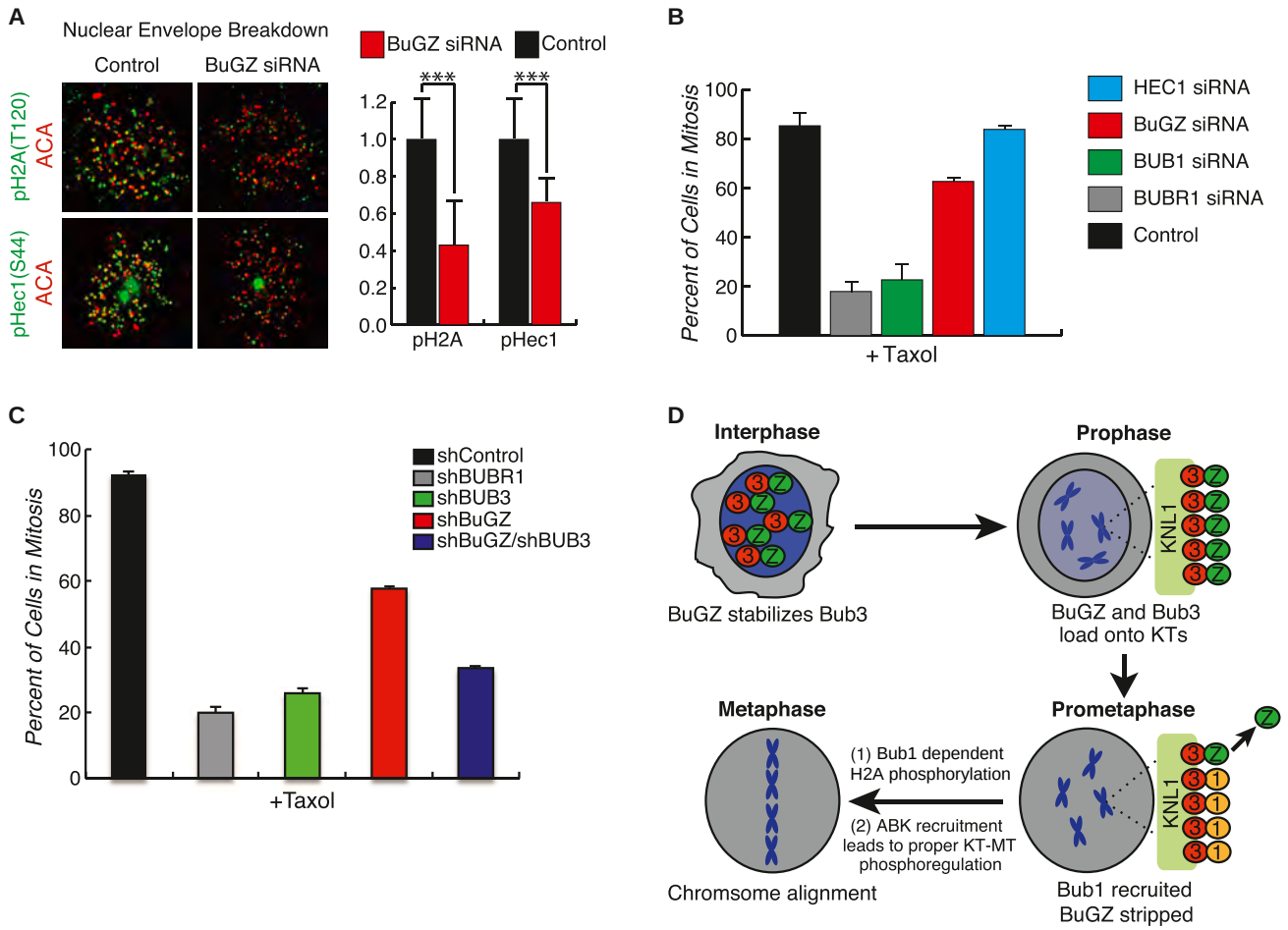

Figure 6. BuGZ Activity Is Required for Localization and Activation of ABK, and the SAC

(A) Immunofluorescence analysis for kinase activity of Bub1 and Aurora B. Representative images (left) and quantitative analysis (right) show that BuGZ depletion decreases phosphorylation of the Bub1 and Aurora B substrates H2A and Hec1, respectively. ***Student's t test $p < 0.001$; n = 2; error bars represent cellular deviation (control) and experimental deviation (*BuGZ* siRNA).

(B) BuGZ-depleted cells sustain a moderate mitotic arrest in MT poisons. A majority of control (black) and attachment factor Hec1 (blue) depleted cells are mitotic after 24 hr in taxol. Depleting the SAC proteins BubR1 (gray) and Bub1 (green) causes premature mitotic exit. BuGZ depletion (red) causes an intermediate phenotype, suggesting that cells establish a SAC response but cannot maintain it (n = 2; >1,000 cells counted/condition; +SD).

(C) BuGZ and Bub3 codepleted cells (blue) do not sustain a checkpoint arrest. A majority of control depleted cells (black) are mitotic after 24 hr in taxol. Depleting the SAC proteins BubR1 (gray) and Bub3 (green) causes a premature mitotic exit, whereas BuGZ depletion (red) causes an intermediate phenotype. Thus, BuGZ-induced arrests require checkpoint signaling (n = 3; >1,000 cells counted/condition; +SD).

(D) Model of BuGZ function.

See also Figure S6.

(BDS). Primary antibodies were diluted in PHEM + 5% BDS and incubated for 16 hr at 4°C. See the Supplemental Experimental Procedures for further details.

Transformed NSCs

Normal CB660 NSCs were simultaneously infected with retrovirus containing pBABE-hTERT + p53DD (Plasmid 11128; Addgene), pBABE-cyclinD1 + CDK4R24C (Plasmid 11129; Addgene), and pBABE-c-mycT58A + HRasG12V (Plasmid 11130; Addgene) for three consecutive rounds of infection (Hubert et al., 2013). After recovery, cells were selected with neomycin for Ras and blasticidin for c-myc.

SSEA1+ Outgrowth Assays

Cells were infected with shControl and *shBuGZ* virus for 48 hr, followed by selection with puromycin for 72 hr. The cells were detached from their respective plate, counted with a NucleoCounter, and mixed with untreated cells. After mixing, the cells were seeded to a six-well tissue-culture dish coated with

BuGZ display aligned chromosomes, compared with 34% for the *BuGZ* allele containing mutations in the GLEBS domain (>445 cells counted/condition; +SD).

(F) BuGZ depletion delays mitotic timing. HeLa cells expressing H2B-GFP fusion protein were imaged at 5 min intervals to determine the time from nuclear envelope breakdown until anaphase onset. The average mitotic timing for BuGZ-depleted cells was 120 min, compared with 60 min in control cells. ***Mann-Whitney test, $p < 0.001$; n > 60 cells/condition; +SD.

See also Figure S5.

laminin for further growth. After 3 days in culture, the cells were harvested, counted, seeded onto a 6-well tissue-culture dish coated with laminin for further growth, or washed with cold PBS containing 0.5% BSA for flow analysis. The cells were analyzed at days 0, 3, 7, 14, and 21. Data analysis was performed using FlowJo (Three Star). See the Supplemental Experimental Proceduresfor further details.

Limiting Dilution Assay

Cells were infected with shControl or *shBuGZ* virus for 48 hr, followed by selection with puromycin for 72 hr (day 0). The cells were detached from their respective plate, dissociated into single-cell suspensions, counted with a NucleoCounter, and then plated onto non-tissue-culture-treated, non-laminin-coated 96-well plates at various seeding densities (0.125–256 cells per well, 10 wells per seeding density). The cells were incubated at 37°C for 3 weeks and fed with 10× EGF and FGF-2 NSC expansion media every 3–4 days. At the time of quantification, each well was examined for the formation of tumor spheres.

Xenotransplantation

For xenotransplantation, 0827 GSCs were infected with pGIPZ shRNA virus and selected for 3 days in puromycin (1 μg/ml). Cells were then harvested using Accutase (Sigma), counted, resuspended in an appropriate volume of culture media, mixed with 90% GIPZ plus 10% untreated cells (noninfected cells), and kept on ice prior to immediate transplantation (Hubert et al., 2013). NOD-*scid* IL2Rgamma^{null} mice (#005557; The Jackson Laboratory) were sedated by inhalation of isoflurane. A small-bore hole was made in the skull using a hand drill with a Meisinger #009 steel burr bit (Hager and Meisinger). Then 1×10^5 cells were slowly injected by pipet into the right frontal cortex approximately 2 mm rostral to bregma, 2 mm lateral, and 3 mm deep through a 0.2–10 μl disposable sterile aerosol barrier tip (#02-707-30; Fisher Scientific). The burr hole was closed using SURGIFOAM (Johnson & Johnson) and the skin was rejoined using Tissumend II (Veterinary Product Laboratories). Seventeen days after the initial transplantation, the mice were injected intravenously through the tail with 100 μl of 10 μM chlorotoxin:indocyanine green (Blaze Bioscience) 4 hr prior to sacrifice by carbon dioxide inhalation. The brain and tumor were removed from the skull and imaged for GFP and indocyanine green fluorescence using the Xenogen IVIS Spectrum imaging system (Caliper Life Sciences). All mouse studies were conducted in accordance with protocols approved by the Institutional Animal Care and Use Committee.

SUPPLEMENTAL INFORMATION

Supplemental Information includes Supplemental Experimental Procedures, six figures, and two tables and can be found with this article online at http://dx.doi.org/10.1016/j.devcel.2013.12.014.

ACKNOWLEDGMENTS

We thank Sue Biggins, Jonathan Cooper, Bob Hevner, Robert Bradley, and members of the DeLuca and Paddison laboratories for helpful discussions, and Pam Lindberg for administrative assistance. This work was supported by the following grants: National Science Foundation Graduate Research Fellowship Program (DGE-0-718124 and DGE-1256082 to C.M.T.), Accelerate Brain Cancer Cure (P.J.P.), DoD Translational New Investigator Award CA100735 (P.J.P.), NIH R21CA170722-01 (P.J.P.), NIH P30CA15704 (P.J.P.), the Pew Biomedical Scholars Program (J.G.D. and P.J.P.), a Phi Beta Psi Sorority Cancer Research Grant (P.J.P.), and NIH R01 GM088371 (J.G.D.).

Received: September 28, 2013
Revised: December 12, 2013
Accepted: December 20, 2013
Published: January 23, 2014

REFERENCES

Bailer, S.M., Siniossoglou, S., Podtelejnikov, A., Hellwig, A., Mann, M., and Hurt, E. (1998). Nup116p and nup100p are interchangeable through a conserved motif which constitutes a docking site for the mRNA transport factor gle2p. EMBO J. *17*, 1107–1119.

Benanti, J.A., and Galloway, D.A. (2004). The normal response to RAS: senescence or transformation? Cell Cycle *3*, 715–717.

Cheeseman, I.M., Chappie, J.S., Wilson-Kubalek, E.M., and Desai, A. (2006). The conserved KMN network constitutes the core microtubule-binding site of the kinetochore. Cell *127*, 983–997.

Chen, X., Skutt-Kakaria, K., Davison, J., Ou, Y.L., Choi, E., Malik, P., Loeb, K., Wood, B., Georges, G., Torok-Storb, B., and Paddison, P.J. (2012). G9a/GLP-dependent histone H3K9me2 patterning during human hematopoietic stem cell lineage commitment. Genes Dev. *26*, 2499–2511.

DeLuca, J.G., Gall, W.E., Ciferri, C., Cimini, D., Musacchio, A., and Salmon, E.D. (2006). Kinetochore microtubule dynamics and attachment stability are regulated by Hec1. Cell *127*, 969–982.

DeLuca, K.F., Lens, S.M., and DeLuca, J.G. (2011). Temporal changes in Hec1 phosphorylation control kinetochore-microtubule attachment stability during mitosis. J. Cell Sci. *124*, 622–634.

Ding, Y., Hubert, C.G., Herman, J., Corrin, P., Toledo, C.M., Skutt-Kakaria, K., Vazquez, J., Basom, R., Zhang, B., Risler, J.K., et al. (2013). Cancer-specific requirement for BUB1B/BUBR1 in human brain tumor isolates and genetically transformed cells. Cancer Discov. *3*, 198–211.

Galli, R., Binda, E., Orfanelli, U., Cipelletti, B., Gritti, A., De Vitis, S., Fiocco, R., Foroni, C., Dimeco, F., and Vescovi, A. (2004). Isolation and characterization of tumorigenic, stem-like neural precursors from human glioblastoma. Cancer Res. *64*, 7011–7021.

Harris, L., Davenport, J., Neale, G., and Goorha, R. (2005). The mitotic checkpoint gene BubR1 has two distinct functions in mitosis. Exp. Cell Res. *308*, 85–100.

Hoffman, D.B., Pearson, C.G., Yen, T.J., Howell, B.J., and Salmon, E.D. (2001). Microtubule-dependent changes in assembly of microtubule motor proteins and mitotic spindle checkpoint proteins at PtK1 kinetochores. Mol. Biol. Cell *12*, 1995–2009.

Howell, B.J., Moree, B., Farrar, E.M., Stewart, S., Fang, G., and Salmon, E.D. (2004). Spindle checkpoint protein dynamics at kinetochores in living cells. Curr. Biol. *14*, 953–964.

Hoyt, M.A., Totis, L., and Roberts, B.T. (1991). S. cerevisiae genes required for cell cycle arrest in response to loss of microtubule function. Cell *66*, 507–517.

Hubert, C.G., Bradley, R.K., Ding, Y., Toledo, C.M., Herman, J., Skutt-Kakaria, K., Girard, E.J., Davison, J., Berndt, J., Corrin, P., et al. (2013). Genome-wide RNAi screens in human brain tumor isolates reveal a novel viability requirement for PHF5A. Genes Dev. *27*, 1032–1045.

Jablonski, S.A., Chan, G.K., Cooke, C.A., Earnshaw, W.C., and Yen, T.J. (1998). The hBUB1 and hBUBR1 kinases sequentially assemble onto kinetochores during prophase with hBUBR1 concentrating at the kinetochore plates in mitosis. Chromosoma *107*, 386–396.

Kalitsis, P., Earle, E., Fowler, K.J., and Choo, K.H. (2000). Bub3 gene disruption in mice reveals essential mitotic spindle checkpoint function during early embryogenesis. Genes Dev. *14*, 2277–2282.

Kawashima, S.A., Tsukahara, T., Langegger, M., Hauf, S., Kitajima, T.S., and Watanabe, Y. (2007). Shugoshin enables tension-generating attachment of kinetochores by loading Aurora to centromeres. Genes Dev. *21*, 420–435.

Kendall, S.D., Linardic, C.M., Adam, S.J., and Counter, C.M. (2005). A network of genetic events sufficient to convert normal human cells to a tumorigenic state. Cancer Res. *65*, 9824–9828.

Kiyomitsu, T., Obuse, C., and Yanagida, M. (2007). Human Blinkin/AF15q14 is required for chromosome alignment and the mitotic checkpoint through direct interaction with Bub1 and BubR1. Dev. Cell *13*, 663–676.

Klebig, C., Korinth, D., and Meraldi, P. (2009). Bub1 regulates chromosome segregation in a kinetochore-independent manner. J. Cell Biol. *185*, 841–858.

Kruse, T., Zhang, G., Larsen, M.S., Lischetti, T., Streicher, W., Kragh Nielsen, T., Bjørn, S.P., and Nilsson, J. (2013). Direct binding between BubR1 and B56-PP2A phosphatase complexes regulate mitotic progression. J. Cell Sci. *126*, 1086–1092.

Lampson, M.A., and Kapoor, T.M. (2005). The human mitotic checkpoint protein BubR1 regulates chromosome-spindle attachments. Nat. Cell Biol. *7*, 93–98.

Lara-Gonzalez, P., Westhorpe, F.G., and Taylor, S.S. (2012). The spindle assembly checkpoint. Curr. Biol. *22*, R966–R980.

Larsen, N.A., Al-Bassam, J., Wei, R.R., and Harrison, S.C. (2007). Structural analysis of Bub3 interactions in the mitotic spindle checkpoint. Proc. Natl. Acad. Sci. USA *104*, 1201–1206.

Liu, S.T., Rattner, J.B., Jablonski, S.A., and Yen, T.J. (2006). Mapping the assembly pathways that specify formation of the trilaminar kinetochore plates in human cells. J. Cell Biol. *175*, 41–53.

Logarinho, E., Resende, T., Torres, C., and Bousbaa, H. (2008). The human spindle assembly checkpoint protein Bub3 is required for the establishment of efficient kinetochore-microtubule attachments. Mol. Biol. Cell *19*, 1798–1813.

London, N., Ceto, S., Ranish, J.A., and Biggins, S. (2012). Phosphoregulation of Spc105 by Mps1 and PP1 regulates Bub1 localization to kinetochores. Curr. Biol. *22*, 900–906.

Malureanu, L.A., Jeganathan, K.B., Hamada, M., Wasilewski, L., Davenport, J., and van Deursen, J.M. (2009). BubR1 N terminus acts as a soluble inhibitor of cyclin B degradation by APC/C(Cdc20) in interphase. Dev. Cell *16*, 118–131.

Meraldi, P., and Sorger, P.K. (2005). A dual role for Bub1 in the spindle checkpoint and chromosome congression. EMBO J. *24*, 1621–1633.

Meraldi, P., Draviam, V.M., and Sorger, P.K. (2004). Timing and checkpoints in the regulation of mitotic progression. Dev. Cell *7*, 45–60.

Musacchio, A., and Salmon, E.D. (2007). The spindle-assembly checkpoint in space and time. Nat. Rev. Mol. Cell Biol. *8*, 379–393.

Pahl, P.M., Hodges, Y.K., Meltesen, L., Perryman, M.B., Horwitz, K.B., and Horwitz, L.D. (1998). ZNF207, a ubiquitously expressed zinc finger gene on chromosome 6p21.3. Genomics *53*, 410–412.

Perera, D., Tilston, V., Hopwood, J.A., Barchi, M., Boot-Handford, R.P., and Taylor, S.S. (2007). Bub1 maintains centromeric cohesion by activation of the spindle checkpoint. Dev. Cell *13*, 566–579.

Powell, S., Szklarczyk, D., Trachana, K., Roth, A., Kuhn, M., Muller, J., Arnold, R., Rattei, T., Letunic, I., Doerks, T., et al. (2012). eggNOG v3.0: orthologous groups covering 1133 organisms at 41 different taxonomic ranges. Nucleic Acids Res. *40* (Database issue), D284–D289.

Primorac, I., and Musacchio, A. (2013). Panta rhei: the APC/C at steady state. J. Cell Biol. *201*, 177–189.

Primorac, I., Weir, J.R., Chiroli, E., Gross, F., Hoffmann, I., van Gerwen, S., Ciliberto, A., and Musacchio, A. (2013). Bub3 reads phosphorylated MELT repeats to promote spindle assembly checkpoint signaling. eLife *2*, e01030.

Pritchard, C.E., Fornerod, M., Kasper, L.H., and van Deursen, J.M. (1999). RAE1 is a shuttling mRNA export factor that binds to a GLEBS-like NUP98 motif at the nuclear pore complex through multiple domains. J. Cell Biol. *145*, 237–254.

Ren, Y., Seo, H.S., Blobel, G., and Hoelz, A. (2010). Structural and functional analysis of the interaction between the nucleoporin Nup98 and the mRNA export factor Rae1. Proc. Natl. Acad. Sci. USA *107*, 10406–10411.

Ricke, R.M., Jeganathan, K.B., Malureanu, L., Harrison, A.M., and van Deursen, J.M. (2012). Bub1 kinase activity drives error correction and mitotic checkpoint control but not tumor suppression. J. Cell Biol. *199*, 931–949.

Santaguida, S., and Musacchio, A. (2009). The life and miracles of kinetochores. EMBO J. *28*, 2511–2531.

Singh, S.K., Hawkins, C., Clarke, I.D., Squire, J.A., Bayani, J., Hide, T., Henkelman, R.M., Cusimano, M.D., and Dirks, P.B. (2004). Identification of human brain tumour initiating cells. Nature *432*, 396–401.

Son, M.J., Woolard, K., Nam, D.H., Lee, J., and Fine, H.A. (2009). SSEA-1 is an enrichment marker for tumor-initiating cells in human glioblastoma. Cell Stem Cell *4*, 440–452.

Suijkerbuijk, S.J., Vleugel, M., Teixeira, A., and Kops, G.J. (2012). Integration of kinase and phosphatase activities by BUBR1 ensures formation of stable kinetochore-microtubule attachments. Dev. Cell *23*, 745–755.

Taylor, S.S., and McKeon, F. (1997). Kinetochore localization of murine Bub1 is required for normal mitotic timing and checkpoint response to spindle damage. Cell *89*, 727–735.

Taylor, S.S., Ha, E., and McKeon, F. (1998). The human homologue of Bub3 is required for kinetochore localization of Bub1 and a Mad3/Bub1-related protein kinase. J. Cell Biol. *142*, 1–11.

Tsukahara, T., Tanno, Y., and Watanabe, Y. (2010). Phosphorylation of the CPC by Cdk1 promotes chromosome bi-orientation. Nature *467*, 719–723.

Vanoosthuyse, V., Valsdottir, R., Javerzat, J.P., and Hardwick, K.G. (2004). Kinetochore targeting of fission yeast Mad and Bub proteins is essential for spindle checkpoint function but not for all chromosome segregation roles of Bub1p. Mol. Cell. Biol. *24*, 9786–9801.

Wang, X., Babu, J.R., Harden, J.M., Jablonski, S.A., Gazi, M.H., Lingle, W.L., de Groen, P.C., Yen, T.J., and van Deursen, J.M. (2001). The mitotic checkpoint protein hBUB3 and the mRNA export factor hRAE1 interact with GLE2p-binding sequence (GLEBS)-containing proteins. J. Biol. Chem. *276*, 26559–26567.

Wang, Q., Liu, T., Fang, Y., Xie, S., Huang, X., Mahmood, R., Ramaswamy, G., Sakamoto, K.M., Darzynkiewicz, Z., Xu, M., and Dai, W. (2004). BUBR1 deficiency results in abnormal megakaryopoiesis. Blood *103*, 1278–1285.

Welburn, J.P., Vleugel, M., Liu, D., Yates, J.R., 3rd, Lampson, M.A., Fukagawa, T., and Cheeseman, I.M. (2010). Aurora B phosphorylates spatially distinct targets to differentially regulate the kinetochore-microtubule interface. Mol. Cell *38*, 383–392.

Yamagishi, Y., Honda, T., Tanno, Y., and Watanabe, Y. (2010). Two histone marks establish the inner centromere and chromosome bi-orientation. Science *330*, 239–243.

Yamagishi, Y., Yang, C.H., Tanno, Y., and Watanabe, Y. (2012). MPS1/Mph1 phosphorylates the kinetochore protein KNL1/Spc7 to recruit SAC components. Nat. Cell Biol. *14*, 746–752.

Published OnlineFirst August 7, 2014; DOI: 10.1158/1078-0432.CCR-13-0645

Clinical Cancer Research

Molecular Pathways: Regulation and Targeting of Kinetochore–Microtubule Attachment in Cancer

Jacob A. Herman[1], Chad M. Toledo[2,3], James M. Olson[4], Jennifer G. DeLuca[1], and Patrick J. Paddison[2,3]

Abstract

Kinetochores are large protein structures assembled on centromeric DNA during mitosis that bind to microtubules of the mitotic spindle to orchestrate and power chromosome movements. Deregulation of kinetochore–microtubule (KT–MT) attachments has been implicated in driving chromosome instability and cancer evolution; however, the nature and source of KT–MT attachment defects in cancer cells remain largely unknown. Here, we highlight recent findings suggesting that oncogene-driven changes in kinetochore regulation occur in glioblastoma multiforme (GBM) and possibly other cancers exhibiting chromosome instability, giving rise to novel therapeutic opportunities. In particular, we consider the GLE2p-binding sequence domains of BubR1 and the newly discovered BuGZ, two kinetochore-associated proteins, as candidate therapeutic targets for GBM. *Clin Cancer Res; 21(2); 233–9.* ©*2014 AACR.*

Background

Regulating kinetochore–microtubule attachment during mitosis

Kinetochores are large protein structures assembled on centromeric DNA during mitosis that bind to microtubules of the mitotic spindle to orchestrate and power chromosome movements. To properly segregate chromosomes during mitosis, kinetochores must attach to the dynamic plus-ends of mitotic spindle microtubules (1). Early in mitosis, attachments are unstable and labile, allowing improperly connected microtubules to be released. This prevents premature stabilization of commonly generated erroneous attachments, which can lead to chromosome mis-segregation (1, 2). Conversely, in late mitosis, KT–MT attachments are stabilized to generate forces required for chromosome movements and to silence the spindle assembly checkpoint (SAC), which prevents mitotic exit until all chromosomes are properly bioriented (1, 2).

Although many of the >100 proteins that comprise the vertebrate kinetochore contribute to the generation of KT–MT attachments, the core attachment factor is the "KMN network," comprised of KNL1, the MIS12 complex, and the NDC80 complex (Fig. 1; refs. 1, 3). Regulation of KT–MT attachments relies on the essential mitotic kinase Aurora B (ABK). Upon nuclear envelope breakdown, kinetochores lack spatial organization and bind microtubules indiscriminately. Thus, early in mitosis, it is common for sister kinetochore pairs to attach to microtubules emanating from the same pole (syntelic attachment) or for a single kinetochore to attach to microtubules from both poles (merotelic attachment; ref. 1). To prevent the accumulation of such attachment errors, ABK phosphorylates multiple kinetochore proteins early in mitosis, including members of the KMN network, to increase KT–MT turnover (Fig. 1A; refs. 2–5). As mitosis progresses, kinase activity decreases and phosphatase activity dominates, resulting in low levels of ABK-dependent kinetochore phosphorylation. Decreased NDC80 complex phosphorylation increases its microtubule-binding activity, resulting in stabilized KT–MT attachments (Fig. 1B; ref. 6). Defects in the ABK regulatory system can result in erroneous KT–MT attachments, which often lead to chromosome segregation errors and chromosome instability, which are observed in many cancers (7).

To prevent mitotic exit until proper KT–MT attachments have formed, the cell uses a surveillance mechanism known as the SAC. The core SAC proteins, MAD1, MAD2, BUBR1, BUB1, BUB3, and MPS1, accumulate at unattached kinetochores and generate a "wait anaphase" signal, which inhibits activation of the anaphase promoting complex/cyclosome (APC/C) and prevents mitotic exit (8, 9). The mechanism by which cells integrate both phosphoregulation and SAC signals is still being characterized, yet interestingly, some SAC proteins have direct roles in KT–MT attachment, independent of their well-defined checkpoint functions. For instance, both BUBR1 and BUB1 function at this interface between KT–MT attachments and the SAC. BUBR1 recruits the phosphatase PP2A to kinetochores to dephosphorylate ABK substrates and promote KT–MT attachment stability (Fig. 1; refs. 10–12). In addition, BUB1 has been implicated in regulating KT–MT attachments both through the recruitment of ABK to centromeres via phosphorylation of histone H2A and through promotion of ABK activity at kinetochores independent of its

[1]Department of Biochemistry and Molecular Biology, Colorado State University, Fort Collins, Colorado. [2]Human Biology Division, Fred Hutchinson Cancer Research Center, Seattle, Washington. [3]Molecular and Cellular Biology Program, University of Washington, Seattle, Washington. [4]Clinical Research Division, Fred Hutchinson Cancer Research Center, Seattle, Washington.

Note: J.G. DeLuca and P.J. Paddison share senior authorship.

Corresponding Authors: Jennifer G. DeLuca, Colorado State University, Fort Collins, CO 80523. Phone: 970-491-6718; Fax: 970-491-0494; E-mail: Jennifer.Deluca@ColoState.edu; and Patrick J. Paddison, Fred Hutchinson Cancer Research Center, Seattle, WA 98109. Phone: 206-667-4312; Fax: 206-667-4023; E-mail: paddison@fhcrc.org

doi: 10.1158/1078-0432.CCR-13-0645

Published OnlineFirst August 7, 2014; DOI: 10.1158/1078-0432.CCR-13-0645

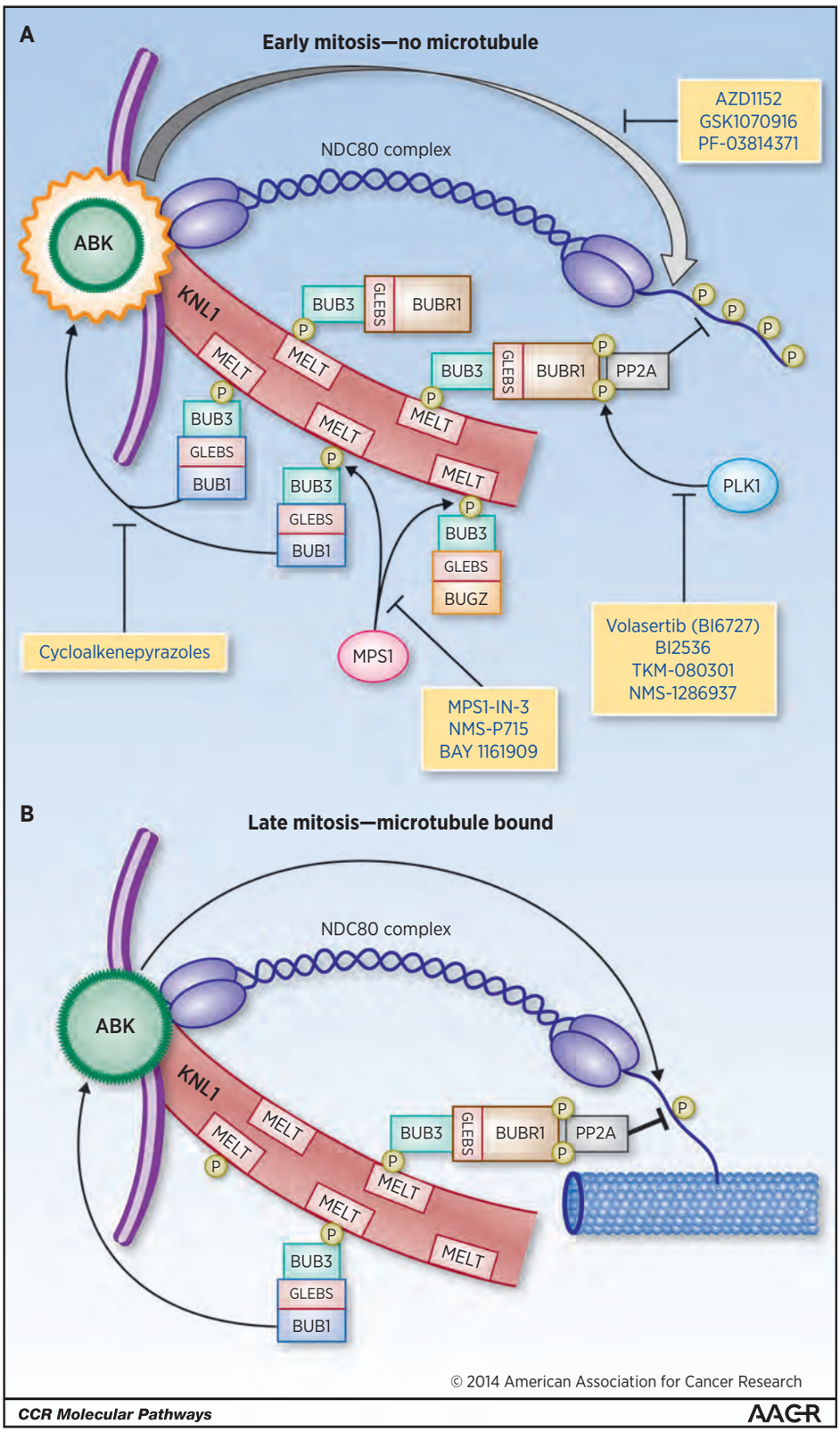

Figure 1.
A, early in mitosis, three GLEBS-containing proteins, BUBR1, BUGZ, and BUB1, accumulate at kinetochores through BUB3 binding to regulate KT–MT attachments. The recruitment of these proteins is dependent on MPS1 phosphorylation of MELT motifs in KNL1. BUB1 and Aurora B kinases increase kinetochore phosphorylation, particularly of the Ndc80 complex, to inhibit stable microtubule attachment. Conversely, BUBR1/PLK1 recruits PP2A to counteract kinetochore phosphorylation to facilitate KT–MT attachment stabilization. B, late in mitosis, phosphatase activity dominates and reduces kinetochore phosphorylation to stabilize microtubule attachments. Clinically relevant chemical inhibitors of kinetochore phosphoregulation are shown in blue.

Published OnlineFirst August 7, 2014; DOI: 10.1158/1078-0432.CCR-13-0645

centromere accumulation (Fig. 1; refs. 13–15). Although SAC activity and SAC protein levels have been commonly characterized in cancers, their secondary role in regulating KT–MT attachments has only recently been evaluated.

Rethinking SAC function in cancer

Cytologic analysis of most late-stage solid tumors such as gliomblastoma multiforme (GBM) reveals dramatic numerical and structural chromosome alterations (16) and intratumoral genomic heterogeneity (16–19). All of these features can promote tumor cell evolution, invasiveness, therapy resistance, and recurrence (7, 20–22). Such chromosomal alterations often arise from aberrant mitoses (e.g., lagging chromosomes, anaphase bridges), consistent with increases in chromosome instability during tumor progression (7, 23, 24). Loss of SAC function is a common explanation proffered for increased chromosome instability and aneuploidy in cancers (25–27). This notion that loss of SAC activity promotes tumorigenesis has found support in studies of certain cancers (25, 26) and model systems (e.g., mouse knockouts of certain SAC genes; refs. 23, 28). However, loss-of function mutations in SAC genes are rare in cancers (27), and many late-stage cancers exhibit high SAC gene expression (29, 30), suggesting hyperactivity (30, 31). Furthermore, as discussed above, there is now evidence that SAC proteins play additional roles in KT–MT regulation. Thus, paradoxically, instead of loss of SAC activity causing chromosome instability and complex karyotypes observed in high-grade glioma and ductal carcinomas, it is likely that SAC proteins become increasingly required to support mitotic defects in KT–MT attachments as low-grade tumors transition to aggressive malignancies such as GBM.

One hypothesis is that oncogenic signaling fundamentally alters regulation of KT–MT attachments in cancers with increased SAC protein expression, resulting in chromosome alignment defects. These defects are suppressed by the contribution of SAC proteins in regulating KT–MT attachments, an otherwise nonessential function. Data supporting this hypothesis are summarized below. If true, the allowance of otherwise lethal KT–MT attachments by SAC proteins leads to the genomic instability observed for such cancers, albeit other factors likely contribute (e.g., tetraploidization, chromothrypsis, telomere fusions, sister chromatid cohesion defects).

The KT–MT attachment activities of SAC proteins may represent much sought-after cancer-specific therapeutic targets for GBM and other refractory late-stage cancers. This particular mechanism may transcend the heterogeneity of molecular subclasses and combinations of oncogenic drivers that has thwarted most pharmacologic interventions for aggressive malignancies in the past.

KT–MT attachments are defective in GBM patient isolates

GBM, or grade IV astrocytoma, is the most aggressive and common form of brain cancer in adults (32, 33). Even with standard-of-care treatments, including surgery, radiation, and the alkylating agent temozolomide, GBM remains among the deadliest cancers, with a median survival period of 12 to 14 months (32, 33). Standard-of-care therapies fail in part due to the fact that GBM tumors are heterogeneous both in cellular composition (e.g., cell morphology and gene expression; ref. 21) and in karyotype (17).

To identify new therapeutic targets for GBM, others and we have performed functional genetic screens in patient-derived GBM stem-like cells (GSC; refs. 30, 34–39). GSCs retain tumor-initiating potential and tumor-specific genetic and epigenetic signatures over extended outgrowth periods (36, 38), under culture conditions that mimic the neural progenitor perivascular niche (40, 41). By performing parallel RNAi screens in GSCs and fetal neural stem cells (a nontransformed candidate cell of origin control), we were able to find genes that when knocked down specifically blocked GSC expansion (i.e., candidate cancer lethal genes). Among these genes were BUB1B/BUBR1 and BUGZ, two kinetochore-associated proteins with roles in regulating KT–MT attachment (30, 39). These studies revealed that GBM cells have two separable defects in kinetochore regulation triggered by oncogenic signaling, which BUBR1 and BUGZ suppress.

BUB1B/BUBR1 function in GBM

BUB1B encodes the highly conserved BUB1-like pseudokinase, BUBR1. BUBR1 has multiple functional domains that have been implicated in mitotic checkpoint control, mitotic timing, and regulating KT–MT attachment (8–10, 27, 42). These include N- and C-terminal KEN box domains required for CDC20 binding and APC/C inhibition (43), a C-terminal kinase domain required for protein stability (44), and a GLE2p-binding sequence (GLEBS) domain necessary for kinetochore localization during mitosis (45, 46). Although BUB1B is essential for mammalian development (31), its essential function is contained solely within the N-terminal KEN box (30, 47), which enables BUBR1 to act as a pseudo-substrate inhibitor of APC/C^{Cdc20} during G_2 and preanaphase mitosis, preventing premature anaphase onset (43, 47).

By contrast, recent studies suggest that BUBR1's GLEBS domain and kinetochore localization are not required for KT–MT attachment in normally dividing somatic cells (e.g., mouse embryo fibroblasts, neural stem cells, astrocytes, retinal pigment epithelial cells). However, in approximately 60% of GBM isolates assayed, RAS-transformed cells, and HeLa cells, the GLEBS domain becomes essential to suppress lethal KT–MT attachment defects (30). BUBR1's GLEBS domain facilitates its interaction with BUB3 and its localization to prometaphase kinetochores, where BUBR1 stabilizes KT–MT attachment by recruiting PP2A to kinetochores to counteract ABK phosphorylation of outer kinetochore substrates (Fig. 1; refs. 11, 12).

Intriguingly, defects in kinetochore regulation are observed in cells that require the BUBR1 GLEBS domain. BUBR1-sensitive cells invariably have shorter distances between sister kinetochores when stable end-on microtubule attachments have formed at metaphase, termed interkinetochore distances (IKD; ref. 30). This distance serves as an indirect measure of the pulling forces generated by dynamic microtubules bound to kinetochores, such that stronger attachments lead to longer IKDs and weaker attachments produce shorter IKDs. A survey of different cell types revealed that, in general, nontransformed cells, including astrocytes, fibroblasts, hematopoietic progenitors, neural stem cells, and retinal pigment epithelial cells, all have "long" IKDs (~1.24 μm), whereas other transformed cell types, including HeLa cells and RASV12-expressing MEFs, exhibit "short" IKDs (~1.12 μm). In cells harboring short IKDs, knockdown of BUBR1 or GLEBS domain inhibition results in profound loss of KT–MT attachment and cell death. This suggests that BUBR1-dependent kinetochore recruitment of PP2A is not essential for normal KT–MT dynamics, perhaps due to functional redundancy with other kinetochore phosphatases, or alternative PP2A recruitment mechanisms. However, in a subset of cancer cells, oncogenic signaling may lead to ABK misregulation,

Published OnlineFirst August 7, 2014; DOI: 10.1158/1078-0432.CCR-13-0645

which prevents stable end-on attachment of KT–MTs in the absence of BUBR1 activity.

BUGZ function in GBM

BUGZ was isolated from an RNAi screen targeting putative human transcription factors to identify key regulators of GSC expansion. This previously uncharacterized C2–H2 zinc-finger domain gene and putative transcription factor was originally named ZNF207 (39, 48). We renamed the gene *BUGZ* (Bub3 interacting GLEBS and Zinc finger domain containing protein) and demonstrated that it is a novel kinetochore component that binds to and stabilizes BUB3 during interphase and mitosis (Fig. 1A). Just like BUBR1, BUGZ binds to BUB3 through a highly conserved GLEBS domain. Inhibition of BUGZ results in loss of both BUB3 and another BUB3 binding partner, BUB1, from kinetochores, but does not result in loss of BUBR1 from kinetochores (39). Localized BUB1 kinase activity helps mediate proper KT–MT attachments through recruitment and activation of ABK to centromeres and kinetochores (13–15). Consistent with BUGZ affecting BUB1 kinetochore localization in GBM isolates, we observe chromosome alignment defects in transformed cells with BUGZ knockdown, but not in untransformed cells. As expected, BUGZ inhibition reduced BUB1 kinase activity at kinetochores as measured by immunostaining the phosphorylated form of its substrate, histone H2AT120, which is key for ABK recruitment. We also observed decreased phosphorylation of HEC1S44, a critical downstream kinetochore substrate of ABK required for regulation of KT–MT attachments. As with BUBR1, we found that the cancer-specific requirement for BUGZ was limited to its GLEBS domain, which mediates BUGZ kinetochore localization.

Intriguingly, the cancer-specific requirement for BUGZ-GLEBS does not correlate to the requirement for BUBR1-GLEBS. Particularly, GBM isolates that do not require the BUBR1-GLEBS for viability do require the BUGZ-GLEBS (39). These independent requirements likely arise from their opposing mechanistic roles; BUBR1 antagonizes ABK activity and stabilizes KT–MT attachments by recruiting the counteracting phosphatase PP2A (Fig. 1B; refs. 10–12, 30). BUGZ instead activates ABK through BUB1 activity, and presumably destabilizes KT–MT attachments (Fig. 1A ref. 39). As opposing regulators, there are likely unique oncogenic pressures that drive the requirement for BUGZ and/or BUBR1. Determining how different oncogenic stresses induce these unique defects, and which, if either, is dominant in GBM will be important for translating these findings into successful therapies.

Clinical–Translational Advances

GLEBS domains as therapeutic targets

A common theme arising from analysis of mitotic defects in GBM patient isolates is the cancer-specific requirement for GLEBS domain activity of BUBR1, BUGZ, and likely BUB1 (30, 39, 49). GLEBS domains are short disordered regions of about 40 amino acids that form a series of salt bridges between the WD40 domains of BUB3 and two glutamate residues in the GLEBS domain (50). As a result of BUB3 binding, the GLEBS domain undergoes a conformational shift from a disordered to a well-ordered structure with fixed interaction points on the top face of BUB3's WD40 propeller (50). This interaction is critical for BUB3-dependent recruitment of BUB1 and BUBR1 to kinetochores (45, 47, 51). For example, a single amino acid change in BUBR1's GLEBS domain (E406K in mouse; corresponds to 409K in human) is sufficient to prevent BUB3 interaction and BUBR1's kinetochore localization (47). In addition to BUGZ, BUB1, and BUBR1, the only other known GLEBS domain–containing protein is NUP98, which binds to the RAE1 WD40 repeat domain protein but not BUB3 (52).

One possible route to new therapeutics for GBM and other cancers with KT–MT attachment defects is targeting the BUB3–GLEBS domain interactions. This would require finding either a GLEBS domain small-molecule mimetic capable of binding BUB3 at its WD40–GLEBS interface and blocking one or all of BUB1/BUBR1/BUGZ GLEBS domain interactions, or alternatively, an allosteric interaction that distorts the GLEBS domain binding interface. Intriguingly, the Structural Genomics Consortium successfully campaigned to find lead compounds that antagonize the WD40 propeller binding pocket of WDR5, which disrupts WDR5 interactions with the MLL1/KMT2 SET domain methyltransferase *in vitro* (53). Moreover, the Tyers lab has recently found allosteric inhibitors (SCF-I2) of the WD40 domain of CDC4, which distort the substrate binding pocket (54). The ideal GLEBS domain drug may be one that would inhibit BUGZ–BUB3 interaction during interphase, which would reduce BUB3 levels by approximately 50% during interphase and prime nonmitotic tumor cells for mitotic catastrophe.

Repurposing current therapies to target KT–MT attachments

More conventional therapies and targets may also take advantage of oncogenically induced kinetochore defects. Both BUBR1 and BUGZ function within complex regulatory pathways to affect kinetochore phosphoregulation, and targeting other mitotic proteins in these pathways may yield GBM-specific cell death. These include kinase activities of MPS1 (55–57), BUB1 (13–15), PKM2 (58), and PLK1 (11). As discussed previously, BUB1 activation of ABK activity requires BUGZ through an unknown mechanism. In addition, BUB1 cannot bind kinetochores without MPS1-dependent phosphorylation of MELT motifs within the kinetochore factor KNL1 (Fig. 1A; refs. 55–57). Thus, kinase inhibitors specific for either MPS1 or BUB1 may exacerbate the same KT–MT attachment defects in GBM that induce the requirement for the BUGZ-GLEBS domain. However, because these kinases are essential for SAC signaling, it remains unclear whether dose-limiting toxicities in noncancer cells will limit the effectiveness of MPS1 or BUB1 inhibitors, albeit there have been promising preclinical trials of MPS1 inhibitors, some of which have initiated phase I trials (59–61). Although cycloalkenepyrazole inhibitors of BUB1 kinase activity have been patented (Patent WO2013167698), no cell-based or *in vivo* studies have been published to date.

Interestingly, PKM2, which has important roles in glycolysis and gene transcription, binds BUB3 during mitosis and phosphorylates residue Y207, a regulatory event required for BUB3-BUB1 complex recruitment to kinetochores in GBM cells (58). PKM2 inhibitors have been previously developed to metabolically target cancers (62). An interesting possibility is that these drugs may have the added effect of destabilizing compromised KT–MT attachments observed in GBM cells which require BUGZ for chromosome alignment; however, this activity has not been assayed.

PLK1 inhibitors have shown efficacy in preclinical work using GBM models (63) and have had clinical success in acute myeloid leukemia. Currently, at least six unique PLK1 inhibitors have

reached phase I or II clinical trails for various cancers, and BI-6727 (volasertib) was recently designated a "breakthrough therapy" by the FDA in the treatment of acute myeloid leukemia after raising complete remission rates 3-fold for patients enrolled in a phase II trial. (64–67)

However, without detailed mechanistic studies, it is difficult to know if the clinical success of these targets is attributable, even in part, to mitotic disruption. As these therapies demonstrate clinical success, it will be important to expand them into cancers with documented KT–MT attachment defects. However, these targets, particularly MPS1 and PLK1, have many roles within the cell cycle, including centrosome duplication and mitotic entry, and thus may exhibit broad antimitotic effects.

Conclusions

Aneuploidy was among the first cytologic features associated with cancer cells (23), and thus chromosome segregation has long been a logical target for cancer therapies. However, our understanding of molecular drivers of chromosome instability in cancer and the interdependency of chromosome instability, tumor initiation, and evolution is only just emerging.

Antimitotic drugs, including microtubule poisons such as taxanes and vinca alkaloids, have long been instrumental in cancer therapy, but unfortunately due to their nonspecific nature can be quite toxic. Even recently developed drugs, such as Aurora kinase or KIF11/EG5 inhibitors, target all dividing cells and thus have performed poorly in clinical trials (68, 69). These failings likely result from targeting mitotic master regulators that are required in healthy cells; inhibiting a ubiquitously essential target dramatically reduces the therapeutic window and efficacy of a treatment. It is clear that the next generation of antimitotic biologic chemotherapies must capitalize on defects already present in cancer cells. Proteins and processes that have become destabilized by oncogenic signaling are ideal targets for a therapy that inhibits accessory or redundant regulators. As observed with BUBR1, healthy cells with robust kinetochore signaling survive BUBR1-GLEBS inhibition, whereas GBM cells, compromised by oncogenic signaling, cannot tolerate this loss. By targeting accessory regulators in defective pathways, healthy cells with redundant or robust regulatory mechanisms are largely unaffected, and the inhibition is amplified or exacerbated in compromised cells.

Kinetochores and their dynamic attachments to microtubules are an exciting area from which to identify targets for precision cancer therapies. Mitotic factors are commonly altered in cancers through mutation, transcriptional changes, or epigenetic and posttranslational modifications. Moreover, a large body of work characterizing the complex pathways, which regulate KT–MT attachments, informs the many targets for chemical intervention. Even more exciting is the possibility of applying previously FDA-approved antimitotic therapies to specific cancers with compromised kinetochore signaling.

Disclosure of Potential Conflicts of Interest

No potential conflicts of interest were disclosed.

Disclaimer

The content is solely the responsibility of the authors and does not necessarily represent the official views of the NIH.

Authors' Contributions

Conception and design: J.A. Herman, C.M. Toledo, J.M. Olson, P.J. Paddison
Acquisition of data (provided animals, acquired and managed patients, provided facilities, etc.): C.M. Toledo, J.M. Olson
Analysis and interpretation of data (e.g., statistical analysis, biostatistics, computational analysis): C.M. Toledo, J.M. Olson
Writing, review, and/or revision of the manuscript: J.A. Herman, J.M. Olson, J.G. DeLuca, P.J. Paddison
Administrative, technical, or material support (i.e., reporting or organizing data, constructing databases): J.G. DeLuca
Study supervision: J.M. Olson, J.G. DeLuca

Acknowledgments

The authors thank members of the DeLuca, Olson, and Paddison laboratories for helpful discussions and Pam Lindberg for administrative assistance.

Grant Support

This work was supported by the NCI and National Institute of General Medical Sciences of the NIH under award numbers R21CA170722-01 (to P.J. Paddison) and RO1GM088371 (to J.G. DeLuca). Further support was provided by the National Science Foundation Graduate Research Fellowship Program (DGE-0-718124 and DGE-1256082; to C.M. Toledo), Accelerate Brain Cancer Cure (to P.J. Paddison), DoD Translational New Investigator Award (CA100735; to P.J. Paddison), and the Pew Biomedical Scholars Program (to J.G. DeLuca and P.J. Paddison).

Received May 12, 2014; revised June 24, 2014; accepted July 18, 2014; published OnlineFirst August 7, 2014.

References

1. Santaguida S, Musacchio A. The life and miracles of kinetochores. Embo J 2009;28:2511–31.
2. Lens SM, Voest EE, Medema RH. Shared and separate functions of polo-like kinases and aurora kinases in cancer. Nat Rev Cancer 2010;10:825–41.
3. Tooley J, Stukenberg PT. The Ndc80 complex: integrating the kinetochore's many movements. Chromosome Res 2011;19:377–91.
4. Lampson MA, Cheeseman IM. Sensing centromere tension: aurora B and the regulation of kinetochore function. Trends Cell Biol 2011;21:133–40.
5. Funabiki H, Wynne DJ. Making an effective switch at the kinetochore by phosphorylation and dephosphorylation. Chromosoma 2013;122:135–58.
6. DeLuca KF, Lens SM, DeLuca JG. Temporal changes in Hec1 phosphorylation control kinetochore-microtubule attachment stability during mitosis. J Cell Sci 2011;124:622–34.
7. Compton DA. Mechanisms of aneuploidy. Curr Opin Cell Biol 2011;23:109–13.
8. Lara-Gonzalez P, Westhorpe FG, Taylor SS. The spindle assembly checkpoint. Curr Biol 2012;22:966–80.
9. Foley EA, Kapoor TM. Microtubule attachment and spindle assembly checkpoint signalling at the kinetochore. Nat Rev Molec Cell Biol 2013;14:25–37
10. Lampson MA, Kapoor TM. The human mitotic checkpoint protein BubR1 regulates chromosome-spindle attachments. Nat Cell Biol 2005;7:93–8.
11. Suijkerbuijk SJ, Vleugel M, Teixeira A, Kops GJ. Integration of kinase and phosphatase activities by BUBR1 ensures formation of stable kinetochore-microtubule attachments. Dev Cell 2012;23:745–55.
12. Kruse T, Zhang G, Larsen MS, Lischetti T, Streicher W, Kragh Nielsen T, et al. Direct binding between BubR1 and B56-PP2A phosphatase complexes regulate mitotic progression. J Cell Sci 2013;126:1086–92.
13. Kawashima SA, Tsukahara T, Langegger M, Hauf S, Kitajima TS, Watanabe Y. Shugoshin enables tension-generating attachment of kinetochores by loading Aurora to centromeres. Genes Dev 2007;21:420–35.

Published OnlineFirst August 7, 2014; DOI: 10.1158/1078-0432.CCR-13-0645

14. Yamagishi Y, Honda T, Tanno Y, Watanabe Y. Two histone marks establish the inner centromere and chromosome bi-orientation. Science 2010;330: 239–43.
15. Caldas GV, DeLuca KF, DeLuca JG. KNL1 facilitates phosphorylation of outer kinetochore proteins by promoting Aurora B kinase activity. J Cell Biol 2013;203:957–69.
16. Szerlip NJ, Pedraza A, Chakravarty D, Azim M, McGuire J, Fang Y, et al. Intratumoral heterogeneity of receptor tyrosine kinases EGFR and PDGFRA amplification in glioblastoma defines subpopulations with distinct growth factor response. Proc Natl Acad Sci U S A 2012;109:3041–6.
17. Harada K, Nishizaki T, Ozaki S, Kubota H, Ito H, Sasaki K. Intratumoral cytogenetic heterogeneity detected by comparative genomic hybridization and laser scanning cytometry in human gliomas. Cancer Res 1998;58: 4694–700.
18. Sottoriva A, Spiteri I, Piccirillo SG, Touloumis A, Collins VP, Marioni JC, et al. Intratumor heterogeneity in human glioblastoma reflects cancer evolutionary dynamics. Proc Natl Acad Sci U S A 2013;110:4009–14.
19. Snuderl M, Fazlollahi L, Le LP, Nitta M, Zhelyazkova BH, Davidson CJ, et al. Mosaic amplification of multiple receptor tyrosine kinase genes in glioblastoma. Cancer Cell 2011;20:810–7.
20. Gao C, Furge K, Koeman J, Dykema K, Su Y, Cutler ML, et al. Chromosome instability, chromosome transcriptome, and clonal evolution of tumor cell populations. Proc Natl Acad Sci U S A 2007;104:8995–9000.
21. Bhat KP, Balasubramaniyan V, Vaillant B, Ezhilarasan R, Hummelink K, Hollingsworth F, et al. Mesenchymal differentiation mediated by NF-kappaB promotes radiation resistance in glioblastoma. Cancer Cell 2013; 24:331–46.
22. Gillies RJ, Verduzco D, Gatenby RA. Evolutionary dynamics of carcinogenesis and why targeted therapy does not work. Nat Rev Cancer 2012;12:487–93.
23. Weaver BA, Cleveland DW. Does aneuploidy cause cancer? Curr Opin Cell Biol 2006;18:658–67.
24. Roschke AV, Rozenblum E. Multi-layered cancer chromosomal instability phenotype. Front Oncol 2013;3:302.
25. Yoon DS, Wersto RP, Zhou W, Chrest FJ, Garrett ES, Kwon TK, et al. Variable levels of chromosomal instability and mitotic spindle checkpoint defects in breast cancer. Am J Pathol 2002;161:391–7.
26. Bie L, Zhao G, Cheng P, Rondeau G, Porwollik S, Ju Y, et al. The accuracy of survival time prediction for patients with glioma is improved by measuring mitotic spindle checkpoint gene expression. PLoS One 2011; 6:e25631.
27. Cahill DP, Lengauer C, Yu J, Riggins GJ, Willson JK, Markowitz SD, et al. Mutations of mitotic checkpoint genes in human cancers. Nature 1998; 392:300–3.
28. Suijkerbuijk SJ, Kops GJ. Preventing aneuploidy: the contribution of mitotic checkpoint proteins. Biochim Biophys Acta 2008;1786:24–31.
29. Yuan B, Xu Y, Woo JH, Wang Y, Bae YK, Yoon DS, et al. Increased expression of mitotic checkpoint genes in breast cancer cells with chromosomal instability. Clin Cancer Res 2006;12:405–10.
30. Ding Y, Hubert CG, Herman J, Corrin P, Toledo CM, Skutt-Kakaria K, et al. Cancer-specific requirement for BUB1B/BUBR1 in human brain tumor isolates and genetically transformed cells. Cancer Discov 2013;3:198–211.
31. Baker DJ, Dawlaty MM, Wijshake T, Jeganathan KB, Malureanu L, van Ree JH, et al. Increased expression of BubR1 protects against aneuploidy and cancer and extends healthy lifespan. Nat Cell Biol 2012;15:96–102.
32. American Cancer Society. Cancer facts and figures 2010. Atlanta, GA: American Cancer Society; 2010. Report No. 500810.
33. Brain Tumor Progress Review Group. Report of the Brain Tumor Progress Review Group. Bethesda (MD): National Cancer Institute and National Institute of Neurological Disorders and Stroke; 2000. Report No. 01–4902.
34. Gargiulo G, Cesaroni M, Serresi M, de Vries N, Hulsman D, Bruggeman SW, et al. In vivo RNAi screen for BMI1 targets identifies TGF-beta/BMP-ER stress pathways as key regulators of neural- and malignant glioma-stem cell homeostasis. Cancer Cell 2013;23:660–76.
35. Hubert CG, Bradley RK, Ding Y, Toledo CM, Herman J, Skutt-Kakaria K, et al. Genome-wide RNAi screens in human brain tumor isolates reveal a novel viability requirement for PHF5A. Genes Dev 2013;27:1032–45.
36. Chudnovsky Y, Kim D, Zheng S, Whyte WA, Bansal M, Bray MA, et al. ZFHX4 interacts with the NuRD core member CHD4 and regulates the glioblastoma tumor-initiating cell state. Cell Rep 2014;6:313–24.
37. Goidts V, Bageritz J, Puccio L, Nakata S, Zapatka M, Barbus S, et al. RNAi screening in glioma stem-like cells identifies PFKFB4 as a key molecule important for cancer cell survival. Oncogene 2012;31:3235–43.
38. Wurdak H, Zhu S, Romero A, Lorger M, Watson J, Chiang CY, et al. An RNAi screen identifies TRRAP as a regulator of brain tumor-initiating cell differentiation. Cell Stem Cell 2010;6:37–47.
39. Toledo CM, Herman JA, Olsen JB, Ding Y, Corrin P, Girard EJ, et al. BuGZ is required for Bub3 stability, Bub1 kinetochore function, and chromosome alignment. Dev Cell 2014;28:282–94.
40. Kazanis I, Lathia JD, Vadakkan TJ, Raborn E, Wan R, Mughal MR, et al. Quiescence and activation of stem and precursor cell populations in the subependymal zone of the mammalian brain are associated with distinct cellular and extracellular matrix signals. J Neurosci 2010;30:9771–81.
41. Lathia JD, Li M, Hall PE, Gallagher J, Hale JS, Wu Q, et al. Laminin alpha 2 enables glioblastoma stem cell growth. Ann Neurol 2012;72:766–78.
42. Musacchio A, Salmon ED. The spindle-assembly checkpoint in space and time. Nat Rev Mol Cell Biol 2007;8:379–93.
43. Lara-Gonzalez P, Scott MI, Diez M, Sen O, Taylor SS. BubR1 blocks substrate recruitment to the APC/C in a KEN-box-dependent manner. J Cell Sci 2011;124:4332–45.
44. Suijkerbuijk SJE, van Dam TJP, Karagoz GE, von Castelmur E, Hubner NC, Duarte AMS, et al. The vertebrate mitotic checkpoint protein BUBR1 is an unusual pseudokinase. Dev Cell 2012;22:1321–9.
45. Wang X, Babu JR, Harden JM, Jablonski SA, Gazi MH, Lingle WL, et al. The mitotic checkpoint protein hBUB3 and the mRNA export factor hRAE1 interact with GLE2p-binding sequence (GLEBS)-containing proteins. J Biol Chem 2001;276:26559–67.
46. Wang Q, Liu T, Fang Y, Xie S, Huang X, Mahmood R, et al. BUBR1 deficiency results in abnormal megakaryopoiesis. Blood 2004;103:1278–85.
47. Malureanu LA, Jeganathan KB, Hamada M, Wasilewski L, Davenport J, van Deursen JM. BubR1 N terminus acts as a soluble inhibitor of cyclin B degradation by APC/C(Cdc20) in interphase. Dev Cell 2009;16:118–31.
48. Pahl PM, Hodges YK, Meltesen L, Perryman MB, Horwitz KB, Horwitz LD. ZNF207, a ubiquitously expressed zinc finger gene on chromosome 6p21.3. Genomics 1998;53:410–2.
49. Morales AG, Pezuk JA, Brassesco MS, de Oliveira JC, de Paula Queiroz RG, Machado HR, et al. BUB1 and BUBR1 inhibition decreases proliferation and colony formation, and enhances radiation sensitivity in pediatric glioblastoma cells. Childs Nerv Syst 2013;29:2241–8.
50. Larsen NA, Al-Bassam J, Wei RR, Harrison SC. Structural analysis of Bub3 interactions in the mitotic spindle checkpoint. Proc Natl Acad Sci U S A 2007;104:1201–6.
51. Taylor SS, Ha E, McKeon F. The human homologue of Bub3 is required for kinetochore localization of Bub1 and a Mad3/Bub1-related protein kinase. J Cell Biol 1998;142:1–11.
52. Pritchard CE, Fornerod M, Kasper LH, van Deursen JM. RAE1 is a shuttling mRNA export factor that binds to a GLEBS-like NUP98 motif at the nuclear pore complex through multiple domains. J Cell Biol 1999;145:237–54.
53. Senisterra G, Wu H, Allali-Hassani A, Wasney GA, Barsyte-Lovejoy D, Dombrovski L, et al. Small-molecule inhibition of MLL activity by disruption of its interaction with WDR5. Biochem J 2013;449:151–9.
54. Orlicky S, Tang X, Neduva V, Elowe N, Brown ED, Sicheri F, et al. An allosteric inhibitor of substrate recognition by the SCF(Cdc4) ubiquitin ligase. Nat Biotechnol 2010;28:733–7.
55. London N, Ceto S, Ranish JA, Biggins S. Phosphoregulation of Spc105 by Mps1 and PP1 regulates Bub1 localization to kinetochores. Curr Biol 2012; 22:900–6.
56. Shepperd LA, Meadows JC, Sochaj AM, Lancaster TC, Zou J, Buttrick GJ, et al. Phosphodependent recruitment of Bub1 and Bub3 to Spc7/KNL1 by Mph1 kinase maintains the spindle checkpoint. Curr Biol 2012;22: 891–9.
57. Yamagishi Y, Yang CH, Tanno Y, Watanabe Y. MPS1/Mph1 phosphorylates the kinetochore protein KNL1/Spc7 to recruit SAC components. Nat Cell Biol 2012;14:746–52.
58. Jiang Y, Li X, Yang W, Hawke DH, Zheng Y, Xia Y, et al. PKM2 regulates chromosome segregation and mitosis progression of tumor cells. Mol Cell 2014;53:75–87.
59. Slee RB, Grimes BR, Bansal R, Gore J, Blackburn C, Brown L, et al. Selective inhibition of pancreatic ductal adenocarcinoma cell growth by the mitotic MPS1 kinase inhibitor NMS-P715. Mol Cancer Ther 2014;13:307–15.

60. Jemaa M, Galluzzi L, Kepp O, Senovilla L, Brands M, Boemer U, et al. Characterization of novel MPS1 inhibitors with preclinical anticancer activity. Cell Death Differ 2013;20:1532–45.
61. Tannous BA, Kerami M, Van der Stoop PM, Kwiatkowski N, Wang J, Zhou W, et al. Effects of the selective MPS1 inhibitor MPS1-IN-3 on glioblastoma sensitivity to antimitotic drugs. J Natl Cancer Inst 2013; 105:1322–31.
62. Chen J, Xie J, Jiang Z, Wang B, Wang Y, Hu X. Shikonin and its analogs inhibit cancer cell glycolysis by targeting tumor pyruvate kinase-M2. Oncogene 2011;30:4297–306.
63. Pezuk JA, Brassesco MS, Morales AG, de Oliveira JC, de Paula Queiroz RG, Machado HR, et al. Polo-like kinase 1 inhibition causes decreased proliferation by cell cycle arrest, leading to cell death in glioblastoma. Cancer Gene Ther 2013;20:499–506.
64. Shi JQ, Lasky K, Shinde V, Stringer B, Qian MG, Liao D, et al. MLN0905, a small-molecule plk1 inhibitor, induces antitumor responses in human models of diffuse large B-cell lymphoma. Mol Cancer Ther 2012;11: 2045–53.
65. Oliveira JC, Pezuk JA, Brassesco MS, Morales AG, Queiroz RGP, Scrideli CA, et al. PLK1 expression and BI 2536 effects in childhood acute lymphoblastic leukemia. Pediatr Blood Cancer 2014;61:1227–31.
66. Danovi D, Folarin A, Gogolok S, Ender C, Elbatsh AM, Engstrom PG, et al. A high-content small molecule screen identifies sensitivity of glioblastoma stem cells to inhibition of polo-like kinase 1. PLoS One 2013;8:e77053.
67. Maertens J, et al.Phase I/II study of volasertib (BI 6727), an intravenous Polo-like kinase (Plk) inhibitor, in patients with acute myeloid leukemia (AML): results from the randomized phase II part for volasertib in combination with low-dose cytarabine (LDAC) versus LDAC monotherapy in patients with previously untreated AML ineligible for intensive treatment [abstract]. In: Proceedings of the 54th ASH Annual Meeting and Exposition; 2012 Dec 8–12; Atlanta, GA.
68. Cheung CH, Coumar MS, Hsieh HP, Chang JY. Aurora kinase inhibitors in preclinical and clinical testing. Expert Opin Investig Drugs 2009;18:379–98.
69. Talapatra SK, Anthony NG, Mackay SP, Kozielski F. Mitotic kinesin Eg5 overcomes inhibition to the phase I/II clinical candidate SB743921 by an allosteric resistance mechanism. J Med Chem 2013;56:6317–29.